



University  
of Glasgow

Cleary, Alison (2004) Integrated optical technologies for analytical sensing. PhD thesis.

<http://theses.gla.ac.uk/6607/>

Copyright and moral rights for this thesis are retained by the author

A copy can be downloaded for personal non-commercial research or study, without prior permission or charge

This thesis cannot be reproduced or quoted extensively from without first obtaining permission in writing from the Author

The content must not be changed in any way or sold commercially in any format or medium without the formal permission of the Author

When referring to this work, full bibliographic details including the author, title, awarding institution and date of the thesis must be given.

# **Integrated Optical Technologies for Analytical Sensing**

Submitted for the degree of Doctor of Philosophy  
to the  
Department of Electronics and Electrical Engineering  
University of Glasgow

by  
Alison Cleary

September 2004

©Alison Cleary 2004

## Acknowledgements

First of all, I would like to thank my supervisors, Prof. Jon Cooper, Prof. Peter Laybourn and Prof. J. Stewart Aitchison, for encouraging me to choose the project, and for their advice throughout the course of the work. In particular I would like to thank Jon for making me worry about the work enough that I did something about it, Peter for coming out of retirement to read my thesis, and Stewart for hosting me at the University of Toronto.

Many thanks are due to the Royal Society of Edinburgh for providing the funding to visit the IEEE Sensors Conference in Toronto, and for the chance to visit the University of Toronto to use their facilities. I would like to thank everyone at the University of Toronto who helped me, in particular Prof. Peter Herman for letting me loose on the laser facilities, and Stephen Ho for patiently helping to run the laser.

I am also very grateful to Gerald Buller, Sara Pellegrini and Carole Helfter at Heriot-Watt University for their advice with the photon counting experiments, for without their help I would have been lost!

There are many people at the University of Glasgow without whose help I could never have completed the project. Ian McNicholl, Mark Dragsnes and Tom Reilly provided ongoing assistance and advice with the FHD system (as well as constantly reminding me how scary it was), while Linda, Eve, Margaret and Lois showed me everything cleanroom-related and Mary and Bill looked after the bio side of things. Everyone in the Level 1 cleanroom helped enormously with electron-beam writing techniques, for which I am very grateful. And many thanks go to Kaz, Joe, Colin and John in the mechanical workshop for cheerily fulfilling 'urgent' requests.

I would like to thank all my colleagues and office-mates from this 'extended' three-year period – especially Sonia for her immense electron beam expertise and encouragement, Duncan for help with FHD, Dong and Marco for being cheerful office-mates.

Finally, I would like to thank Gerry and all my family for their patience!

## **Abstract**

Recent diversification of the telecommunications industry has resulted in the adaptation of optical materials and their associated fabrication technologies for use in the bioanalytical sensor industry.

Flame hydrolysis deposited (FHD) planar silica is one such material. Capable of producing high quality films for optical waveguides, the chemical inertness of the deposited silica makes it an ideal substrate from which to fabricate a biological fluorescence sensor.

The aim of the work contained in this thesis was to utilise the FHD silica in optical fluorescence sensors suitable for use at visible and in particular red wavelengths where several fluorophores can be excited, and background fluorescence from the silica is small. New technologies for producing waveguides have been evaluated in the context of their usefulness in optical sensors, with the intention of producing devices with as few fabrication steps as possible to reduce fabrication time and cost.

The design, fabrication and testing of a number of sensor configurations is described, in which optical waveguides were interfaced with microfluidic chambers to provide excitation of a fluorophore in solution. New waveguide fabrication technologies were used for the first time in sensor systems with integrated microfluidic circuits.

Waveguides written by electron beam densification were evaluated in terms of their performance in splitting an excitation signal into several different components, as would be appropriate for excitation of multiple microfluidic chambers – an ‘array sensor’. Both Y-branch waveguides and multimode interference (MMI) splitters were successfully used to split the excitation signal.

In addition to electron beam densification, UV irradiation at a wavelength of 157 nm was used to write waveguides in FHD silica. The application of a metal surface mask to define the waveguide structures is described.

To allow sensitive detection and identification of fluorophores from FHD silica sensor chips, a single chamber device was successfully interfaced to a system to make time resolved fluorescence measurements, a technique known as time correlated single photon counting (TCSPC). The use of TCSPC allowed measurement of the decay time of the fluorescent dye, by which different fluorescent molecules could be identified, as well as the possibility of low concentration measurements.

The research has allowed new technologies for creating waveguides in FHD silica to be adapted for sensing purposes, leading to a platform for creating devices in a number of different configurations.

# Publication List

## First Author

### Journal Papers

**Cleary, A., García-Blanco, Glidle, A., Aitchison, J.S., Laybourn, P., Cooper, J.M.,** “An integrated fluorescence array as a platform for lab-on-a-chip technology using multimode interference splitters”, in press, IEEE Sensors, 2004.

### Conference Proceedings

**Cleary, A., García-Blanco, Glidle, A., Aitchison, J.S., Laybourn, P., Cooper, J.M.,** “Direct-write asymmetric Y-branch waveguides on flame hydrolysis silica for sensing applications”, Proc. Eurosensors XVII, 478-481, 2003.

**Cleary, A., García-Blanco, S., Glidle, A., Aitchison, J.S., Laybourn, P., Cooper, J.M.,** “Towards optical fluorescence sensing using multimode interference splitters”, Proc. IEEE Sensors II, 279-282, 2003.

## Named Author

**Ruano, J.M., Glidle, A., Cleary, A., Walmsley, A., Aitchison, J.S., Cooper, J.M.,** “Design and fabrication of a silica on silicon integrated optical biochip as a fluorescence microarray platform”, Biosensors and Bioelectronics 18, 175-184, 2003.

**Ho, S., Aitchison, J.S., García-Blanco, S., Herman, P.R., Cleary, A.,** “Direct F<sub>2</sub> laser fabrication of Y-junction waveguides in flame hydrolysis deposited germanium-doped silica”, Paper CThT15, Proc. CLEO 2004.

# List of Abbreviations

<b>ADC</b>	Analogue to Digital Converter
<b>APD</b>	Avalanche Photodiode
<b>AWG</b>	Arrayed Waveguide Grating
<b>BP</b>	Bandpass
<b>CCD</b>	Charge Coupled Device
<b>EIM</b>	Effective Index Method
<b>FHD</b>	Flame Hydrolysis Deposition
<b>IR</b>	Infrared
<b>MCA</b>	Multi Channel Analyser
<b>MMI</b>	Multimode Interference
<b>NA</b>	Numerical Aperture
<b>NB</b>	Narrow Band
<b>ND</b>	Neutral Density
<b>PDMS</b>	Poly(dimethylsiloxane)
<b>PMMA</b>	Poly(methylmethacrylate)
<b>PMT</b>	Photomultiplier Tube
<b>RF</b>	Radio Frequency
<b>RO</b>	Reverse Osmosis
<b>SPAD</b>	Single Photon Avalanche Diode
<b>TAC</b>	Time to Amplitude Converter
<b>TBC</b>	Transparent Boundary Condition
<b>TCSPC</b>	Time Correlated Single Photon Counting
<b>TRPL</b>	Time Resolved Photoluminescence
<b>UV</b>	Ultraviolet

# Contents

Acknowledgements	II
Abstract	III
Publication List	V
List of Abbreviations	VI
<b>1 Introduction</b>	<b>1</b>
1.1 Lab-on-a-Chip and Optical Sensors	1
1.2 Integrated Optics and Planar Silica Lightwave Circuits	2
1.3 Microfluidics	2
1.4 Motivation	3
1.5 Synopsis of Thesis	3
<b>2 Planar Silica for Waveguides and Sensors</b>	<b>5</b>
2.1 Planar Silica Waveguides in Integrated Optics	5
2.2 Flame Hydrolysis Deposition of Planar Silica	6
2.3 Defects in FHD Glass	9
2.4 Fluorescence Sensing Using Waveguides	9
2.4.1 Array Sensors	10
2.5 Microfluidics	11
2.6 Fabrication of Waveguides and Microchannels	11
2.6.1 Fabrication of Dry Etched Waveguides and Microchannels	12
2.6.1.1 Deposition of FHD Silica Layers	12
2.6.1.2 The Etch Process	13
2.6.1.3 Pattern Masking	14
2.6.1.4 Sample Preparation and Photolithography for Etching	15
2.6.1.5 Tailoring the Waveguide Dimensions to Suit the Application	20
2.6.2 Waveguides Written using Electron Beam Densification	21
2.6.2.1 Fabrication Process for Electron Beam Written Waveguides	22
2.6.3 Waveguides Defined by UV Irradiation	26
2.7 Polymers for Waveguide Cladding and Device Sealing	26
2.7.1 Selection of an Appropriate Cladding Material	27

2.7.1.1	Possible Choices	27
2.7.1.2	Other Examples of Polymer Cladding	28
2.7.2	Definition of Channels in PDMS Films	29
2.8	Device Design	31
2.8.1	Waveguide Design using the Beam Propagation Method	31
2.8.2	Microfluidic Circuit Dimensions	32
2.9	Device Characterisation	32
2.9.1	Coupling of Light into Waveguides	33
2.9.2	Loss Measurement	34
2.9.3	Fluorescence Detection	34
2.9.3.1	The CCD Detector	34
2.9.3.2	The Photomultiplier Tube (PMT) Detector	34
2.9.3.3	Choice of Fluorophore	35
2.10	Summary	36
<b>3</b>	<b>Y-branch Waveguides and Polymers for Biological Sensors</b>	<b>37</b>
3.1	Y-branch Waveguides as Optical Beamsplitters	37
3.1.1	Symmetric Y-branch Waveguides	37
3.1.2	Asymmetric Y-branch Waveguides	39
3.2	Y-branch waveguides in Optical Sensor Devices	39
3.2.1	Design of Asymmetric Y-branch Waveguides	39
3.2.2	Fabrication and Optical Characterisation of Asymmetric Y-branch Waveguides	43
3.2.3	Fabrication and Optical Characterisation of Symmetric Y-branch Waveguides	46
3.2.4	Microfluidic Circuitry	47
3.2.5	PDMS as Waveguide Cladding	49
3.3	Fluorescence Measurements on an Asymmetric Y-branch Waveguide Sensor with an Etched Microfluidic Chamber	50
3.4	Fabrication of Unclad Dry Etched Ridge Waveguides	52
3.5	Evanescent Excitation Sensors using Y-branch Waveguides	53
3.5.1	Fabrication of the Evanescent Excitation Chip	54
3.5.2	Fluorescence Measurements	55
3.6	Summary	57

<b>4</b>	<b>Multimode Interference (MMI) Splitters for Fluorescence Applications</b>	58
4.1	Multimode Interference in Strong Guiding Media	58
4.2	Silica-Based MMI Devices	60
4.2.1	Multimode Interference in Dry Etched Silica	60
4.2.2	Electron beam Defined Multimode Interference Structures	63
4.2.3	Fabrication Tolerances	67
4.3	Fabrication and Waveguide Characterisation	70
4.3.1	Waveguide Fabrication	70
4.3.2	Microfluidics	71
4.3.3	Optical Characterisation	72
4.4	Fluorescence Measurements using MMI Splitters	74
4.5	Summary	78
<b>5</b>	<b>Time Correlated Single Photon Detection of Fluorescence from an FHD Planar Silica Sensor Chip</b>	79
5.1	Time Correlated Single Photon Counting (TCSPC)	79
5.2	The Single Photon Avalanche Diode (SPAD) as a Detector	83
5.3	Chip Fabrication	83
5.3.1	Optical Components	84
5.3.2	Microfluidic Components	84
5.4	Experimental Setup	87
5.5	Measurement of Different Fluorescent Dye Concentrations	88
5.5.1	Limitations on the Minimum Detectable Concentration	89
5.6	Measurement of the Decay Time of Nile Blue Dye	91
5.7	Summary	92
<b>6</b>	<b>UV Laser Irradiation for Optical Waveguide Definition</b>	94
6.1	UV Photosensitivity of Silica	94
6.1.1	Photosensitisation	95
6.1.2	Gratings Written in Fibres by UV Irradiation	95

6.1.3	Channel Waveguides Fabricated by UV Irradiation	96
6.2	F <sub>2</sub> UV Lasers for Photonic Fabrication	97
6.2.1	Background to Waveguide Fabrication	97
6.2.2	Refractive-Index Modification of Ge-doped FHD Silica	98
6.2.2.1	Sample Preparation	98
6.3	Results from UV Irradiation of FHD Silica	102
6.3.1	Mask Preparation	102
6.3.2	Fabrication and Characterisation of Straight Waveguides	103
6.3.2.1	Losses in the Irradiated Waveguides	105
6.3.3	Writing of Symmetric and Asymmetric Y-branch Waveguides	105
6.3.3.1	Y-branch Design	105
6.3.4	Grating Fabrication	108
6.4	Summary	109
<b>7</b>	<b>Conclusions and Future Work</b>	<b>110</b>
7.1	Conclusions	110
7.2	Suggestions for Future Work	111

# Chapter 1: Introduction

## 1.1 Lab-on-a-Chip and Optical Sensors

The requirement for sensitive compact sensors in the areas of healthcare and biotechnology has driven the development of integrated analytical systems, known as “Lab-on-a-Chip”, or micro total analysis systems ( $\mu$ TAS). The concept, where the goal is to integrate all sensing and reagent handling components on a single chip, has been the subject of a great amount of interest [Manz 1990, Reyes 2002, Auroux 2002, Bilenberg 2003, Erickson 2004]. In many of these systems there are micro-scale components interfaced with larger ‘off-chip’ instruments, including sensors, detectors and pumps (for microfluidics). Often light guiding is performed off-chip, using either free space optics or fibres. However, it has been a challenge to both industry and researchers to achieve complete integration, as many components of sensor systems are still somewhat bulky.

Many different types of miniaturised sensors have been developed since the concept was first introduced [Harrison 1992, Seiler 1993, Göpel 1998, Moore 2001]. One of the most successful has been the DNA microarray, used to investigate gene expression, which was successfully commercialised by Affymetrix Inc. from the work of Stephen Fodor. Tagging of DNA with fluorescent labels allows sensors specific to a given DNA sequence to be created. Other well-established firms with interests in the semiconductor, optical and computer industries have also been adapting their existing technologies to produce biological sensing devices. One example is Agilent, who have adapted their inkjet printer technology for DNA microarrays.

As an addition to the reduced size of complete devices, the advantages of Lab-on-a-Chip include increased speed of assays, reduced reagent consumption, cheaper manufacturing and a greater degree of automation [Erickson 2004].

Planar optical sensors, where waveguides control the delivery of light to a particular detection area, have previously been developed, allowing on-chip detection to be performed [Heideman 1999, Duvencek 2002]. The many advances in microfabrication technologies and integrated optics allow these devices to be easily fabricated. Fluorescence detection is an attractive method due to its sensitivity [Plowman 1999, Verpoorte 2003],

and it has been successfully used in optical fluorescence sensor systems where waveguides have been integrated with microfluidics [Zhou 1993, Kunz 1997]. There are numerous advantages to using a planar substrate rather than a fibre for optical sensing purposes [Robinson 1995], including robustness, alignment and the possibility of integrated manufacturing on a single sheet or wafer.

## **1.2 Integrated Optics and Planar Silica Lightwave Circuits**

One of the principal advantages of silica-based planar lightwave circuits is their inherent compatibility with optical fibres. Of the different fabrication methods, flame hydrolysis deposition (FHD) of doped silica glass provides extremely high quality and robust waveguides [Kawachi 1990, Okamoto 1998]. FHD of planar silica was developed from a method for optical fibre fabrication, with a silicon wafer coated with a layer of silica thermal oxide used as the undercladding. Industrially, FHD technology has been proposed as a key technology in the new generation of planar optical networking components [Astle 2000], although the more recent slowdown in the telecommunications industry has forced the development of new technologies in this area to take a lower profile.

Traditional microfabrication techniques such as photolithography and dry etching have been adapted for use on silica substrates, resulting in the production of high quality, low-loss, low autofluorescence waveguide components [Barbarossa 1992, McLaughlin 1998, Ruano 2000 (a,b)].

## **1.3 Microfluidics**

Microfluidic systems are increasingly used as a replacement for macrofluidic systems for a number of purposes, including pumping, flow sensing, separation and chemical delivery [Gravesen 1993]. When used for chemical and biological analysis, the reduced size of the devices presents several advantages, such as the reduction of the amount of reagents used, the increase in the speed of reactions and an increase in the density of analytical sites. The potential for integration of microfluidics with sensor systems has resulted in a wide variety of analytical devices [Erickson 2004]. Integration of microfluidic channels with optical waveguides provides one such implementation, creating a miniaturised portable analysis chip [Ruano 2000 (a), Mogensen 2001]. By integrating waveguides with microfluidics, light can be directed to one or many specific points of analysis within an area of a few mm<sup>2</sup> or even less.

## 1.4 Motivation

The purpose of this work was to develop new integrated optical biosensor systems, based upon FHD planar silica-on-silicon technology. One particular aim was to investigate systems where the high performance integrated optical waveguide elements were retained, exploring alternative methods of integrating microfluidic channels with the waveguides. Reduction of the fabrication and processing time, and therefore the cost required to produce the optical sensor chips, was a major goal of the work.

Specifically, the aims of the research were firstly to understand the requirements of optical sensors for biological applications, in particular silica-based waveguide systems. A study to determine if the use of polymers as part of the system, which could help to reduce the fabrication cost without compromising chip performance, was then required. Identification and design of optimum waveguide layouts for chip compactness and performance, allowing microfluidics to be easily integrated with the optical sections was considered necessary before fabrication could be carried out.

Thorough familiarisation with the FHD system was essential to design and fabricate the sensor chips and evaluate their performance in comparison with other systems. All devices described within this thesis were fabricated and tested by the author. Fundamental limits on the performance of this family of optical sensors were found, and any emerging technologies that may provide future improvements were evaluated.

## 1.5 Synopsis of Thesis

After this brief introduction, Chapter 2 provides a review of the basic technologies involved, and the fabrication and characterisation processes used throughout this work. Any processes specific to a detailed section of the work are described in the chapter with which they are associated. The polymers employed in the work are also described, and methods for processing are discussed.

The work described in Chapter 3 investigates Y-branching waveguides for the excitation of multiple assay points or reference branches, and their suitability to sensor structures. Asymmetric branching guides are also described. Two sensor chip formats are presented using Y-branches to give an excitation guide and a reference, employing both direct

excitation of fluorescent molecules and evanescent excitation. The purpose of using two different types of excitation was to determine the ease of fabrication of both devices, and to compare their performance. The reproducibility of the branched waveguides was studied.

An alternative and more recently discovered method of splitting an excitation wave is the multimode interference (MMI) splitter, which is described in Chapter 4. While generally considered to be capable of more accurate beam splitting than Y-branches, the MMI splitter has not, to the author's knowledge, been previously used in a fluorescence sensor. Its suitability for both single-point and multipoint excitation chips was evaluated.

The limit of detection of planar silica fluorescent sensor chips was investigated in Chapter 5, where the interfacing of a single photon avalanche detector (SPAD) to a sensor chip is shown. The decay time of the fluorescent dye used was also measured with this system.

In Chapter 6, the fabrication of straight and Y-branch waveguides using ultraviolet (UV) radiation is presented. A new technique for masking the sample was evaluated during this work. The suitability of UV written waveguides for sensing applications is discussed, and future possibilities outlined.

Finally, Chapter 7 concludes the work, with suggestions for future work included in this section.

## 2 Planar Silica for Waveguides and Sensors

This chapter introduces the basic theory behind the work contained in the thesis. Detailed descriptions of well-known theory are not included; instead the reader is referred to relevant sources. Details of materials, fabrication processes and technology used throughout the thesis work are provided, but if a fabrication process is specific to only one device, it will be described in more detail in that chapter. Finally, the methods used for characterisation and testing of devices are described.

### 2.1 Planar Silica Waveguides in Integrated Optics

Planar silica or silica-on-silicon technology has found many applications in the telecommunications industry due to its excellent compatibility with optical fibre components [Okamoto 1999, Astle 2000]. The term planar implies that the devices or constituents are all on the same substrate or wafer rather than optical fibre-based, and different layers of silica can be formed sequentially one on top of the other. By controlling the refractive index of the different layers, light can be confined within a layer that is sandwiched between two other layers of lower refractive index. Use of microfabrication techniques allows waveguide structures of different sizes and layouts to be defined so that the path of the light can be controlled [Miya 2000]. Arrayed Waveguide Gratings (AWGs), multi/demultiplexers, filters and couplers have all been realised in planar silica, and can easily be coupled to fibres, as the fibres are typically silica-based also, allowing index and dimensional matching at the fibre-device interface.

Other materials can also be used for waveguide devices. Silicon,  $\text{LiNbO}_3$  (lithium niobate), semiconductor and various polymers are among the most common. The basic requirements for a waveguide material is that it should be easily processable, of an optical quality or purity such that losses are not prohibitive, and with a refractive index that can either be controlled or is of a value that it can be sandwiched between other materials of suitable index to give the required difference in refractive index [Ward 1974].

Flame hydrolysis deposition (FHD) of silica was used for the work in this thesis and is described in Section 2.2. Several other methods exist to produce silica on silicon wafers, the most common of these currently being sol-gel deposition and Plasma Enhanced

Chemical Vapour Deposition (PECVD) [Almeida 1999, Wosinski 2003]. While both of these may possess certain advantages over the FHD process used in the work detailed in this thesis, they also have disadvantages that may make them less useful or reproducible.

Sol-gel silica deposition involves the preparation of a solvent-based 'sol', to which a photosensitising agent is often added [Coudray 1997]. The sol is then spun onto a wafer and consolidated at around 900 °C. Fabrication of ridge waveguides can be achieved by exposing the waveguide pattern to UV radiation, for example in a mask aligner, to crosslink and harden the exposed polymer. The remaining unexposed silica can then be removed using acetone, leaving the gel waveguides on the substrate.

Layers of spun sol-gel silica tend to be much thinner than those possible with FHD, around 0.2 µm, necessitating the use of a multi-layer technique to produce even a single-mode guiding layer. Even when thin layers are used, sol-gel silica has a tendency to crack at the edges of the wafer, and much current research is focussed on reducing this effect to produce high optical quality films. Typical dopants used to enhance the properties of the silica are zirconium, titanium, ytterbium, erbium and aluminium [Livage 1997, Almeida 1999].

PECVD bears more similarities to FHD than sol-gel in that the silica can be deposited inside a plasma reaction chamber from reactive gas precursors, and the films produced can be of several microns thickness in one step [Wosinski 2003]. Electrons are accelerated inside the reaction chamber by creating a field using a radio frequency (RF) source. Silicon precursors (normally SiH<sub>4</sub>, SiCl<sub>4</sub> or SiF<sub>4</sub>) then react with oxygen precursors (O<sub>2</sub>, N<sub>2</sub>O or CO<sub>2</sub>) to form silica that is then deposited on to silicon wafers or oxidised silicon wafers inside the chamber. To control the refractive index of the films, dopants are added. The dopants germanium, phosphorus and boron, which are also used in the FHD process, are commonly used. For further details on PECVD, as well as a number of lesser-used types of silica and their deposition methods, there are many references available [Sahu 1999, Mogensen 2002, Wosinski 2003].

## **2.2 Flame Hydrolysis Deposition of Planar Silica**

In the work described in this thesis, the method of producing planar silica or 'glass' substrates used was FHD. FHD was first pioneered by Hyde in the 1930s at Corning, and

then patented [Hyde 1942]. The technology was widely developed from the 1980's onwards, mainly by Kawachi [Kawachi 1983, Kawachi 1990, Kitoh 1992] and was further developed from the late 1980's [Barbarossa 1991, Barbarossa 1992 (a,b), Bebbington 1993, Bonar 1998]. FHD deposition of planar silica is in many ways similar to the more widely used FHD production of optical fibres and is a particular type of Chemical Vapour Deposition (CVD) giving a very high optical quality, low-loss glass. The definition of low-loss changes as technology improves, but a general figure is that waveguides possessing a propagation loss of less than 1 dB/cm can be classified as low-loss, although a lower figure is both desired and attainable [Li 2003]. For example, propagation losses of 0.1 dB/cm in PECVD waveguides have been observed [Wosinski 2003].

The hydrolysis reaction occurs in an oxy-hydrogen flame, to which  $\text{SiCl}_4$  is added to produce fine glass soot. The flame is positioned above a rotating turntable containing the target wafers to allow the soot to be uniformly deposited on the wafers before it is sintered at high temperature. Three dopants,  $\text{BCl}_3$ ,  $\text{GeCl}_4$  and  $\text{POCl}_3$  can be added to the flame in defined concentrations to alter the refractive index of the final glass. The range of refractive index increase that could be obtained with the FHD system used is from zero to 1% with respect to the index of the  $\text{SiO}_2$  undercladding [McLaughlin 1998]. The addition of B or P can also reduce the sintering temperature needed, which is important as the furnace liner and wafer holders must be able to withstand the sintering temperature also.

Other dopants, such as Ti-based halides, could also be added to produce similar refractive index and glass sintering temperature effects. Normally an FHD system will only have a choice of three different dopants, as this should be sufficient to produce the required range of refractive indices and to manipulate the sintering temperature to within a practical range. Sintering temperatures of greater than around 1400 °C can lead to devitrification of the furnace liner, and warping of the Si base layer of the wafers. The hydrolysis equations are shown below in Equations 1-4.



Equation 1 shows the production of the silica soot, while the three below (Equations 2-4) are the reactions that occur when the dopants are added to the soot. The dopants become part of the glass network when the soot is consolidated in the furnace.

Nitrogen is used both to cool the flame and to bubble through Drechsel bottles containing the  $\text{SiCl}_4$ ,  $\text{GeCl}_4$  and  $\text{POCl}_3$ , acting as a carrier gas to transport them to the torch. The  $\text{BCl}_3$  is supplied as a gas and therefore does not require nitrogen to be bubbled through it. After deposition, the soot-covered wafer is removed from the deposition chamber and consolidated in a furnace at temperatures greater than  $1000\text{ }^\circ\text{C}$ . A schematic of the deposition equipment is shown in Figure 2.1.

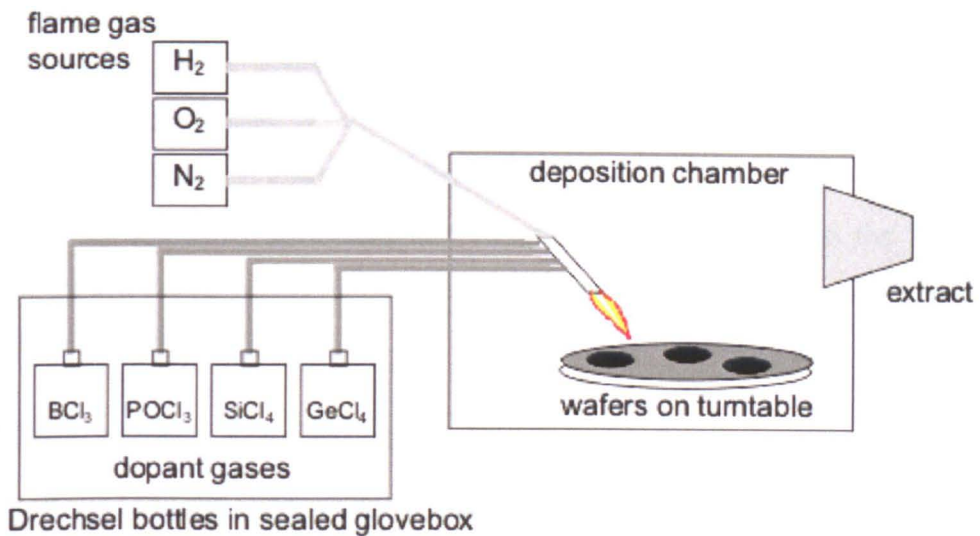


Figure 2.1: Schematic of the FHD deposition apparatus. An oxy-hydrogen flame burns the chlorides, which are carried to the torch by bubbling nitrogen gas through the Drechsel bottles.  $\text{BCl}_3$  is the exception as it is supplied as a gas and therefore does not need to be carried by nitrogen. The turntable rotates while the torch traverses linearly across the table to give an even soot deposition.

The sintering program varies with the type of glass to be produced. Ge-core waveguides are normally sintered for several hours, with the furnace temperature being gradually increased from  $1050\text{ }^\circ\text{C}$  up to the maximum ( $1350\text{ }^\circ\text{C}$ ), where it is normally held for 2 hours and then decreased to the removal temperature ( $600\text{ }^\circ\text{C}$ ) at the end of the program. P-doped core layers, however, require only a short 15-minute sinter at  $1375\text{ }^\circ\text{C}$  with no increase or decrease to the furnace temperature [Barbarossa 1992 (b)]. These sintering

requirements have previously been found empirically and more recently verified by the author.

### **2.3 Defects in FHD Glass**

Defects found in the FHD glass layer are often pinhole or point defects caused by contamination. The pinholes can be any size in the range of a few tens of microns where they can only be seen clearly through an optical microscope up to around 0.5 mm in diameter. Contamination is minimised by housing the deposition equipment in a cleanroom environment.

Air bubbles may also appear in a wafer after consolidation, particularly when the layer being consolidated is a second or third FHD waveguide cladding layer, and may be covering ridge waveguide structures that have been fabricated after a previous deposition. Where the existing ridge structures have particularly fine features, such as branching or closely spaced waveguides, the air bubbles can form between two adjacent guides. Experimentally it has been observed, both by the author and by previous users of the FHD system, that by gradually increasing the sintering temperature up to the maximum, in particular for Ge-doped cores, reduces the occurrence of the bubbles, such that none are observed over a full 3-inch wafer.

### **2.4 Fluorescence Sensing using Waveguides**

Recently, the potential for planar silica devices in biological sensing has been realised, and utilised in several studies. Ruano et al have shown the viability of both a single assay and array devices as fluorescence sensors, using Y-branch waveguide structures leading to microfluidic chambers filled with fluorophore [Ruano 1999, Ruano 2000]. Silica waveguide devices are amenable to use in biological sensors due to their robust nature, chemical inertness, and transparency at the visible wavelengths that are of interest in fluorescence sensors.

An alternative approach to fluorescence detection is that of absorbance, as shown by the micro-TAS group at the Mikroelektronik Centret in Denmark [Mogensen 2002]. However, absorbance detection does not provide such high sensitivity as fluorescence, and is often limited by the optical path length of the detection cell.

Both of the sensor types mentioned above were based on direct excitation of analyte, where the microfluidic channels and chambers for the fluorophore or analyte are etched through the full waveguide height, allowing the excitation light to propagate directly into the analyte, thus exciting as much of it as possible. Figure 2.2 illustrates this concept.

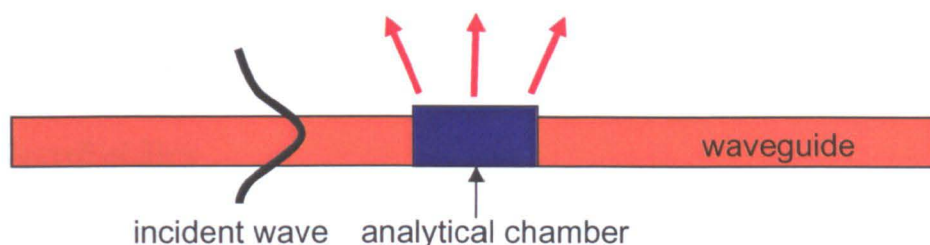


Figure 2.2: Schematic of a direct-excitation optical fluorescence sensor. Excitation light is directed by the waveguide to the microfluidic analytical chamber that contains the fluorophore or fluorescently labelled biomolecules. Emitted fluorescent light can be collected either through an output waveguide or from directly above the chamber.

The alternative to direct excitation is evanescent field excitation of the analyte, where the microfluidics are positioned directly on top of the waveguide structure. The evanescent field from the waveguide excites only the first few hundred nanometres of analyte closest to the waveguide, which in practice means that normally a monolayer of analyte would have to be attached to the waveguide surface to allow it to be probed efficiently [Zhou 1993, Heideman 1999].

For a fluorescent assay in solution, it is normally required that the substance under test be labelled with a fluorophore that is compatible with the excitation wavelength of the sensor. Therefore, detection of a particular substance relies on the ability of the sensor to detect the fluorophore to which the substance is attached.

#### 2.4.1 Array Sensors

In biological sensing, an array or microarray is normally used to sense a variety of different ‘elements’ such as different sequences of DNA or proteins within the one chip. The main advantage of arrays is the potential for simultaneous sensing of multiple analytes on one array or ‘substrate’, rather than performing several separate assays for different analytes, as was previously the case [Rowe-Tait 2000]. While DNA microarrays have become

industrially commonplace, arrays for proteins require different binding chemistry and therefore took longer to develop in terms of miniaturisation, although they have also been made available industrially [Bernard 2001]. Assays that were once performed in well plates, which are arrays of small fluidic chambers, are gradually being adapted so that they can use the least amount of analyte possible. For a fluorescence array, the device is normally imaged from the top using a charge coupled device (CCD) camera attached to a fluorescence microscope.

## **2.5 Microfluidics**

In recent years, research into microfluidic systems has resulted in an array of technologies being developed. Controlling the flow of fluid inside the channel is important, in that many applications require the sample to be pumped at a certain rate, or its components separated. The role of microfluidics in delivering samples to a sensing area is critical when aiming to reduce reagent usage, as only a few molecules may be present in the sample, and thus none of the sample should be lost before it reaches its destination [Polson 2001].

Controlling the flow of fluid inside channels is often achieved by electroosmotic flow, for which an external electric field is applied. Differently charged molecules can then be controlled and delivered to different places within the microfluidic chip [Jacobsen 1999, Fu 2002]. Pressure driven flow using a micropump is also possible, but suffers from less control and greater expense. Handling of samples of extremely small volume is difficult, but has been achieved successfully on the picolitre scale [Hosokawa 1999].

Valves for stopping fluid flow are also commonly used in microfluidic devices. Often made from an elastomer-type polymer, they normally consist of a tiny flap within the channel that can be forced to close and therefore stop fluid flow, or only allow fluid flow in one direction [Felton 2003]. The use of plastic microfluidic devices that can be fabricated by injection moulding, casting or embossing, greatly reduces the cost of devices compared to the older style glass or silicon ones [Boone 2002].

## **2.6 Fabrication of Waveguides and Microchannels**

Silica-on-silicon channel waveguides have traditionally been defined by plasma-assisted Reactive Ion Etching (RIE) [Kawachi 1990, Okamoto 1999], an anisotropic etch method which removes unmasked or unprotected areas of the substrate. More recently, studies

have confirmed the feasibility of waveguide definition using electron beam lithography or UV irradiation to cause densification of the silica and therefore refractive index increase [Syms 1994]. This subsection explains the technology behind all three methods and draws brief conclusions on the advantages of each.

## 2.6.1 Fabrication of Dry Etched Waveguides and Microchannels

### 2.6.1.1 Deposition of FHD Silica Layers

The starting point of any device was the deposition of the Ge doped silica to be used as the waveguide layer. All waveguides used in this work were formed in Ge doped silica, mostly with a  $\text{GeCl}_4$  flow rate of 100 sccm, according to the process given below in Table 2.1. The thickness of the final FHD layer was chosen by altering the number of torch traversals used, with each traversal of the torch giving a final FHD silica layer of around  $0.7 \mu\text{m}$ . The example shown in Table 2.1 shows that 3 traversals were used to give a layer thickness of  $2.1 \mu\text{m}$ . Two warm up traversals were used prior to the addition of the halides (that is, with just the oxygen/hydrogen/nitrogen flame) to heat the wafer so that the soot particles would begin to sinter on contact with the wafer.

Prior to the deposition of the silica, a Si wafer with  $7 \mu\text{m}$  thermal oxide (Compart, UK) was cleaned in an ultrasonic bath of acetone for 5 minutes, followed by methanol for 5 minutes and then rinsed in RO water. A 10 minute acid clean using a 7:1 ratio of  $\text{H}_2\text{SO}_4:\text{H}_2\text{O}_2$  (sulphuric acid:hydrogen peroxide) was used immediately prior to the deposition to remove any final debris from the wafer surface.

	Warming Step		Deposition Step	
<b>Initial Turntable Temperature</b>	120°C		150°C	
<b>No. of Traversals</b>	2		3	
<b>Flame Parameters</b>	Oxygen	7 l/min	Oxygen	7 l/min
	Hydrogen	5 l/min	Hydrogen	5 l/min
	Nitrogen	3 l/min	Nitrogen	3 l/min
<b>Halide Flows</b>	-	-	SiCl <sub>4</sub>	150 sccm
	-	-	GeCl <sub>4</sub>	100 sccm
	-	-	BCl <sub>3</sub>	65 sccm
	-	-	POCl <sub>3</sub>	-

Table 2.1: Summary of the process parameters used to fabricate the FHD Ge doped core layers for the waveguides used in the work.

The sintering cycle began at 1050 °C, rising to 1350 °C where it was held constant for 2 hours, and the wafers were removed from the furnace once the temperature had fallen to 600 °C. The wafers were then diced into pieces, normally 1 x 1.5 cm, using a fine diamond saw. Polishing of the device edges to improve light coupling was also possible, using a fine abrasive to remove rough edges, but was considered too time consuming for normal practice.

The thickness of the FHD layer was found by etching through the FHD silica into the thermal oxide, and using a Talystep (Taylor-Hobson, UK) or Dektak (Veeco, UK) profilometer to measure the thickness of the layers. Refractive index characterisation of the FHD slab was by the prism coupler method [Tien 1970, Ulrich 1970, Ulrich 1973].

### 2.6.1.2 The Etch Process

RIE of silica waveguides is achieved in a sealed chamber, in which a plasma reacts with the surface atoms of the unmasked silica surface. The product molecules are drawn away, resulting in etching wherever a mask does not exist. Figure 2.3 shows a schematic of the reaction chamber.

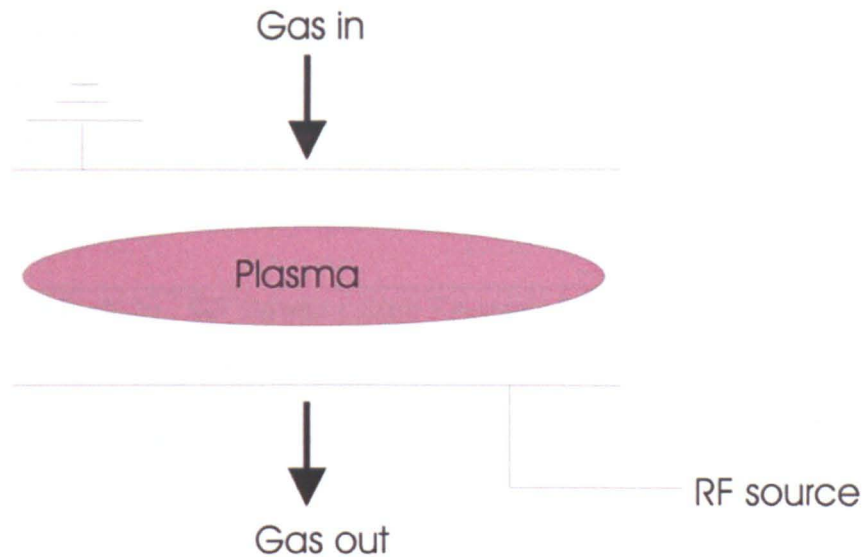


Figure 2.3: Schematic diagram of the RIE process chamber (after McLaughlin 1998). Ions from the plasma attach to the sample surface, where a reaction takes place to remove some of the silica sample. The product is then removed from the chamber by a pump to prevent redeposition.

The gases used for all work in this project were  $\text{CHF}_3$  for etching and  $\text{O}_2$  for sample and chamber cleaning. Other gases such as  $\text{CF}_4$  and  $\text{C}_2\text{F}_6$  can also be used for silica etching in the Oxford PlasmaTechnology BP80 machine used in this work, or in other similar machines, but  $\text{CHF}_3$  has been found to produce the best combination of etch rate and quality [McLaughlin 1998].

### 2.6.1.3 Pattern Masking

The mask can be produced by the traditional photolithographic techniques used by the microelectronics industry, which are suitable for feature sizes of greater than around 1 micron. If smaller features such as gratings, which require nanometre resolution, have to be etched, a polymethylmethacrylate (PMMA) mask patterned by electron beam lithography can be used [García-Blanco 2003 (b)].

Previous studies have shown that a bilayer etch mask of NiCr and photoresist provides a reliable mask for the higher powers needed to etch the FHD silica [McLaughlin 1998]. Polysilicon has also been used in similar systems where PECVD silica is to be etched [Mogensen 2002]. In this work, previously established mask thicknesses and RIE etch recipes developed within the department have been utilised, as the same machines and chemicals were that were used for the development were still available. Table 2.2 shows

the etch parameters used for a deep FHD silica etch, and the resulting average etch rate. The etch rate was found by measuring the depth etched in the silica in a known time using a Dektak surface profiler. The maximum length of an etch run is 30 minutes, after which an oxygen plasma clean is needed to remove reacted residue from the sample surface and the chamber.

Machine	RF Power	Etch Pressure	Etch Rate
BP80	190 W	30 mTorr	Approx. 65 nm/min

Table 2.2: Etch parameters for the dry etching of silica waveguides and microchannels in the Oxford PlasmaTechnology BP80 machine.

Omission of the cleaning step results in redeposition of photoresist onto the sample. To remove the redeposited photoresist is difficult, requiring an O<sub>2</sub> plasma cleaning step followed by an acid clean in sulphuric acid and hydrogen peroxide after the normal mask removal process. It was found that redeposition started to occur, even when the etch chamber was cleaned every 30 minutes, at etch depths in the silica of around 10 µm and more.

#### 2.6.1.4 Sample Preparation and Photolithography for Etching

Figure 2.4 shows the process for patterning and etching FHD silica using photolithography and dry etch [Ruano 2000 (b)]. Prior to NiCr deposition, an extensive cleaning step was required to ensure that the NiCr adhered to the FHD glass. The sample was cleaned in an ultrasonic bath of acetone for 5 minutes, followed by methanol for 5 minutes, and rinsed in RO water to remove any organic debris. Immersion for 10 minutes in a 7:1 ratio of sulphuric acid:hydrogen peroxide was then used to ensure that all surface contamination was removed.

Two types of photoresist were used in the work. The first, S1828 (Shipley, UK), gave a thickness of 2.8 µm when spun at 4000 rpm for 30 seconds, and was used for definition of features of greater than 2 µm wide, and requiring etch depths of less than 6 µm. After depths of greater than 6 µm had been etched, resist redeposition would occur. Therefore, a thicker resist, AZ4562 (Clariant, UK), was used for larger features and those requiring

deeper dry etches, such as microfluidic channels. When spun at 4000 rpm for 30 seconds, AZ4562 gave a thickness of 6.2  $\mu\text{m}$ .

For S1828 photoresist, the UV exposure time used was 18 seconds, followed by development in 1:1 MF312 developer (Shipley, UK) to RO water for 60 seconds. AZ4562 was exposed for 20 seconds and developed for approximately 2 minutes in 1:4 AZ400K developer (Clariant, UK) to RO water.

Etching of the NiCr pattern layer to leave the FHD silica exposed for dry etching was achieved using a standard chrome etch solution for 1 minute (ceric ammonium nitrate, acetic acid and RO water). After the dry etching, acetone was used to remove the photoresist pattern mask, and Cr etch to remove the NiCr mask.

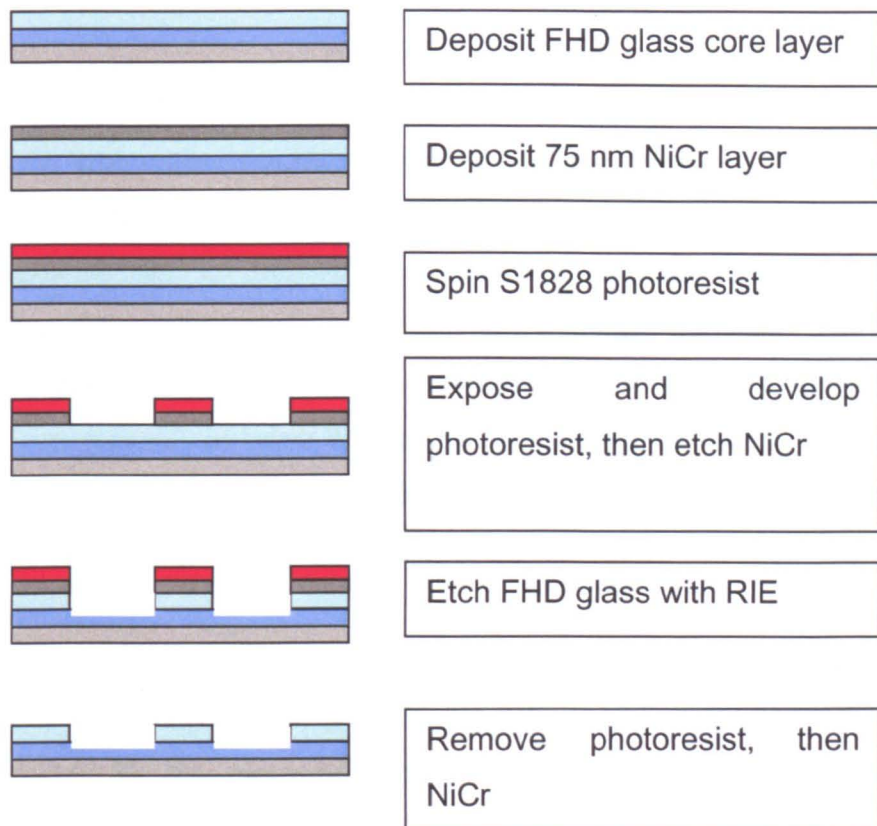


Figure 2.4: Process steps for the fabrication of waveguides and microchannels in FHD glass. To etch features deeper than 6  $\mu\text{m}$ , AZ4562 photoresist is used in place of S1828.

An alternative to the acid cleaning step to prepare the sample for NiCr deposition is a two-minute O<sub>2</sub> plasma clean, as used for photoresist removal. This has a similar effect on the FHD silica surface as the acid cleaning; activation of the bonds near to the surface, making the surface hydrophilic and allowing the NiCr to adhere more easily. If the acid cleaning or the plasma cleaning step is omitted, it was observed that the NiCr would peel off soon after deposition, sometimes even before photoresist could be spun on the surface. Visual inspection under an optical microscope also showed a less smooth surface of the NiCr if the cleaning step had been insufficient. Thus it is essential that the NiCr layer be applied as soon as possible after the cleaning step. It was found that the NiCr stuck sufficiently well if the layer was applied in the same working day as the cleaning was performed.

Resist reflow, that is melting the resist so that the profile becomes slightly less square, for 20 minutes at 120 °C was used after photoresist development to harden the photoresist for the dry etching steps.

The composition of the NiCr masking layer used could be either 60:40 or 90:10 (Ni:Cr) depending on the evaporation machine used, and was determined by the size of feature required. Smaller features such as waveguides normally require the thermally evaporated 90:10 NiCr deposited using an evaporator built in-house as a mask to provide a smoother sidewall [McLaughlin 1998]. Larger feature microfluidics normally use the 60:40 deposited by a Plassys MEB450 electron beam evaporator (Plassys, France). As the microfluidics were typically of larger dimensions than waveguides (at least several tens of μm rather than a few μm), photolithography of the channels was therefore much more straightforward than for dry etched waveguides due to the tolerances involved.

An example of an etched channel is shown in Figure 2.5, taken using a Hitachi S800 scanning electron microscope (SEM) from Hitachi, UK, at 10 keV. To prevent charging of the silica substrate by the electrons and therefore picture degradation, a layer of approximately 100 nm Au-Pd was sputtered onto the device. The layer can be removed by an acid clean as described above.

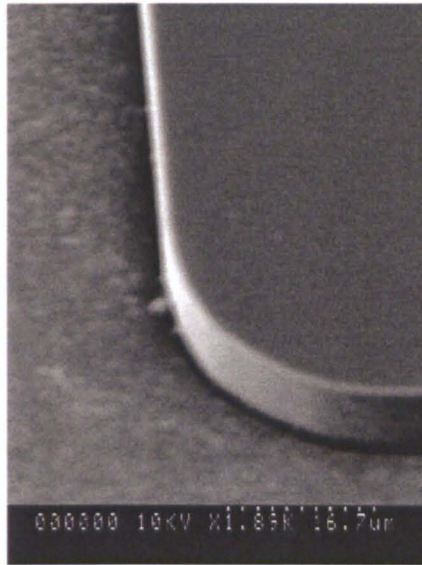


Figure 2.5: SEM micrograph showing an example of a channel wall etched with the photolithography and dry etch processes described above. The roughness observed at the base of the sample often occurred when the FHD glass was etched through to the thermal oxide underneath.

Similarly, the type of photoresist used was determined by the feature size of the silica structure required. S1828 was used for waveguides and shallow ( $<6 \mu\text{m}$ ) depth features, whereas AZ4562 was used for deeper microfluidic structures where the resist was required to last for a longer dry etch. The deep dry etching of microchannels was described in more detail by Ruano [Ruano 1999]. It was more difficult to resolve small waveguide features with the more viscous AZ4562 resist, as the resist layer was much thicker than that of S1828 ( $6.2 \mu\text{m}$  rather than  $2.8 \mu\text{m}$ ).

An inherent problem with waveguides defined by RIE is sidewall roughness. It occurs when the mask edges become eroded during the long etch process, a necessary step in deep dry etching of silica. This eroded pattern is then copied into the waveguide, as in Figure 2.6. The effect of waveguide sidewall roughness is an increased propagation loss [Marcuse 1969].

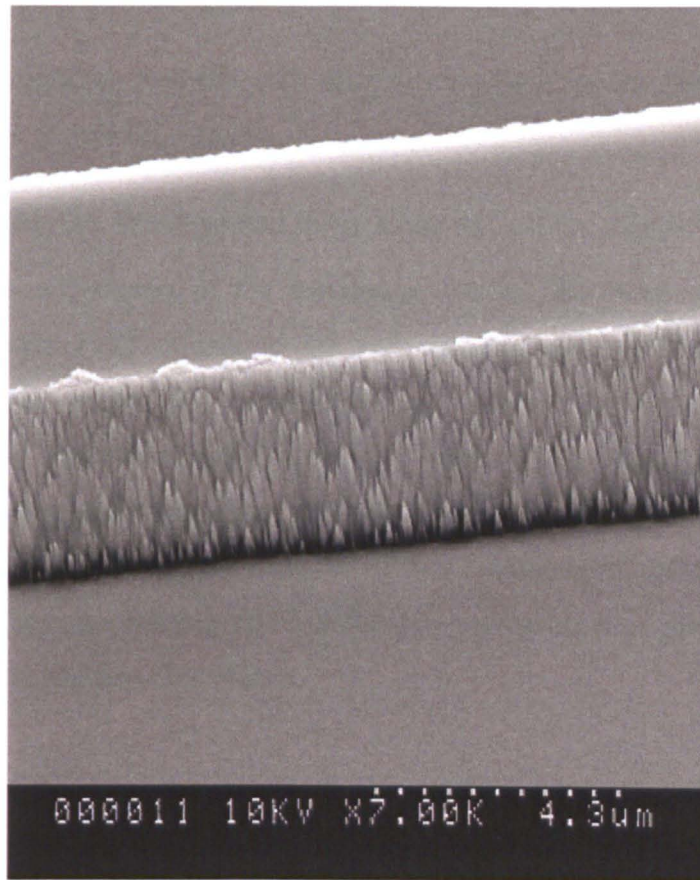


Figure 2.6: SEM image of a dry etched waveguide in FHD silica. The sidewall roughness that is clearly visible here is a significant source of loss in the waveguide.

To overcome this problem in FHD glass, two approaches are possible: reflow and hydrofluoric (HF) acid smoothing. Reflow involves leaving the waveguide structure in a furnace until the glass begins to melt, thus smoothing the surface of the guide. Immersion of the waveguide in a 4:1 HF to water solution etches the structure anisotropically at a rate of approximately 70 nm / minute. In both cases the mask is removed prior to smoothing. One result of both types of smoothing is that the waveguide profile is changed from a defined ridge to a more rounded structure. The waveguide would then be more asymmetric, as the base of the guide would still be flat, in contrast with the rounded profile of the three other ‘edges’. This makes the structure more difficult to simulate accurately, in return for a smaller loss due to sidewall roughness. However, the effect of adding a cladding layer of FHD glass to these waveguides may also have a similar smoothing effect as the whole waveguide structure is then subject to another furnace sintering cycle, although it cannot be examined thoroughly as the cladding layer is irremovable. The only way to examine the roughness after cladding deposition is by cleaving through the sample.

Both of these smoothing methods add considerable time to the fabrication stage, and therefore should be avoided if possible.

#### 2.6.1.5 Tailoring the Waveguide Dimensions to Suit the Application

Depending on the application of the waveguides to be fabricated, and the operational wavelength, different FHD dopant levels and waveguide dimensions must be chosen carefully. Typically, monomode waveguides are required for any type of Y-branch structure, to allow consistent splitting ratios [Isutzu 1982, McLaughlin 1998]. Other structures, such as straight waveguides, normally possess less stringent mode requirements. With dry etched FHD waveguides, there exist three methods of reducing the number of modes: reducing the core-cladding index difference, increasing the operational wavelength, or decreasing the waveguide dimensions.

Reducing the core-cladding index difference by a few tenths of a percent, for example from 0.5 % to 0.3 % in FHD silica, can reduce the number of allowed modes in a waveguide, with the trade-off being weaker coupling inside the guide as the difference decreases. The evanescent field, however, would be stronger as the light is less strongly confined to the guide. Increasing the operational wavelength is not normally an option in biological applications, as most useful wavelengths are in the visible range, and the higher telecommunications wavelength of 1550 nm will not normally excite any relevant biological fluorophores.

In practical terms, reducing the waveguide dimensions produces significant fabrication complications; a single-mode ridge waveguide with a refractive index difference of 0.75% between the core and upper / lower cladding at 1550 nm can be around  $6 \mu\text{m}^2$ . However, a similar waveguide at 632.8 nm, where a number of fluorophores can be excited, must possess a core-cladding index difference as low as 0.25% and be  $3 \mu\text{m}^2$  to be single-mode. Features of less than  $2 \mu\text{m}$  were difficult, although not impossible, to resolve using photolithography and dry etch, particularly when the waveguide dimensions are critical in providing accurate splitting ratios in branching structures.

## 2.6.2 Waveguides Written using Electron Beam Densification

A more contemporary mechanism to define waveguides in silica is to use electron beam densification. This was first demonstrated in fused silica by Houghton in 1976 [Houghton 1976], who used electron energies of 11 to 16 keV and current densities of several  $\mu\text{A}$  per  $\text{cm}^2$  and proposed that optical waveguides could be fabricated in this manner. Houghton's idea was revisited by Madden, Green and Barbier, using a gold surface mask to define the waveguide areas to be irradiated [Madden 1990, Barbier 1991]. Peak refractive index changes of approximately  $10^{-2}$  for electron doses of several  $\text{C}\cdot\text{cm}^{-2}$  were observed by Barbier.

Surface masks fabricated by electroplating were used by Syms to define waveguide areas for near-infrared wavelengths. The writing of S-bends, symmetric Y-branches and directional couplers was also reported, the first comprehensive report on devices successfully fabricated using electron beam densification [Syms 1994, Syms 1995, Syahriar 1998]. However, their mask-making process was dependent on photolithography, thus limiting the resolution of the waveguides to the resolution of the photolithographic process. The principal advantage in Syms' method of waveguide fabrication was that electron beam irradiation rather than dry etch was used after the masking process, so the need for a cladding layer to protect the guide was eliminated.

The use of a high-resolution, focussed electron beam to write waveguide structures in Ge-doped FHD silica has been extensively studied by García-Blanco [García-Blanco 2003 (b), García-Blanco 2001 (c)]. In all work, a Leica model EBPG 5HR100 electron beamwriter with a minimum resolution of  $0.3125 \mu\text{m}$  was used (Leica Microsystems, UK). The refractive index profile of the area densified by the electron beam was characterised using the m-lines technique, based on the measurement of modes observed from grating couplers [García-Blanco 2003 (a)].

Irradiation of silica by electron beam produces a refractive index increase, which occurs mainly by compaction of the silica [García-Blanco 2001 (a,b), García-Blanco 2002 (a,b)]. Additional effects include a change in polarisability from the Si-O bond rearrangement [Barbier 1991]. The addition of the Ge dopant enhances this effect to the point where waveguides can be written [García-Blanco 2001 (a)]. In comparison to dry etched ridge

waveguides, the irradiated waveguide is embedded in the FHD silica slab layer, as illustrated in Figure 2.7.

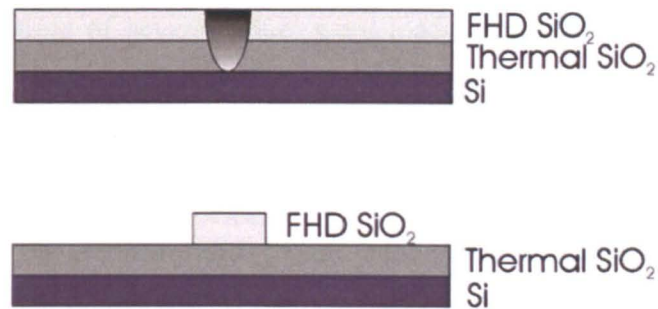


Figure 2.7: Comparison of a dry etched and an electron beam written waveguide. The electron beam waveguide requires no etching or cladding, and is protected on either side by the FHD slab.

Waveguides formed by the electron beam densification of FHD silica form the basis of the devices presented in Chapters 3, 4 and 5, in which the suitability of such waveguides to biological sensing is explored.

#### 2.6.2.1 Fabrication Process for Electron Beam Written Waveguides

Compared to dry etched waveguides, the process for writing waveguides on FHD silica with an electron beam is relatively simple. The first step in both processes would be to design the waveguide structure using an optical design package, such as the Beam Propagation Method (BPM) from Optiwave Corp., Canada, as described later in Section 2.8.1. For the dry etch process, a photolithographic mask would have to be written using the electron beamwriter, a process that normally takes several hours, depending on the pattern. For the electron beam process, no mask was needed, as the computer generated files were used directly to write the pattern onto the FHD silica substrate.

The optical design for the electron beam written waveguides was transferred directly to the beamwriter using a software package called CATS. The pattern was split up into small sections, as the beamwriter writes a small area, then moves along and writes the next area stepwise until the full pattern is written. At this point, the position of the pattern on the sample was specified, and then all data was stored until the sample was ready for the pattern to be written.

To prepare the sample for writing, the FHD silica wafer was diced to the size of the final devices. This way it was easier to position the pattern on the sample, and more separate devices could be written in the same run of the beamwriter. Normally enough samples to give a total writing time of several hours were loaded into the beamwriter and then the patterns were written overnight.

A thin (around 30 nm) metal layer must be deposited on the top of the silica sample to prevent charging by the electron beam [Syms 1995, García-Blanco 2003 (b)]. If charging occurs, a number of extra sharp lines can normally be seen at the edges of the intended pattern, and there are normally too many defects to allow the device to function properly. A similar effect is seen when examining silica devices in an SEM, and a thin layer of sputtered palladium-gold was used to prevent it. In our case, 30 nm NiCr was evaporated using the Plassys MEB450 electron beam evaporator. The deposition time was variable, but was typically less than five minutes. The NiCr can be easily removed by immersion in a standard Cr etch solution for 1 minute. The electrons pass easily through the metal layer, and therefore do not affect the resolution or amount of densification of the silica sample.

The silica sample should be thoroughly cleaned prior to NiCr deposition. Firstly, the NiCr will only adhere well to a clean surface, and secondly, any particles that are on the sample surface may affect the quality of the pattern written by the electron beam. An ultrasonic clean with organic solvents (acetone and methanol) followed by an acid clean (7 parts sulphuric acid  $\text{H}_2\text{SO}_4$ : 1 part hydrogen peroxide  $\text{H}_2\text{O}_2$ ) as described in Section 2.6.1.4 should be used. Alternatively, a 1 minute oxygen plasma clean in an ashing machine (ET Plasmafab 505) can be used in place of the acid clean.

The sample was then placed in the beamwriter and the pattern written. For most work contained in this thesis, an electron dose of  $1 \text{ C.cm}^{-2}$  at 50 keV was used, with a resolution of  $0.3125 \mu\text{m}$ . The dose was set on the beamwriter prior to writing, and the resolution defined when transferring the pattern with the CATS software. This dose of  $1 \text{ C.cm}^{-2}$  has been measured to give an average refractive index change of  $6 \times 10^{-3}$  using the grating coupler method to obtain the effective index of the propagating modes in the densified area [García Blanco 2003 (b)]. The lower the resolution of the pattern, the faster the writing time. As the patterns written were normally waveguides of approximately  $2 \mu\text{m}$  width, this

resolution was considered sufficient. Writing times at this resolution were typically less than 1 hour to write a chip containing up to 10 waveguides, including Y-branch devices.

To summarise the differences between the dry etch and electron beam methods of producing waveguides, Figure 2.8 shows the process flow for fabrication of both types of waveguide.

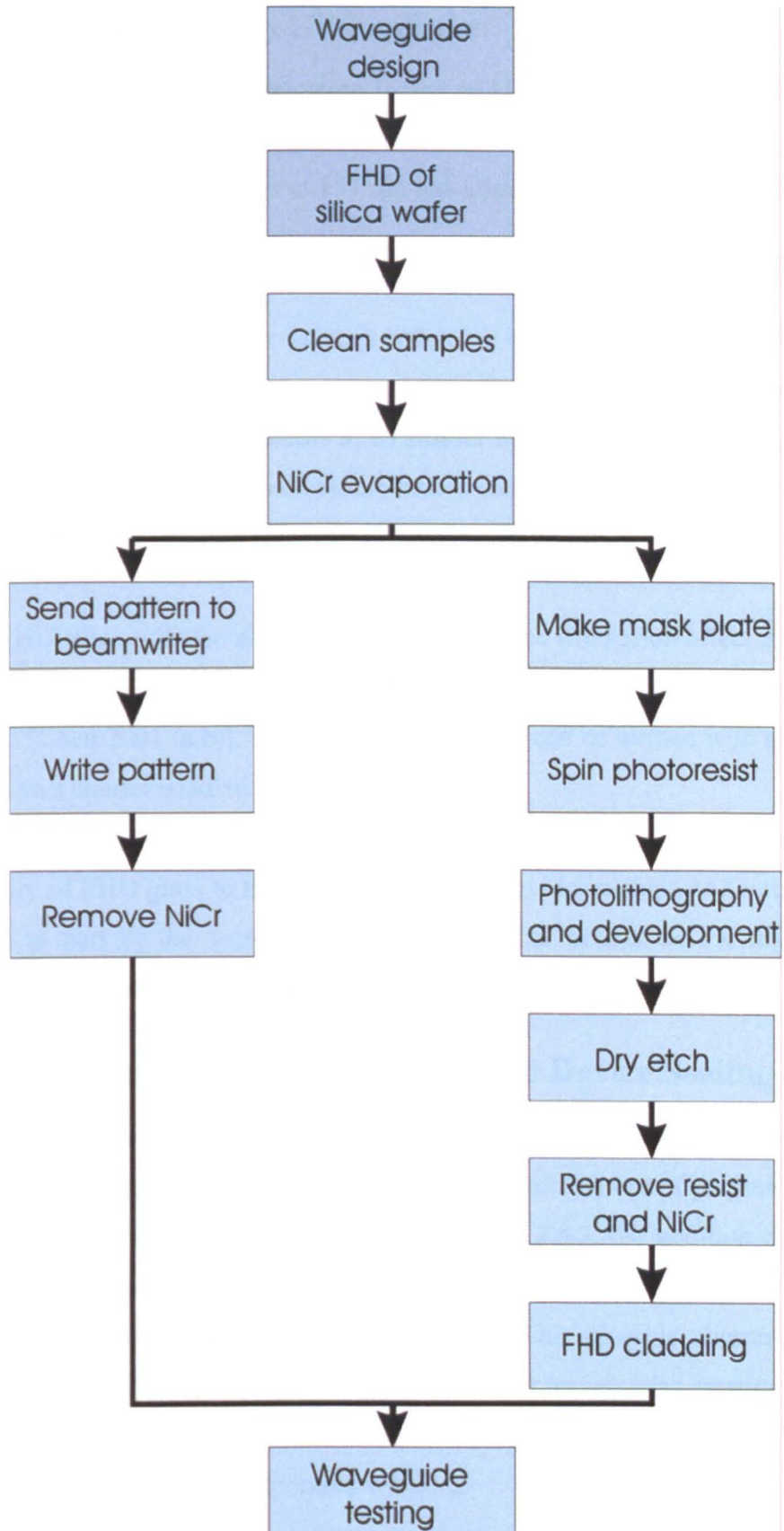


Figure 2.8: Process flow to create waveguides with both dry etched and electron beam written waveguides, showing that there are fewer steps involved in producing electron beam written waveguides, and cladding is not needed.

### 2.6.3 Waveguides Defined by UV Irradiation

A third method for waveguide fabrication is that of UV irradiation [Hill 1978, Svalgaard 1994]. Several UV wavelengths have been used, including 195 nm, 215 nm and 248 nm, and the advent of deeper UV lasers at 157 nm has allowed this wavelength also to be used [Herman 2000].

The exact mechanism for UV laser-induced refractive index change is as yet unknown, but material compaction of a few hundred nm in the irradiated area can be observed. Structural changes are believed by several authors to be similar to those observed with electron beam irradiation, namely the formation of colour centres and bond rearrangement, but have not yet been experimentally verified [Ebendorff-Heidepriem 2004].

Doping of FHD silica with Ge allows enhancement of the irradiation effect at 157 nm due to the close match of the laser bandgap with that of Ge-doped silica (7.9 and  $\sim$ 7.1 eV respectively) [Chen 2001 (a,b)]. Therefore, a waveguide can be written with a smaller total fluence, and so a shorter irradiation time.

The suitability of FHD glass to the fabrication of waveguides using a 157 nm F<sub>2</sub> laser was investigated as part of the work for this thesis. Further details on the fabrication and characterisation of these waveguides are contained in Chapter 6.

## 2.7 Polymers for Waveguide Cladding and Device Sealing

One of the overall aims of the project was to reduce the cost and fabrication time of producing integrated optical fluorescence sensors, in which the use of polymers could play a significant role. As mentioned previously in Section 2.6.2, the addition of FHD silica cladding to dry etched waveguides becomes an expensive bottleneck when fabricating optical sensors with integrated microfluidic channels. One possible alternative is to use another material instead of FHD silica as cladding for the waveguides, bearing in mind that the material should have the potential to be either moulded or formed in such a way that microfluidic channels can be incorporated within it.

## 2.7.1 Selection of an Appropriate Cladding Material

### 2.7.1.1 Possible Choices

Polymer materials would appear to possess the characteristics described above to fulfil the purpose of waveguide cladding and microfluidics. A number of polymers are routinely used in cleanroom fabrication, including polymethylmethacrylate (PMMA), SU-8 and poly(dimethylsiloxane) (PDMS). PMMA, or Perspex™, which can be obtained from Microchem Corp., USA, is normally used for high-resolution masking purposes, and can be patterned using electron beam lithography, or by irradiation with a UV source. It has also been successfully used as a waveguide material [Zhao 2000]. SU-8, a spinnable polymer from Microchem Corp., USA, that can be crosslinked by exposure to UV light, has found a number of applications from a masking material to a microfluidic device material and even as optical waveguides [Mogensen 2002, Chuang 2003]. While SU-8 and PMMA could be used as the waveguide material here, they would not be of the same high optical quality of FHD silica waveguides. Therefore it was decided that the FHD glass would be kept as the optical waveguide section.

PDMS (RS supplies, UK) is a silicone-based elastomer-type material that has recently found extensive use in microfluidic circuitry due to its mouldability, low-cost and non-toxicity [Duffy 1998, Wheeler 2004]. It is optically transparent at visible wavelengths, and is also non-autofluorescent at visible wavelengths. A common use for PDMS is to create microfluidic channels by fabricating a master mould of silicon or SU-8, then pouring on uncured PDMS [Duffy 1998]. The silicone monomer is mixed with an activator, usually in a 10:1 ratio, and cured at either room temperature overnight or in an oven. The PDMS is allowed to set on the mould and then peeled off and sealed to a flat surface to give a complete microfluidic circuit. This process is known as soft lithography.

The initial consideration when choosing a polymer as a possible cladding material for silica waveguides is its refractive index. The polymer index should be lower than that of the silica waveguides to enable guiding in the FHD silica, but close enough so that the possibility of producing single-mode waveguides exists. The single-mode waveguides are a necessary part of Y-branch structures, described more in Chapter 3. An extensive search of literature, plus measurements on a Abbé refractometer (Bellingham and Stanley, UK) confirmed that the refractive index of most easily-processable and available polymers at

632.8 nm (the wavelength primarily used throughout this work), including PMMA and SU-8, is higher than that of silica waveguides and is therefore unsuitable as a cladding material. PDMS, however, has a refractive index of around 1.43 at 632.8 nm, which is lower than the index of FHD silica waveguides. Further details of the suitability of PDMS as waveguide cladding are given in Chapter 3. For the reasons given above, PDMS was chosen as a waveguide cladding and device sealing material for the sensor devices presented in this work.

The swelling of PDMS in solvents is less important than the index change, as microfluidic circuitry dimensions are typically of the order of tens of microns, and a small change in volume should not affect the detected signal significantly. In smaller microfluidic circuits this may become a problem, and the possibilities of surface modification of PDMS channels is a current subject of investigation in several institutions.

All PDMS used in this work was a ratio of 10:1 precursor:activator by volume. The mixture was left for 30 minutes to allow air bubbles introduced in the mixing process to disperse, and, if the PDMS was to be used as a cladding, it was degassed under vacuum to remove other bubbles which were too small to be seen by the naked eye. This was an important step, as these bubbles, if left in the film, could cause a lowering of the bulk refractive index. The mixture was then spun, typically ramping up to 500 rpm over 10 seconds, then spinning for a further 20 seconds at 500 rpm. Curing was performed at 90 °C for 30 minutes. When spinning over waveguides, the 10:1 mixture was sufficiently viscous not to drip over and cover the waveguide ends.

#### 2.7.1.2 Other Examples of Polymer Cladding

Bosc first described the use of a methacrylate copolymer doped with fluorine as a top cladding for silica waveguides [Bosc 1999], where refractive index tuning was accomplished by varying the amount of fluorine in the copolymer. Some silica cladding was still deposited at the edges of the device, therefore the purpose of the polymer was only to eliminate the problem of filling small spaces between waveguides such as at the apex of a Y-branch with the cladding material. When using FHD or PECVD silica claddings, bubbles often appear between small waveguide features, thus degrading the optical performance. As the cladding step was retained, the device fabrication time and expense were not improved.

## 2.7.2 Definition of Channels in PDMS Films

Section 2.7.1 describes the reasons for choosing PDMS as waveguide cladding and as a microfluidic sealing layer. Here, the twofold use of PDMS as waveguide cladding as well as microfluidic channels in the one fabrication step is described. By using PDMS as the microfluidic channel material, the need for dry etching of the FHD silica is eliminated. However, the problem of integrating the waveguides with the channels becomes more complex, as without etching it more difficult to access the waveguides directly. The problem is addressed in Chapter 3, Section 3.5, where evanescent excitation of the fluorophore was used, thus eliminating the need for microfluidic channels to be etched through the waveguides.

A convenient method of integrating microfluidic channels into PDMS films was developed by Yasukawa [Yasukawa 2001] and has been successfully employed in the integration of silica waveguides and PDMS cladding.

Following the method of Yasukawa, photolithography of a thick layer of positive AZ4562 photoresist was used to define the desired microfluidic pattern in relief; that is, after developing, the photoresist left formed tracks where the microfluidic channels would be. A PDMS layer was spun and cured on the top, then the remaining photoresist was flushed away using acetone, leaving the buried channels intact and the PDMS sealed to the substrate. The whole process can be achieved in a few hours, and is illustrated in Figure 2.9. A slower spin speed (1000 rpm) for the photoresist was used to enable thicker layers to be formed, thus making deeper channels.

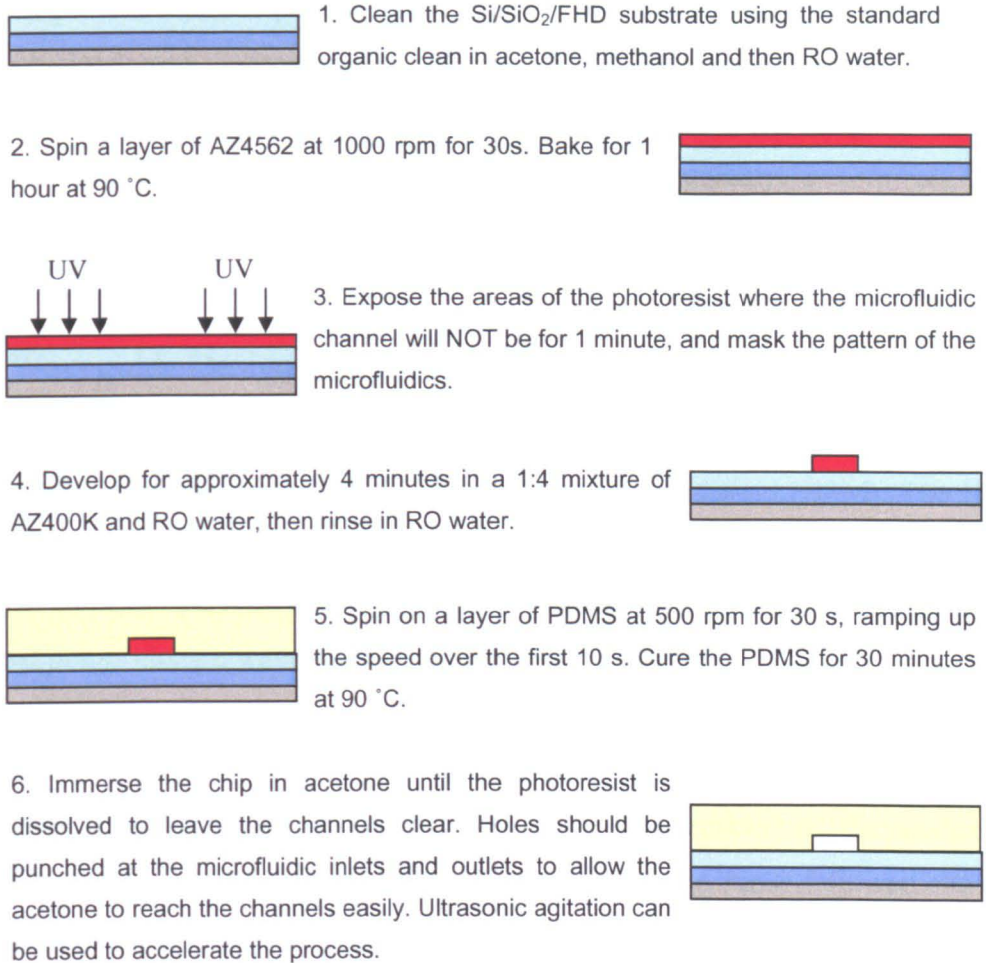


Figure 2.9: Summary of the process steps needed to fabricate an embedded microfluidic channel in PDMS, when attached to an FHD silica chip. The entire process takes less than 3 hours.

When the PDMS is spun onto the chip, there is sufficient surface tension to prevent it from spilling over the sides, and thus obscuring the waveguide facets. Similarly, the same happens with most photoresists, especially the more viscous ones, and is commonly referred to as the ‘edge bead’. There is a slight build up of PDMS at the chip edges, as described in Chapter 2, but the overall film is reasonably flat. As the top surface of the PDMS was the top of the final chip, it would not be in contact with any other layer, and so the flatness was not so important as the flatness of the surface in contact with the waveguides.

As it is a photolithographic process, alignment of the channels to the waveguides is straightforward using standard mask alignment techniques, and by using a slow spin speed (1000 rpm) the thickness of the photoresist covers any dry etched ridge waveguides

enough to provide a planar photoresist surface for the photolithography. The final channel height obtained was approximately 10  $\mu\text{m}$ , found by measuring the height of the photoresist after developing with 1 part AZ400K to 4 parts RO water. The channel widths had to be at least 80  $\mu\text{m}$  to allow the photoresist to dissolve quickly.

## 2.8 Device Design

### 2.8.1 Waveguide Design using the Beam Propagation Method

Prior to device fabrication, waveguide layouts and dimensions were designed using a commercially available version of the Beam Propagation Method (BPM). The BPM is a numerical method based on a paraxial approximation of the scalar wave equation, and can be used to calculate the optical field and modal propagation constants in a stepwise fashion at defined points along a waveguide structure [Marcuse 1991].

Feit and Fleck first proposed their propagating beam method in 1978, applied to graded-index fibres [Feit 1978]. More recently, they have also reported on the analysis of rib waveguides in this manner [Feit 1990]. Numerous papers have followed the original publication, offering corrections and modifications to the original method, and showing examples of its applicability [Van Roey 1982, Baets 1982, Hadley 1992]. It has been shown by the authors listed to be a suitable method for analysing the performance of weakly guiding materials such as silica, and has been successfully applied to bending, branching and coupling structures. Further details of the method can be found in the references given above.

To minimise processing time, 3D structures were reduced to 2D using the Effective Index Method (EIM) [Marcuse 1991], and the resulting effective indices used in a 2D BPM simulation. It has been shown, and is widely accepted, that close agreement between modal propagation constants found by the EIM and exact solutions can be obtained [Marcuse 1991].

The EIM for a three-layer (undercladding-core-cladding) ridge waveguide device can be summarised in Figure 2.10.

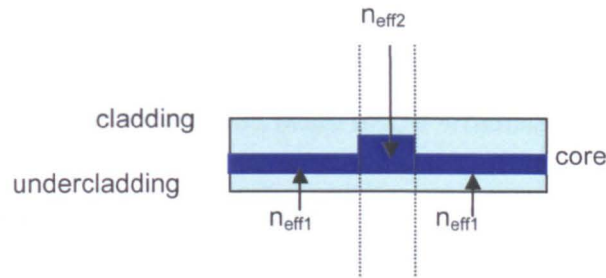


Figure 2.10: The EIM for a ridge waveguide structure. The device was sliced into three sections; the two outer sections and the inner guide region. Here the regions on either side of the guide were assumed to be equal. The effective indices were found for each slice, and then the overall effective index was found by taking the three effective indices and again finding the effective indices for these.

For a waveguide embedded in a guiding slab such as an electron beam written waveguide or a UV written waveguide, only the vertical effective indices for the two regions were used for the 2D BPM.

For all BPM simulations of FHD silica devices, the base or undercladding refractive index was 1.4582, with a thickness of  $7\ \mu\text{m}$ . The index of the waveguide region varied with each individual device, but was normally  $6 \times 10^{-3}$  greater than the index of the FHD silica for waveguides written by electron beam. The standard FHD recipe of 100 sccm  $\text{GeCl}_4$  gave a refractive index increase in the FHD silica layer of approximately 0.75 % from the undercladding index (1.4582).

### 2.8.2 Microfluidic Circuit Dimensions

Fabrication technology allows microfluidic circuits of a few  $\mu\text{m}^2$  or even sub- $\mu\text{m}$  to be easily formed [Felton 2003]. However, the typical dimensions of microfluidic channels are tens or hundreds of  $\mu\text{m}$ , as sample delivery into the channels can prove problematic. Another potential problem is the trapping of dust or air bubbles inside the channels, which can impair the fluid flow. For these reasons, microfluidic circuits used in this project were normally at least  $50\ \mu\text{m}$  wide, while the depths were between 4 and  $8\ \mu\text{m}$ , limited by the depth of the FHD silica on the device.

## 2.9 Device Characterisation

Prior to testing, devices were examined under a microscope to ensure that the pattern had been written correctly. The microscope used was a Leica INM 20 with a SPOT Insight QE

CCD camera. All optical micrographs of devices were taken using this camera. Interference contrast filters were used for observation of the densified waveguide patterns that had been written with an electron beam or UV irradiation.

### 2.9.1 Coupling of Light into Waveguides

Microscope objective lenses were used for both input and output coupling to devices throughout this work, unless otherwise stated. Lenses were chosen above fibres due to the availability of a number of different lenses, allowing coupling to a variety of waveguide sizes.

Most waveguides used in this work were approximately 2-3  $\mu\text{m}$  square. For these, a x40 lens with numerical aperture (NA) of 0.65 was used for input, and a x20 lens with NA of 0.45 for output, unless otherwise stated. All lenses were from Ealing, UK.

A 2.5 mW HeNe laser at 632.8 nm was used for most waveguide characterisation and fluorescence experiments. Light was directed to the input lens via two mirrors, as shown in Figure 2.11.

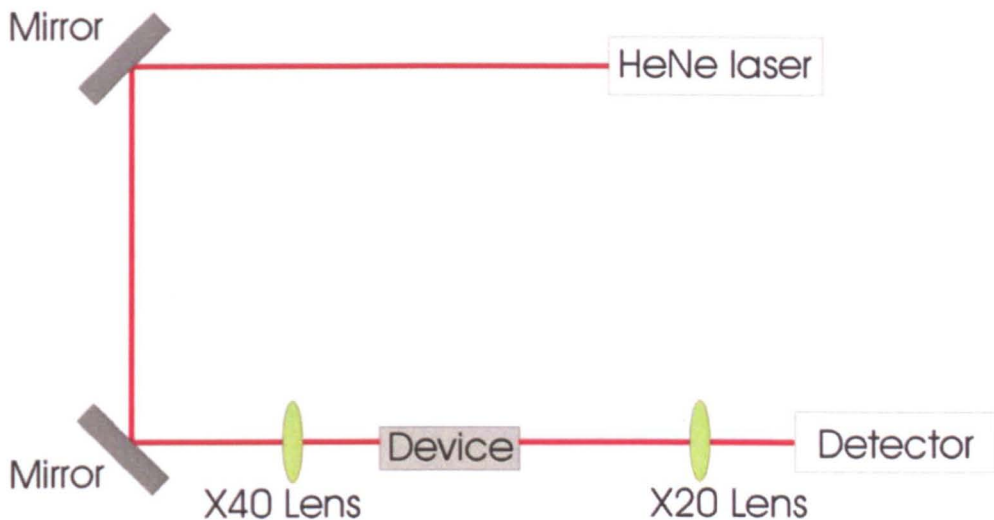


Figure 2.11: Typical optical test setup. The excitation was provided by a 632.8 nm, 2.5 mW HeNe laser. Use of visible light makes waveguide alignment simpler than if UV light were to be used. The lenses help to focus the light into the waveguides and to collect the output from the device. The detector was a Labmaster optical power meter.

## 2.9.2 Loss Measurement

To measure the propagation loss of a single mode waveguide, the modified Fabry-Perot technique was used. For this to work using a standard setup, a single-mode waveguide at  $1.55\ \mu\text{m}$  with good quality polished facets was required to allow reflections inside the waveguide cavity. As most waveguides used in the work described here were designed for  $632.8\ \text{nm}$ , this method was only used to examine a small number of test waveguides.

Another loss measurement method is the cut-back technique, which involves taking readings of the waveguide output, then cutting the sample across the waveguide in half before repeating the output power measurement. This is repeated several times, then the propagation loss of the guide can be found. As this technique destroys the sample it was decided that it would not be suitable to use routinely.

To monitor waveguide performance, once a test waveguide of a certain type had been measured and the losses determined, it was assumed that differences in output between different waveguides were mostly caused by facet roughness. Every chip that was fabricated contained a set of straight waveguides in an unobtrusive area, and the output power of these was checked before measurement of the actual device waveguides.

## 2.9.3 Fluorescence Detection

### 2.9.3.1 The CCD Detector

To fully exploit the potential sensitivity of a fluorescent sensor, the method of detecting the fluorescent signal must be capable of sensitivity sufficient to allow small fluorophore concentrations to be detected. While CCD cameras are often used for fluorescence imaging, they are more suited to taking a photo of the image, which can then be analysed for intensity variations.

### 2.9.3.2 The Photomultiplier Tube (PMT) Detector

A more sensitive method of detection is via a PMT, which in principle should be capable of single photon detection. A PMT consists of a vacuum tube containing a photocathode and an electron multiplier section made up of a series of dynodes. Light passing into the detector tube is incident on the photocathode, generating photoelectrons that are focussed

by an electrode and then multiplied by secondary emission through the dynodes to generate a measurable electrical signal [Hamamatsu 2004].

Single photon sensitivity is however difficult to achieve, but the sensitivity to the wavelength of interest can be enhanced by using a lock-in amplifier (EG&G, UK) and an optical chopper to chop the laser excitation light. A PMT detector was used for most fluorescence measurements described in this thesis. The lock-in amplifier ensures that the PMT only detects signals that are of the same frequency as the chopper, that is only light that has passed through the device under test should be measured. Figure 2.12 shows a plan view of the setup. The lock-in amplifier is not shown, but is connected to the chopper and PMT. The PMT used was model H5700-50 from Hamamatsu, Japan.

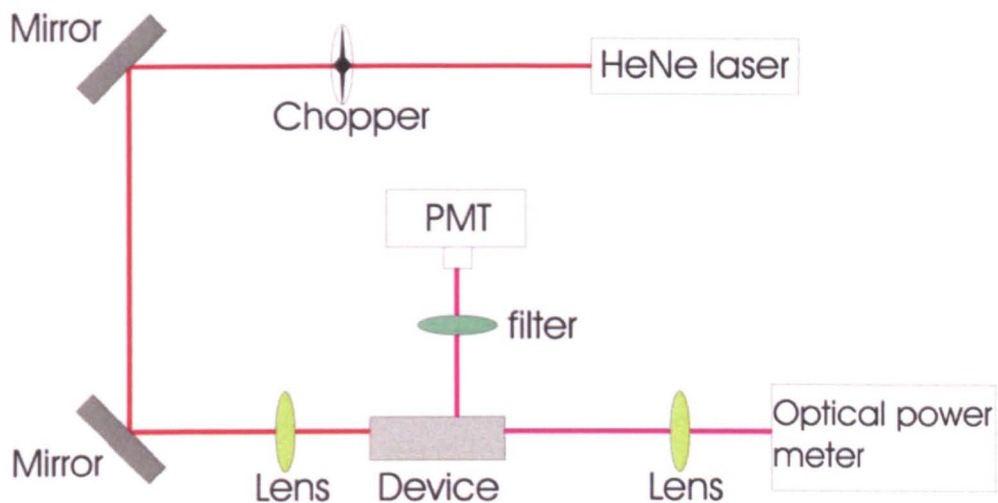


Figure 2.12: Optical setup for waveguide characterisation and fluorescence detection. The chopper and PMT are connected through a lock-in amplifier for fluorescence measurements so that only light pulses at the frequency of the chopper are detected by the PMT.

### 2.9.3.3 Choice of Fluorophore

For all measurements of integrated devices in this work, the fluorophore Nile Blue dissolved in methanol, was chosen. With excitation and emission maxima at 636 and 686 nm respectively, Nile Blue was compatible with the available HeNe laser at 632.8 nm, and standard commercially-available filters could be used to block the excitation light at the detector. The low cost and relative safety in comparison with other dyes, as well as stability and six-month shelf life in solution of this dye provided additional reasons for

selecting this particular dye above others with similar fluorescent properties such as Cy5 or Alexa Fluor 633 [Sigma-Aldrich, 2001].

Methanol was chosen as the solvent due to the solubility of Nile Blue in methanol. However, water or another organic solvent could equally be used. Water permeates PDMS the least of all possible solvents for Nile Blue [Lee 2003], but it was decided that to ensure complete solvation of the dye, methanol would be more suitable.

## **2.10 Summary**

A short review of optical sensing and how it relates to silica-on-silicon technology has been presented. Fabrication processes that have been used throughout the thesis work have been described. Optical characterisation of waveguides, and the detection of fluorescence from the sensors fabricated has been outlined.

## **3 Y-branch Waveguides and Polymers for Biological Sensors**

Y-branch waveguides have long been established as a convenient beamsplitting or coupling mechanism in the telecommunications industry [Burns 1976, Sasaki 1978, Cullen 1984], and have more recently been utilised in a number of biological sensing applications [Heideman 1999, Ruano 2000, Mogensen 2002]. This chapter describes the application of waveguides directly-written by electron beam to Y-branches, and the incorporation of microfluidic channels to form an optical biological sensor.

### **3.1 Y-branch Waveguides as Optical Beamsplitters**

Waveguide fabrication requires precise control of the width and depth of the core, particularly in single-mode waveguides, which are a requirement for a predictable splitting ratio in Y-branch structures. Microfluidic circuits however, possess a more generous tolerance, as their main function in optical sensors is normally to deliver a liquid sample to the waveguide region for probing. Therefore, it would be rather wasteful of resources to use the relatively expensive but precise FHD silica as the microfluidic part of a sensor chip, where other types of microfluidic circuits in industry use lower quality glass or plastics.

Included in this chapter are details of the practical implementation of the polymer PDMS as waveguide cladding, microfluidic circuitry and device sealing. PDMS was found to be suitable as cladding for both straight and branched electron beam written waveguides.

#### **3.1.1 Symmetric Y-branch Waveguides**

Switching and multiplexing of optical signals were among the original uses for Y-branch waveguides, and their behaviour at the junction has been subject to analysis by a number of authors [Yajima 1978, Burns 1980, Isutzu 1982, Baets 1982, Cullen 1984]. Improvements to the original simple splitting structure shown in Figure 3.1 have been investigated by a number of authors [Wang 2002].

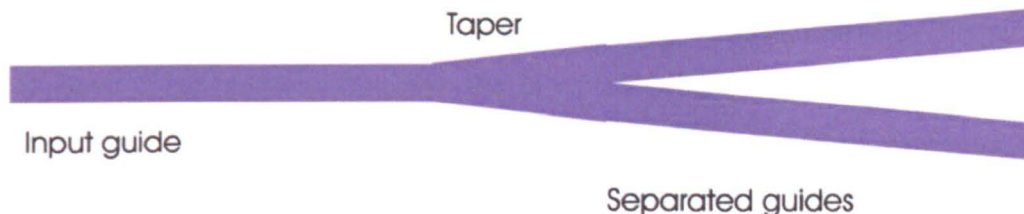


Figure 3.1: A simple Y-branch structure. Three distinct sections are present: the input waveguide, a taper section leading to the splitting guides, and the two separate guides. An even simpler guide may have no taper, and S-bends can be used for the separated guides. Most recent improvements to the design have been made in the taper section between the input and output guides.

Detailed analysis of the behaviour of the waveguide modes at the junction can be found in the above references and will not be reproduced here. However, a simplified view of the problems that may occur when a branching waveguide has more than one propagating mode is presented below in Figure 3.2, to emphasise the necessity for single-mode waveguide structures.

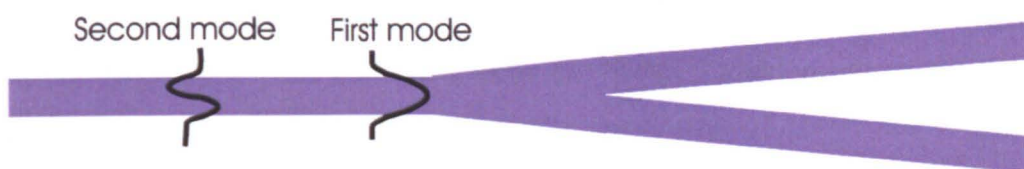


Figure 3.2: Plan view of the effect of 2 different modes propagating down a branching waveguide. Clearly, when the uneven mode reaches the branch, splitting will not be equal. As it is not simple to select which mode is to be launched down the waveguide, fabrication of guides that only support one fundamental mode is desirable.

When launching light into a multimode waveguide, any of the possible modes may be excited depending on the exact orientation of the device with respect to the incident light, and the quality of the waveguide facet. Each mode, in particular asymmetric modes, will provide a different splitting ratio than expected at the junction of a Y-branch, especially in the real case where some imbalance due to practical limitations of the fabrication methods may exist between the two branches. In the case of a symmetric splitter, the effect will be non-symmetric splitting and a measurably unbalanced output. In the case of an asymmetric splitter, the splitting ratio will depend on which mode has been excited in the waveguide, and will therefore be unpredictable.

Isutzu provided a detailed analysis of a completely single-mode Y-branch [Isutzu 1982], whereas most other authors describe the situation where part or all of the joining waveguide is multimode. The completely single-mode Y-branch is of particular interest here, as all branching waveguides used in the work described in this thesis were intended to be entirely single-mode. The main point to note in Isutzus analysis, which uses the concept of local normal modes, is that any higher order modes that may exist in the branching section will be converted to radiation modes upon reaching the single mode guide again.

### 3.1.2 Asymmetric Y-branch Waveguides

Asymmetric dry etched Y-branch structures in silica for optical interferometers were reported by Takato [Takato 1988], and have recently been employed in sensors [Ruano 1999, 2000 (a,b)]. At the shorter wavelengths required for biological sensing applications, the waveguide dimensions required for single-mode guiding decrease to the point where they reach the limits of photolithographic possibilities. Therefore, the use of electron beam irradiation, which can write with nanometre precision, should result in more reliable waveguide structures.

## 3.2 Y-branch Waveguides in Optical Sensor Devices

### 3.2.1 Design of Asymmetric Y-branch Waveguides

The Optiwave 2D BPM program was used to predict the asymmetric Y-branch splitting ratios. Cosine S-bends with a horizontal length of 9000  $\mu\text{m}$  were used, as cosine S-bends have previously been found to produce the lowest bend losses [Ruano 2000 (b)]. The length of 9000  $\mu\text{m}$  was chosen to allow for a gradual change in waveguide separation over the waveguide chip, which was normally 15 mm (15000  $\mu\text{m}$ ) long. Initial simulations showed that this length was appropriate for the range of cosine amplitudes to be used, that is, over the range of final distances 'd' between the two output branches, losses were reasonably small.

Before fabrication, a series of simulations were carried out to examine the effect of varying the final distance 'd' between the straight arm of the guide and the branch, as shown below in Figure 3.3. The purpose of the investigation was to determine a design guide for asymmetric Y-branches, allowing an estimation of the expected power splitting ratio prior

to fabrication. Asymmetric branches such as those shown here have potential in both Mach-Zehnder type sensors and devices that require a reference branch, for example to monitor input power.

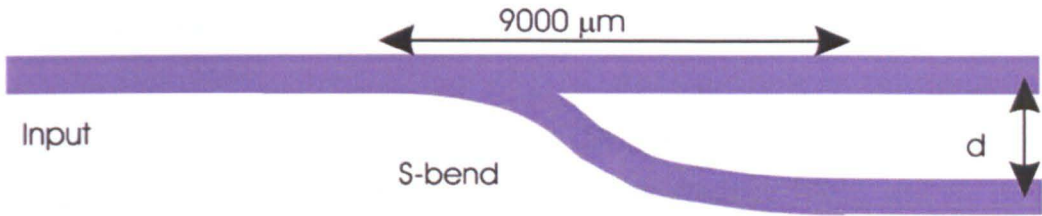


Figure 3.3: Schematic (not to scale) of the asymmetric Y-branches used in simulations and in the devices described later in this chapter. ‘d’, the final distance between the output waveguides, was varied by altering the cosine S-bend amplitude.

The simulations were performed using real thickness and refractive index data from FHD wafers that had been prepared for the purpose of fabricating a range of asymmetric Y-branch waveguides. Table 3.1 shows the values used for the 2D BPM simulation.

Device Length	15000 $\mu\text{m}$
FHD refractive index	1.4679
Densified FHD refractive index ‘ $n_D$ ’	1.4739 (FHD silica index + 0.006)
FHD film thickness, ‘t’	2 $\mu\text{m}$
Waveguide width	2 $\mu\text{m}$
S-bend length	9000 $\mu\text{m}$

Table 3.1: Values used in the initial BPM simulation of asymmetric Y-branches written by electron beam densification of FHD silica to investigate the effect of changing the final separation ‘d’ of the output waveguides.  $n_D$  is the FHD silica refractive index plus the increase caused by the electron beam densification, and the FHD film thickness, ‘t’, is equal to the height of the densified waveguide.

An initial BPM simulation was carried out for the case of a 2  $\mu\text{m}$  square electron beam densified Y-branch structure with air as the cladding ( $n=1$ ) on the top surface of the guide. The thermal oxide undercladding had a refractive index of 1.4582, giving a core-undercladding refractive index difference of approximately 0.7 %.

The split between the output waveguides 'd' was varied between 30 and 100  $\mu\text{m}$ , and the resulting field plotted, as shown in Figure 3.4. The field was found for the final splitting distances 'd' at intervals of 5  $\mu\text{m}$ , and then the graph points were smoothed to produce the final graph given here.

The simple Transparent Boundary Condition (TBC) option for treatment of the optical field at the boundaries of the simulation area was used [Hadley 1992], and the excitation wavelength was 632.8 nm. In BPM simulations, it is important to set the correct boundary conditions to avoid unwanted reflections at the boundary of the simulation window, on either side of the waveguides in the plane of the FHD glass. The TBC allows most of these reflections to be absorbed, or to 'pass through' the boundaries set in the simulation, to allow for the case in real life where the device size is normally larger than the boundary sizes imposed in the BPM.

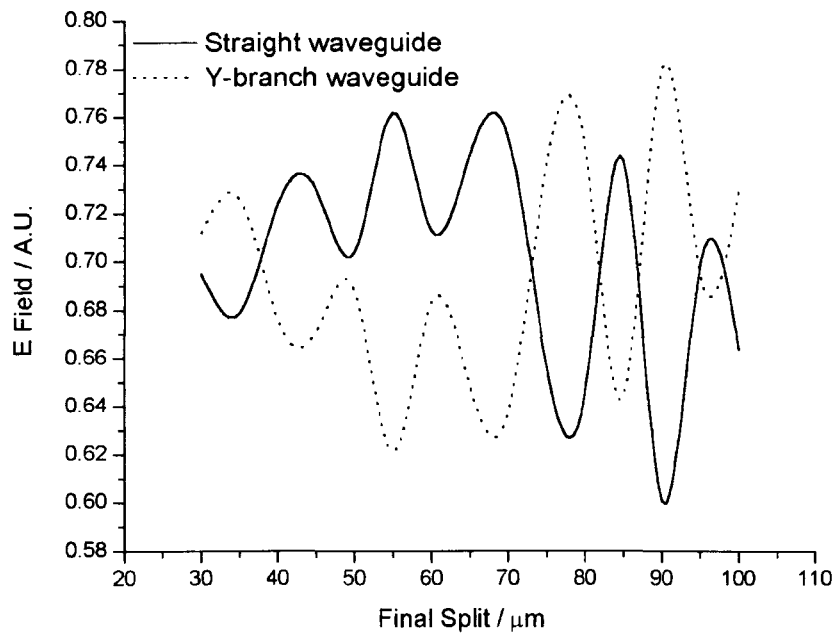


Figure 3.4: Variation of the waveguide outputs for different splitting distances, d, for an asymmetric single-mode Y-branch waveguide written by electron beam. The output of the asymmetric branch appears to mirror that of the straight branch, although without crossing over the x-axis.

While the behaviour of the field at the output of each branch approximates a sinusoid, it is clear that just one or two  $\mu\text{m}$  difference in splitting distance can have a significant effect on the final ratio of the outputs (straight branch output : Y-branch output). Therefore it was also important that the material refractive index and thickness were determined accurately prior to waveguide fabrication, or the expected splitting may not be observed. The output power, as measured with an optical power meter, is equivalent to the square of the E field.

For comparison, a similar simulation was carried out when the vertical thickness of the waveguide was just large enough to give 2 propagation modes in the guide. In this case a vertical FHD thickness of  $2.5 \mu\text{m}$  was used instead of  $2 \mu\text{m}$ . All other parameters in the simulation were kept the same. The result is given in Figure 3.5.

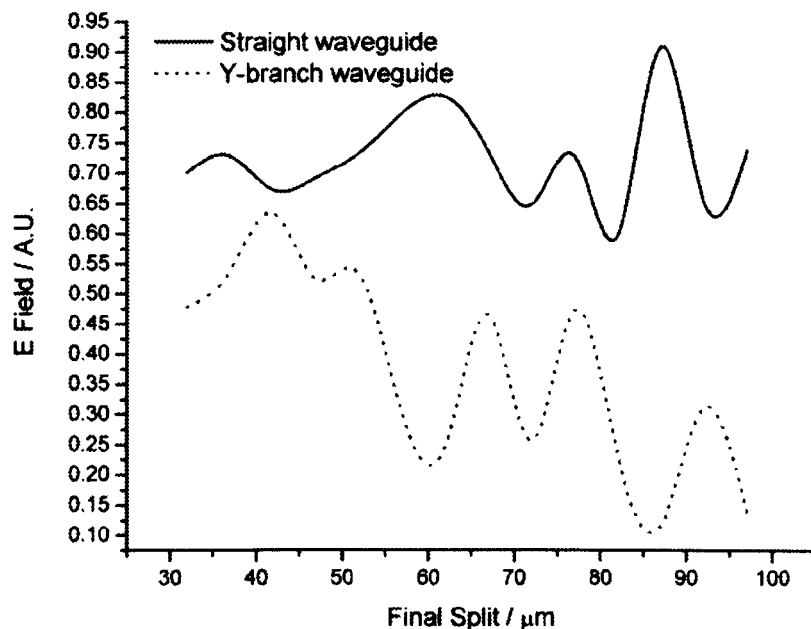


Figure 3.5: Variation of the waveguide outputs for different splitting distances,  $d$ , for an asymmetric branching waveguide where there are 2 modes in the vertical direction. The output of the asymmetric branch no longer mirrors that of the straight guide, as in the single-mode case.

The branching waveguide has a consistently smaller output than the straight one, allowing for much less versatility in the design of different power splitting ratios. In addition, the total output magnitude of both outputs is less than that in the single-mode case, implying that more losses are occurring in the branch, shown in Figure 3.6. The losses were observed in the simulation to originate in the S-bend area.

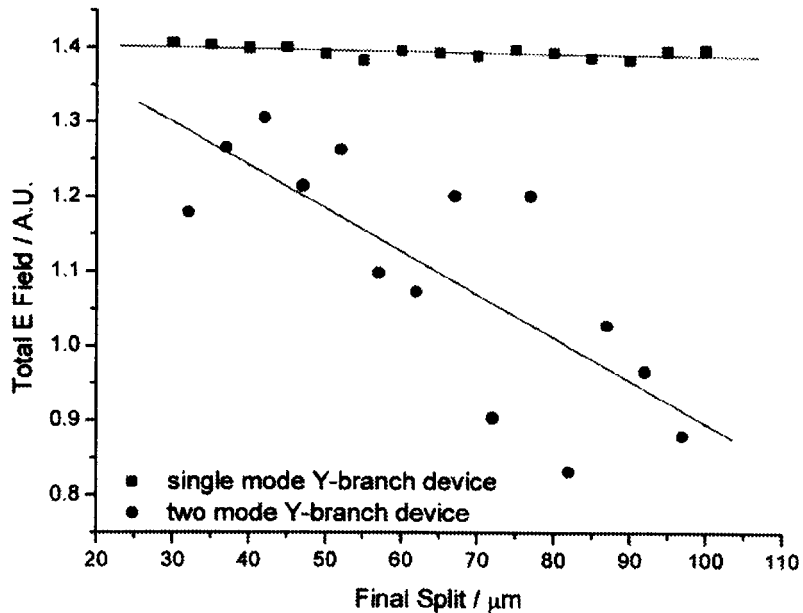


Figure 3.6: Sum of the output fields of the two asymmetric branches for the single mode device and the two mode device. The single mode device shows a much more consistent total output field.

### 3.2.2 Fabrication and Optical Characterisation of Asymmetric Y-branch Waveguides

As described in Chapter 2 for the preparation of substrates for FHD, a Si wafer with  $7\ \mu\text{m}$  thermal oxide was cleaned in an ultrasonic bath of acetone followed by methanol and then rinsed in RO water. An acid clean was used immediately prior to the deposition to remove any final debris from the wafer surface. FHD silica wafers were grown with a core-undercladding index difference of 0.7 %. Ge and B doping was used, as described in Chapter 2 for the standard FHD process.

All waveguides were written on FHD silica substrates deposited in the same deposition run. A thin layer (30 nm) of NiCr was evaporated onto the FHD silica using a Plassys electron beam evaporator prior to electron beam irradiation to prevent charging. The samples were cleaned in an ultrasonic bath of acetone followed by methanol and rinsed in RO water, followed by an acid clean to remove any contamination accumulated in the cutting process before evaporating the NiCr. The NiCr was removed using a standard Cr etch solution and rinsing in RO water after the electron beam irradiation.

The refractive index change produced in the irradiated area of FHD silica was  $6 \times 10^{-3}$  for a dose of  $1 \text{ C cm}^{-2}$  and electron energy of 50 keV. A series of test Y-branch waveguides was written sequentially on one  $1 \times 1.5 \text{ cm}$  FHD silica chip each time to minimise the effect of any thickness variations that may be present over a 3-inch wafer.

The Y-branches were characterized before the fabrication of any microfluidics in order to verify their splitting ratio, and to compare the expected ratio calculated from the BPM with that obtained experimentally. To that aim, end-fire coupling was used to launch 632.8 nm wavelength light from a 2.5 mW HeNe laser (Coherent Inc., UK) into the input waveguides. A x60 magnification objective lens with a numerical aperture (NA) of 0.85 was used to focus the light into the guides, while a x40 objective lens with a NA of 0.65 was used for collection. Y-branch output measurements were made using a LabMaster optical power meter, and an aperture was used to remove any stray light from the FHD slab around the waveguide outputs.

Table 3.2 shows the measured (with the optical power meter) and expected (from BPM) power splitting ratio of Y-branches with different branching angles, indicated by the separation 'd' between the two output waveguides. All of the measurements were taken from the waveguides on one chip.

A number of symmetric (50:50) Y-branches were also fabricated on the same chip. The worst-case measured branching ratio for the symmetric Y-branches was 53:47.

<b>Final distance 'd' (<math>\mu\text{m}</math>)</b>	<b>Predicted branching ratio</b>	<b>Measured branching ratio</b>
57.5	59:41	56:44
60	53:47	55:45
65	61:39	63:37
80	56:44	53:47
93	75:25	65:35

Table 3.2: Comparison of expected and actual output field ratios of an asymmetric Y-branch waveguide in densified FHD silica. The relatively wide separations were chosen to ensure that crosstalk between waveguides was minimised, although further work should be carried out to investigate further the effect of having more closely spaced waveguides.

A separation 'd' of 93  $\mu\text{m}$  between the output waveguides was selected for the final chip that would include the microfluidics. Experimentally, this configuration provided the smallest easily measurable reference branch due to the quality of the waveguide facets. Polishing of the facets was an option, but due to the long turnaround time of the polishing process (approximately 3-4 weeks), the diamond saw dicing was decided to be the most time-efficient method of facet preparation.

The measurement error was estimated to be  $\pm 10\%$ . The estimation of the error was found by repeating the measurement of the output of a straight reference waveguide that had been written onto the chip at the same time as the branching waveguides. Point defects due to contamination in the FHD silica layer were believed to contribute to the error, and to the deviations from the expected splitting ratios. A reasonable agreement between the measurements and simulations was observed, and it is believed that the main contribution to the difference between the expected and measured values was a variation in the thickness of the FHD silica layer from that measured on the test piece. As the thickness measurement using HF etching destroys the sample, it was not possible to measure the thickness of the actual sample that was to be used in this way.

Waveguide propagation losses of several sample waveguides were typically measured as  $0.5 \text{ dB cm}^{-1}$ , using the modified Fabry-Perot technique, described in Chapter 2. Losses in electron beam written waveguides written in Ge-doped FHD silica have previously been extensively investigated by García-Blanco [García-Blanco 2003]. Coupling losses due to the roughness of the waveguide end-facets were estimated to provide a more significant contribution to the total loss than the actual waveguide propagation loss.

Figure 3.7 shows a photograph of a typical Y-branch output, taken after the in-line x40 output lens using a webcam (Logitech, UK). The non-uniformity of the slab was believed to be due to several factors: in-plane scattering in the FHD material, end-polishing inhomogeneity and inefficient coupling. An aperture was used to eliminate light from the slab when taking measurements.

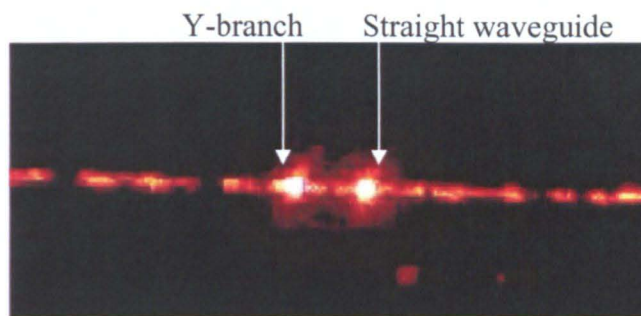


Figure 3.7: Digital image of the output of an asymmetric Y-branch written by electron beam. The light seen on either side of the waveguide outputs is from the FHD slab, which is more weakly guiding than the waveguides themselves. Further optimisation of the FHD process and electron beam dosage could reduce or eliminate the light in the slab.

After the initial waveguide characterisation, a waveguide separation, ‘d’, of  $93\ \mu\text{m}$  was chosen to give an expected output ratio of 75:25 for the final sensor chip, although the measured ratio was 65:35. The majority of the excitation light should be guided into the microfluidic chamber to excite the fluorophore, with only a small amount passing into the reference branch to monitor the coupling into the guide.

### 3.2.3 Fabrication and Optical Characterisation of Symmetric Y-branch Waveguides

Symmetric Y-branch waveguides were modelled and fabricated in the same manner as the asymmetric waveguides. Figure 3.8 shows an optical micrograph of a section of a  $1 \times 4$  array that was written by electron beam radiation. Interference filters were used in the microscope to enable observation of the refractive index contrast. An array such as the one shown could form the optical section of a biological array sensor to excite fluorophores in multiple microfluidic chambers.

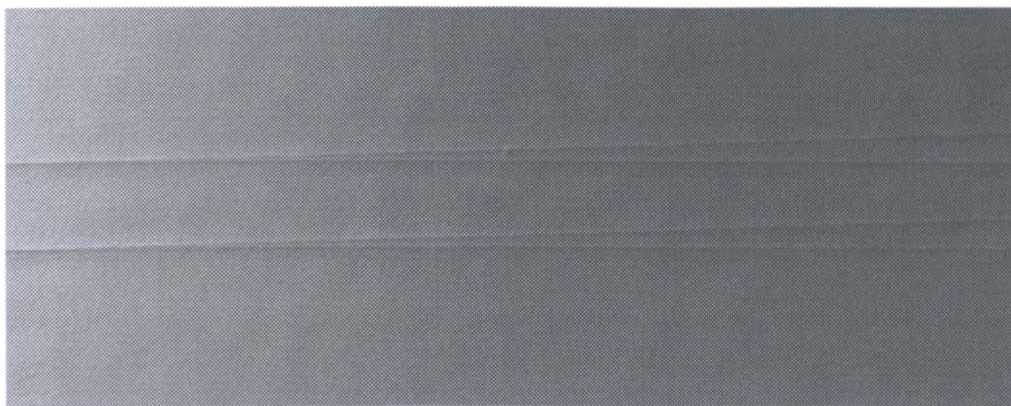


Figure 3.8: Optical micrograph of symmetric Y-branch waveguides forming part of a 1 x 4 array for multipoint excitation of fluorescent molecules in microchannels. The total chip length was 15 mm, and the width of the waveguides 2  $\mu\text{m}$ .

The Y-branches used were simple structures with a straight waveguide leading to two symmetric cosine S-bends in each case. However, despite repeated attempts at coupling light into the waveguides, the four separate output signals were unbalanced. It is thought that there were two main factors contributing to the problem, all mentioned previously as possible problems. The first is the possibility of an uneven thickness of the FHD layer, which would lead to asymmetric splitting at one or more of the branches. If a branch splits unevenly and then leads to other branches, then the effect will carry through to those branches also.

The second problem is that the Y-branch design may need to be optimised further to minimise losses. Several alternatives or enhancements to the simple design used here were available, but these would have to be investigated fully for the case of electron beam written waveguides in FHD glass. Syms et al successfully used a similarly simple structure to fabricate symmetric Y-branch waveguides in PECVD silica [Syms 1995]. Their writing process, however, still required photolithography of the required pattern, followed by flood exposure by electron beam.

### 3.2.4 Microfluidic Circuitry

The asymmetric Y-branch structure was written again for a complete sensor chip with the final separation of the output waveguides being 93  $\mu\text{m}$ . A 90  $\mu\text{m}$  wide orthogonal output waveguide was also included in the design, to collect the fluorescence from the

microfluidic chamber and deliver it to the PMT detector with the minimum amount of laser light included in the signal.

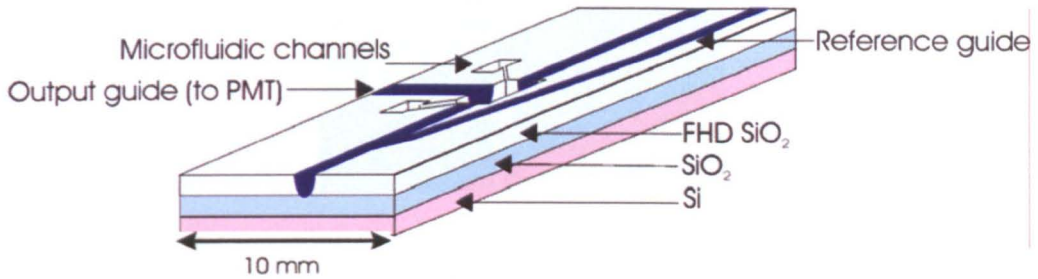


Figure 3.9: Schematic of the asymmetric Y-branch sensor chip prior to sealing with PDMS. The microfluidics intersect the excitation waveguide to allow direct excitation, and the output from the orthogonal waveguide was monitored with a PMT detector.

A low-cost laser-printed acetate mask plate was used for photolithography of the microfluidic circuitry in place of a more expensive mask plate written by electron beam, as the dimensions were less critical than those of the waveguides. The mask layout was designed in CorelDraw (Corel Corp., USA). A bilayer mask of 75nm NiCr and AZ4562 photoresist was used. Channels were dry etched 4  $\mu\text{m}$  deep through the waveguide core using  $\text{CHF}_3$  chemistry with the BP80 machine, at a measured rate of 60  $\text{nm min}^{-1}$ , as described in Chapter 2. The chamber dimensions were 600 x 50  $\mu\text{m}$ , and the channels were approximately 150  $\mu\text{m}$  wide. Figure 3.10 shows part of the microfluidic chamber and channel. However, as can be seen in the image, lines that are at an angle to the vertical or horizontal have not been resolved well, resulting in a ‘step’ from the pixellation of the mask image. The actual test chamber where the waveguides intersect the microfluidics was a rectangular structure, so the pixellation was not expected to affect the measured signal in any way.

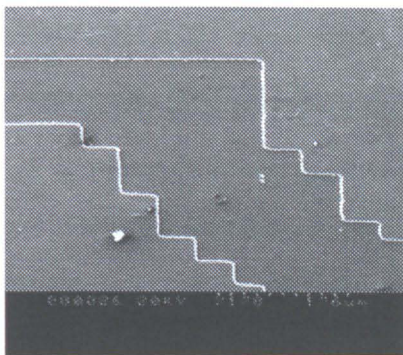


Figure 3.10: SEM image of a microfluidic channel etched into FHD glass, where an acetate mask has been used for the photolithography stage.

### 3.2.5 PDMS as Waveguide Cladding

PDMS has a refractive index of around 1.43 at 632.8 nm, (measured using an Abbé refractometer from Bellingham-Stanley, UK), which is lower than that of typical FHD silica waveguides (around 1.468). Several films were examined by the author with precursor:activator ratios ranging from 1:1 to 20:1, and no appreciable index difference was observed, thus allowing the assumption that the two parts are of equal refractive index. Therefore, it was decided that PDMS possessed the qualities desired of the cladding material, and it was adopted as a cladding, sealing and microfluidic material for most of the work described here.

One disadvantage of PDMS is that it is permeable by organic solvents such as acetone [Lee 2003]. This could prove to be a disadvantage if fluorescent dyes in solvent, such as Nile Blue, are to be used for analysis in chips containing PDMS. To verify that PDMS is indeed suitable, experiments into the index change during prolonged exposure to acetone were conducted.

A spun PDMS film was immersed in acetone, and its index measured after several time intervals up to 48 hours. The same experiment was repeated for methanol, in which PDMS swells relatively slowly according to Lee [Lee 2003]. The refractive index, within the measurement error, was found to remain constant over the 48 hours, and so it was concluded that index change due to solvent exposure would not affect waveguide performance.

### **3.3 Fluorescence Measurements on an Asymmetric Y-branch Waveguide Sensor with an Etched Microfluidic Chamber**

The reference waveguide shown in Figure 3.9 was used to ensure that the excitation light was always coupled to the input while fluorescence measurements were being made, and the output waveguide was orthogonal in order to prevent most of the excitation light from reaching the detector.

Preliminary tests were conducted to establish the feasibility of integrating microfluidic channels into the electron beam written waveguide chip to allow fluorescence measurements to be made. As this was the first time that electron beam written waveguides had been used for this purpose, the low-cost acetate printed mask was used for the microfluidics before writing a traditional (and much more expensive) photolithographic mask plate.

The channels were etched through the waveguide to allow direct excitation. PDMS was used to seal the channels and to provide an upper cladding for the waveguides. This polymer was one of the few suitable for use as cladding for FHD waveguides, and was chosen for its suitable refractive index (1.43) and low autofluorescence, as discussed in Chapter 2.

The PDMS cladding was prepared using a 10:1 mixture of precursor and activator. The resulting mixture was spun onto clean glass slides at 500 rpm for 30 seconds including a ramp up to 500 rpm for the first 10 seconds, and cured at 90 °C. Once cured, the PDMS was peeled from the slides and sealed to the waveguide chip.

Initial fluorescence measurements of the output from the orthogonal waveguide were made using a Hamamatsu H5700-50 PMT connected through an EG&G lock-in amplifier and optical chopper. Nile Blue dye in methanol, with excitation and emission maxima at 636 and 686 nm respectively was used. An Omega optical emission filter (670DF40) was used to remove stray excitation light from the detected signal. The fluorophore was added by placing a droplet at one of the microfluidic inlets, and allowing capillary forces to fill the channel. Figure 3.11 shows the plan view of the setup.

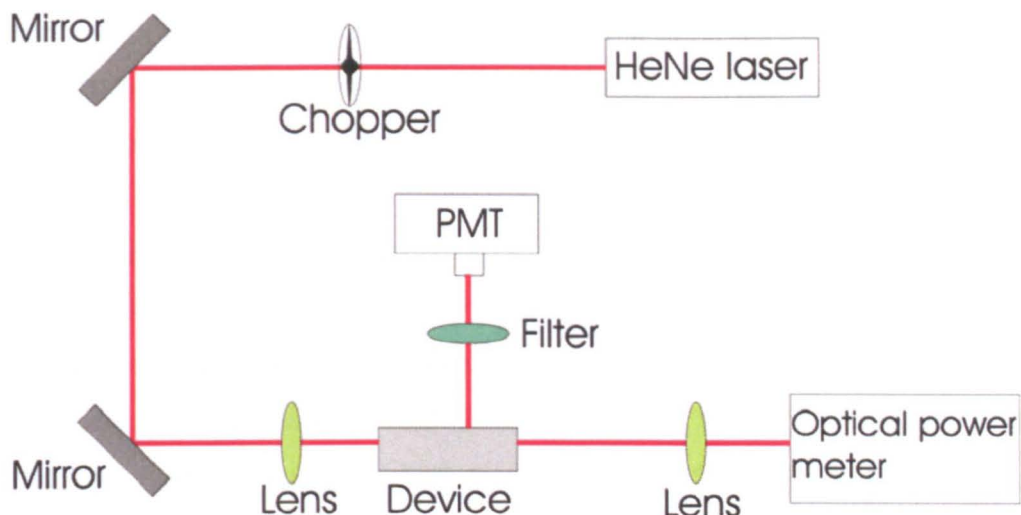


Figure 3.11: Optical setup used for fluorescence measurements and also for waveguide characterisation. The lock-in amplifier is not shown, but was connected to the PMT, with the chopper as a reference.

Figure 3.12 shows the measured fluorescent signal for various concentrations of Nile Blue. These values were obtained by subtracting the measured signal when the chamber was filled with methanol (blank signal) from the signal when fluorescent dye was present.

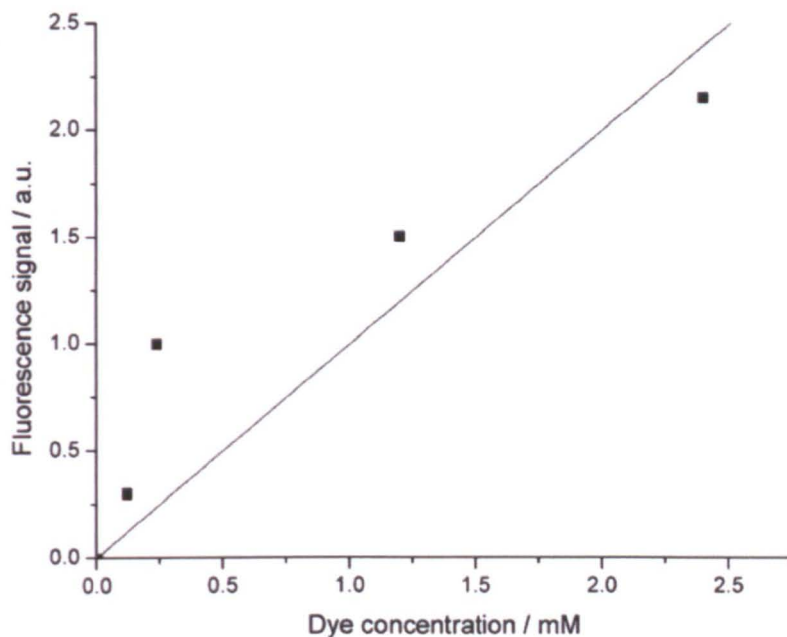


Figure 3.12: Measured fluorescence signal for various concentrations of Nile Blue dye. The line is given as a guide for the eye.

The sensitivity of measurement was comparable to that observed by Ruano [Ruano 1999], using similar concentrations. The minimum detectable concentration was 200  $\mu\text{M}$ . The measurement error was estimated to be  $\pm 7\%$ , by repetition of each measurement.

The quality of the microfluidic chamber walls of the chip was poor, attributed to the use of the acetate mask, and indicated in Figure 3.10. Therefore, although the results here show that the electron beam written waveguides were suitable for such a sensor, the sensitivity achieved is not the optimum. A second chip, this time with microfluidics defined by photolithography with a traditional high-resolution mask plate written by electron beam, was fabricated. The results of measurements with this chip are given in Chapter 5, where a single photon avalanche detector (SPAD) was used in place of the PMT detector.

### **3.4 Fabrication of Unclad Dry Etched Ridge Waveguides**

In order to use a polymer as cladding for silica-based waveguides, the dry etched silica waveguides must be prepared for optical coupling prior to addition of the polymer. That is, the waveguide end facets must be prepared to as high a quality as possible, which normally requires polishing of the facets, or at the very least dicing with a fine diamond blade.

With traditional, silica-clad waveguides, once the cladding has been added, the waveguide structure is protected and the facets were easily diced or polished without affecting any other part of the buried waveguides. Often, an entire wafer was patterned, etched and clad at the one time, and only then was the wafer cut up to separate individual devices.

When producing unclad ridge waveguide devices, however, the wafer must be diced before the waveguides are fabricated, as they were found to break when being held in the cutting machine.

The fabrication of unclad, or polymer clad, silica waveguides was then found to present a new problem: degradation of the waveguide ends due to photoresist edge bead formation during spinning. This was a common problem when spinning all types of photoresist onto devices, and was usually worse for non-circular substrates. Web-based discussion forums often contain problems of this nature [see for example [www.memsnet.org](http://www.memsnet.org)]. It is not a problem when spinning a full wafer as described in the previous paragraph, as the edges of

the wafer will be cut away at a later stage. Figure 3.13 illustrates the problem, showing the edge of an unclad waveguide after dry etching.

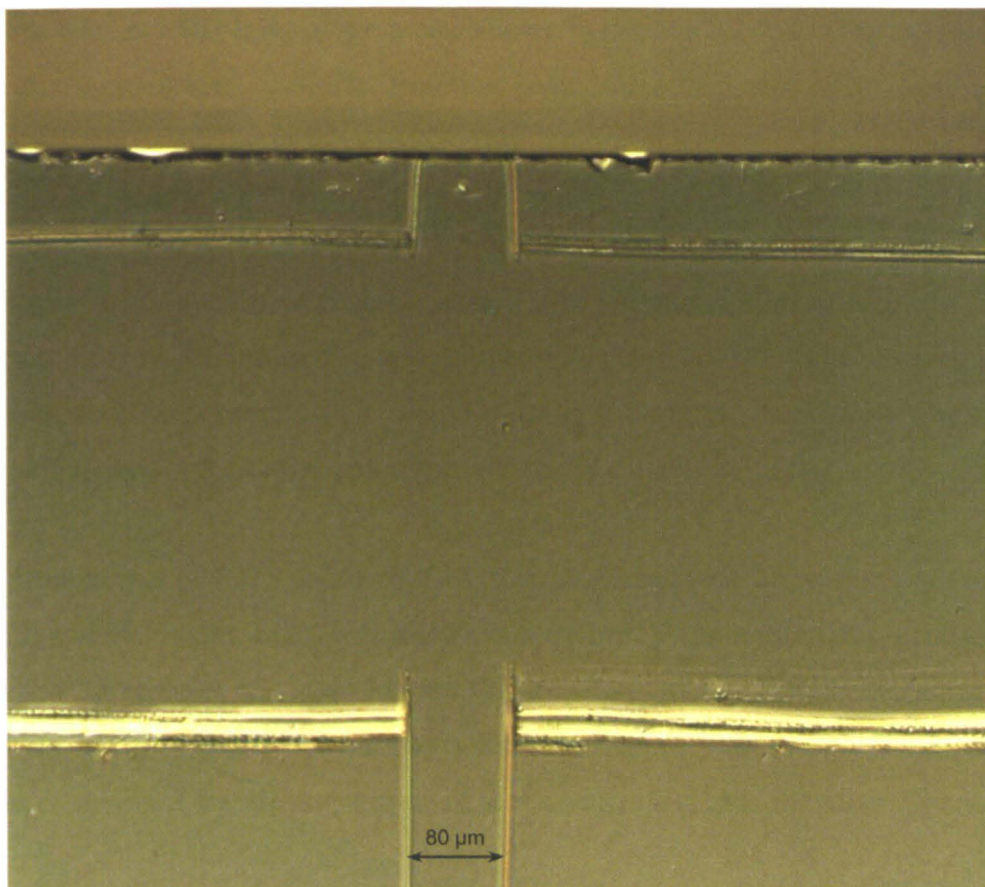


Figure 3.13: Optical micrograph at the edge of a chip with a dry etched unclad ridge waveguide showing the effect of resist edge bead. The build up of photoresist at the edge of the chip during spinning results in a thicker area that does not develop properly, and subsequent dry etching of the waveguides is affected by the resist.

### 3.5 Evanescent Excitation Sensors using Y-branch Waveguides

In the quest for a chip that requires the minimum of fabrication steps, the suitability of a chip that provided evanescent excitation of the fluorophore was evaluated, that is, a chip that has no dry etched microfluidic chambers. The same electron beam written waveguide layout as in Section 3.2 was used, that is, a straight waveguide to excite the fluorophore with an asymmetric branch for the reference. The collection waveguide was a 4  $\mu\text{m}$  deep, 80  $\mu\text{m}$  wide dry etched guide to collect the fluorescence directly from the microfluidic chamber. In future chips, an optical fibre could be incorporated in the PDMS sealing stage to replace the dry etched output waveguide, thus a completely 'etchless' chip could be produced.

To allow for both the 4  $\mu\text{m}$  deep etched output waveguide and the 2  $\mu\text{m}$  needed for the electron beam written excitation waveguides, a total FHD silica layer of 6  $\mu\text{m}$  was needed. To achieve this, an FHD layer of the recipe shown in Section 3.2.2 was deposited, but with 8 torch traversals instead of 3. The resulting layer had a thickness of 5.8  $\mu\text{m}$ , measured using HF etching of the layers followed by Talystep profilometry.

### 3.5.1 Fabrication of the Evanescent Excitation Chip

The electron beam written waveguide section was written in the full 6  $\mu\text{m}$  of the FHD silica layer first, to minimise the possibility of damage to the etched waveguide. An adiabatic taper from 2  $\mu\text{m}$  up to a width of 9  $\mu\text{m}$  in the straight waveguide was added, to allow a larger area for excitation under the microfluidic chamber.

Next, a 30 nm layer of NiCr, followed by S1828 photoresist was deposited as described in Chapter 2, and the output waveguide pattern was defined by photolithography. A  $\text{CHF}_3$  dry etch for 2 x 30 minutes was used to etch the complete guide, also etching away the top layer of the electron beam written waveguides so that they were only 2  $\mu\text{m}$  deep. An optical micrograph of the sensing section of the waveguide chip is shown in Figure 3.14.

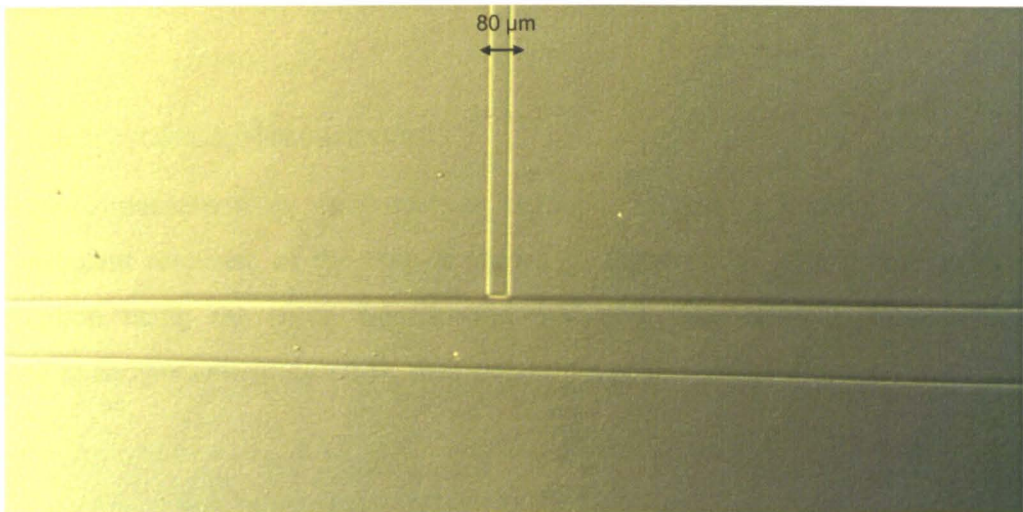


Figure 3.14: Micrograph of the optical part of the evanescent excitation chip. The branch area consists of electron beam written waveguides that have then been etched, allowing the dry etched ridge waveguide to be defined.

A microfluidic channel was then incorporated, following the process steps shown in Section 2.7.2. The resulting chip is shown in Figure 3.15, where the view is taken through the PDMS layer.

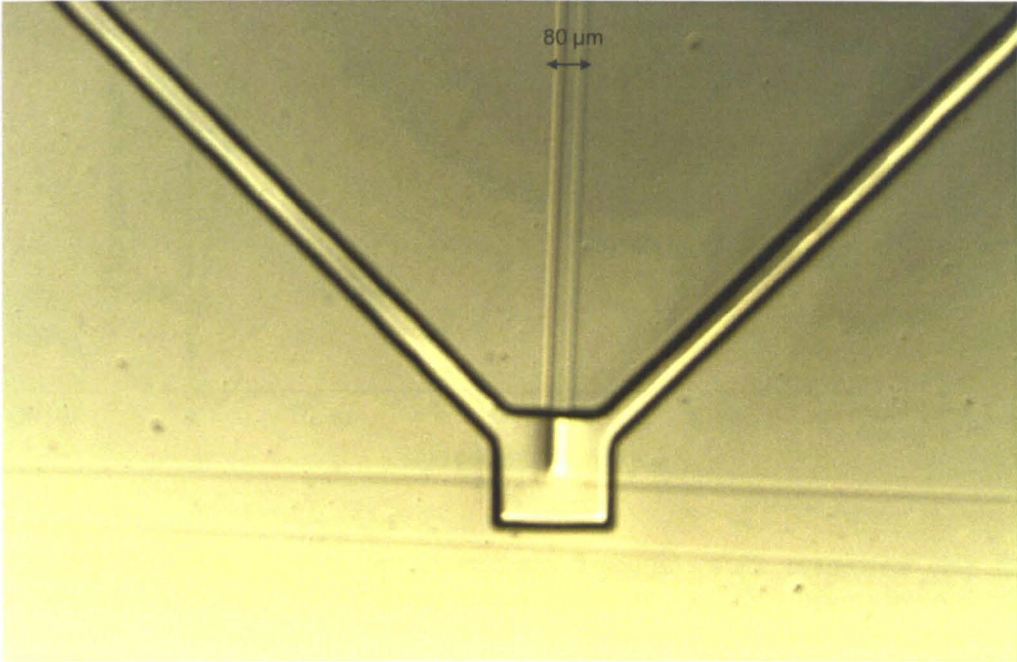


Figure 3.15: Micrograph showing the complete evanescent excitation chip, with the embedded channels defined in PDMS using photolithography. A complete description of the fabrication is included in the text.

### 3.5.2 Fluorescence Measurements

Fluorescence measurements were made as before in Section 3.3, using a PMT detector. The fluorescent response of the chip is shown in Figure 3.16. The minimum detectable concentration using the setup was around 500 nM. The error in measurement was estimated to be approximately 10 %, from repetition of the measurements.

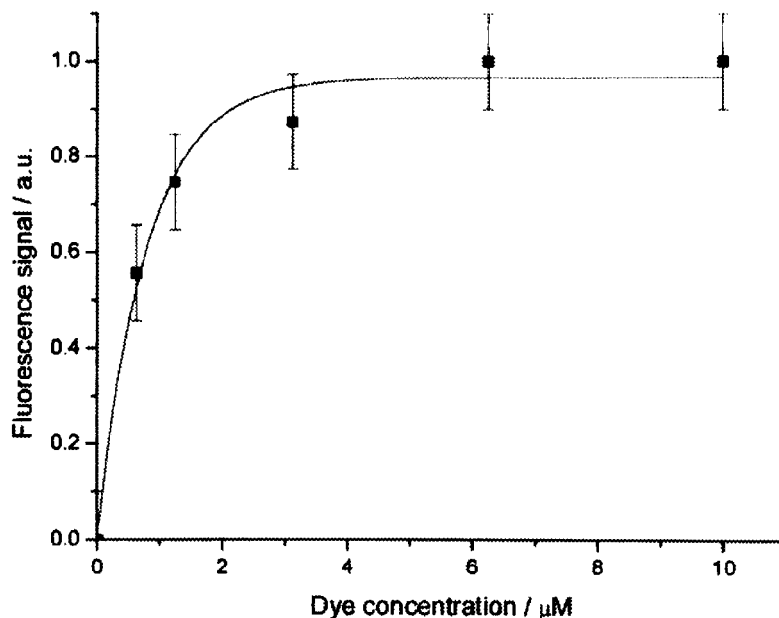


Figure 3.16: Graph showing the fluorescence response of the evanescent chip for various concentrations. As the concentration increases, the graph begins to level off, even though a different concentration range was used than in previous measurements.

The response begins to saturate after a certain concentration, around  $2 \mu\text{M}$ . This effect was originally thought to be due to quenching above a certain concentration, perhaps brought on by dye particle aggregation. However, the concentration range used here was much lower than the range used in Section 3.3, therefore the reason for the levelling off may be more complex. The channel becoming blocked by small dust particles is another possibility, as this effect has occasionally been observed through an optical microscope while monitoring the fluid flow in the channels. However, the most likely explanation for the saturation is that the positively charged dye molecules are adsorbed onto the negatively charged silica channel walls. As each successive sample of increasing concentration is injected into the channel, a gradually thicker layer of dye molecules may become attached to the walls, thus reducing the channel size available for sample flow and so reducing the number of dye molecules that can reach the analytical chamber.

At present, the easiest solution would be to remove the chip and clean it thoroughly in an acetone and methanol ultrasonic bath. However, the chip must then be realigned with the laser and detectors, and so the measured signal is unlikely to be completely consistent each time. To reduce the probability of dust blocking the channels, the device optical testing

system could be housed in a cleaner area, where dust is less likely to be a problem. A complete integrated flow system could also be incorporated.

### 3.6 Summary

Symmetric and asymmetric Y-branch waveguides have been written in Ge doped FHD silica using an electron beam. The splitting ratio obtained in the case of asymmetric branches has been compared with BPM simulations of the devices. Reasonable agreement of experimental splitting ratio with that predicted by the BPM was observed, although some error was evident, possibly introduced by thickness variations in the FHD silica film in which the waveguides were written.

Microfluidic circuits were defined by photolithography and etched through the waveguides using dry etch. PDMS was used as a top lid to seal the microfluidic channels and therefore form a complete optical fluorescence sensor chip. Trials of the chip with increasing concentrations of fluorescent dye excited by the light guided into the microfluidic chamber showed that the different concentrations could easily be detected with a PMT.

Symmetric Y-branching electron beam written waveguides were fabricated, mainly to establish the standard and reproducibility of branching waveguides. Consistently equal splitting ratios were obtained for single 1 x 2 splitters, thus helping to reinforce confidence in measurements of the less well characterised asymmetric branches. The symmetric branches would also be suitable for use in an array sensor with multiple excitation points, as described by Ruano for dry etched channel waveguides [Ruano 2000]. Further optimisation of the design of the symmetric branches would be needed to minimise losses over the full device.

An alternative, 'etchless' chip was also fabricated, in which the excitation of the fluorophore was evanescent rather than direct. In this case, the PDMS sealing layer also contained the microfluidic channels. While encouraging results show sensitivity just into the nM range, the problem of channel blocking reduced the number of measurements that could be made.

## 4 Multimode Interference (MMI) Splitters for Fluorescence Applications

This chapter addresses the problem of the splitting nonuniformity observed in Chapter 3 in arrayed Y-branch waveguides. The aim was to investigate waveguide array devices by examining the multimode interference (MMI) splitter as an alternative type of splitter to the Y-branches. Its suitability for fluorescence sensing purposes at the biologically-relevant and fluorophore compatible excitation wavelength of 632.8 nm was examined by the fabrication of two prototype chips; one for use as a single-assay device, and the second as an array structure for excitation of multiple sites. Electron beam densification of FHD silica was evaluated as the waveguide fabrication method.

### 4.1 Multimode Interference in Strong Guiding Media

MMI 3 dB splitters and combiners have long been recognised as valuable devices in communications technology due to their ability to split an input signal into a predetermined number of outputs with high uniformity, or to combine or couple several input signals [Themistos 2002]. A combiner is essentially a splitter in reverse, so the discussion from this point will refer to an MMI splitter, but many of the design and technological issues will be consistent for a combiner/coupler.

MMI devices have been employed in numerous applications, including Mach-Zehnder switches, ring lasers, modulators and demultiplexers [Bachmann 1994]. Natarajan et al suggested that MMI devices might be used for sensors, based on BPM simulations of an InP device [Natarajan 2001]. In this latter work, an example of a fibre optic gyroscope was given, but no method for fabrication was described.

The basic concept of the MMI splitter is based on the self-imaging principle [Soldano 1995], in which multiple images of an excitation field are reproduced at periodic intervals along a waveguide. A single-mode input guide 'feeds' a wider multimode section, in which constructive interference occurs at specific points along the guide. Choosing the length 'L' of the guide to be the length at which the desired number of outputs is imaged by the constructive interference allows accurate beamsplitting to be performed. Figure 4.1 shows

a plan view of an MMI splitter, where the output waveguides are equally spaced at a pitch 'p' of  $W/N$ .  $W$  is the splitter width and  $N$  the number of outputs.

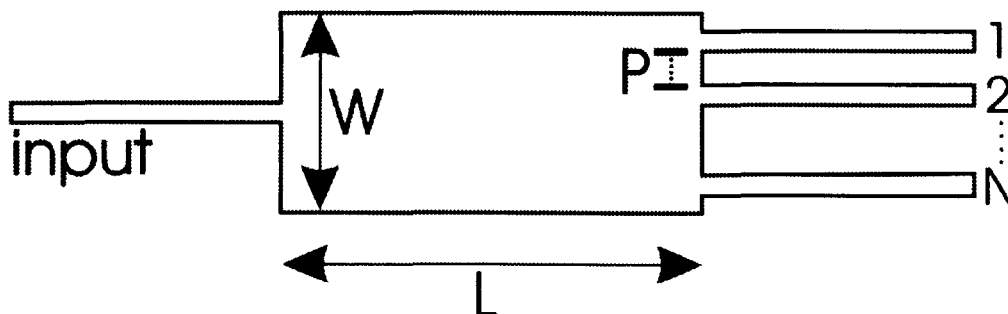


Figure 4.1: Schematic of a MMI splitter with  $N$  outputs. The input and output waveguides are typically single-mode, and the length  $L$  is chosen according to the number of outputs required. For equal power splitting, the pitch  $p$  between each output waveguide is equal.

For further details on the analysis of MMI structures, the reader is referred to papers concerning this topic [Soldano 1995, Rajarajan 1996, Błahut 2002]. Soldano in particular provides a comprehensive review.

The excellent fabrication tolerances of MMI devices have been widely reported [Besse 1994]. Leuthold investigated the effects of intentionally modifying the dimensions of the multimode section of the fabricated MMI device from the designed layout and found that the splitting ratio was still reliable [Leuthold 1997], while Campillo used a near-field scanning optical microscope (NSOM) to directly image the guided light [Campillo 2003]. Shibata also reported that the performance of cascaded MMI couplers was superior to that of Y-branch waveguides [Shibata 2002], although to obtain a division of more than  $1 \times 2$  with an MMI splitter requires still only one multimode section.

A number of alternative designs for the multimode section have recently been proposed, with the intention of further improving the fabrication tolerances and allowing the splitting ratios to be tuned [Besse 1996, Lagali 1999, Yin 2000, Leuthold 2001, Mašanović 2003]. As yet, to the author's knowledge, none of these designs have been brought into common use in place of the original rectangular design.

Several materials have been used to realise MMI splitters, using either dry etched or Na<sup>+</sup> ion exchanged waveguides. Devices in LiNbO<sub>3</sub>, GaAs compounds, InP compounds and silica have all been reported [Soldano 1995]. Excluding silica, these materials can normally be classified as ‘strongly-guiding’ due to the magnitude of the refractive index difference between core and cladding. The length needed for a particular width in the strongly guiding case is given by Equation 4.1 below, where  $n_{\text{eff}}$  is the effective refractive index of the MMI region,  $W$  is the MMI width,  $N$  the number of outputs and  $\lambda_0$  the operational wavelength, as shown in Figure 4.1 [Heaton 1992].

$$L = \frac{n_{\text{eff}} W^2}{N \lambda_0} \quad (4.1)$$

## 4.2 Silica-Based MMI Devices

### 4.2.1 Multimode Interference in Dry Etched Silica

MMI splitters in dry etched silica-on-silicon have previously been examined both experimentally and theoretically by Lai and Leick [Lai 1997, Leick 2001]. PECVD silica was used in both cases. Core-cladding refractive index differences used by these authors were around 1% (~0.015) and 0.7% (~0.01) respectively. A switching device has also been reported using silica-on-silicon [Lai 1998]. Ruano fabricated prototype MMI splitters in FHD glass with a core-cladding index difference of 0.25%, demonstrating the possibility of using FHD glass in a splitter [Ruano 2000].

Weaker guiding observed as a result of the lower index difference introduces a number of design problems not observed with the strong guiding structures described previously. The most significant is the increase in phase errors at the MMI boundary resulting in greater splitting imbalance. The error leads to the need for the splitter length ‘L’ to be modified from the calculated optimum length in Equation 1. In our case, the 2D BPM simulation package was used to calculate the optimum length for minimal splitter imbalance.

Using BPM simulation, it was found that the length correction needed increases linearly with increasing width for a dry etched silica-on-silicon structure compared to a strongly guiding MMI structure [Cleary 2003]. An example of this is shown in the following two

figures for a 1 x 2 splitter that is a ridge structure, with core-cladding difference of 0.25 %. The index difference of 0.25 % was chosen so that the single-mode input waveguides would be relatively large ( $\sim 3 \mu\text{m}$ ) square, to enable photolithography to be used as a method to fabricate the device. Figure 4.2 shows the actual calculated length for a strong guiding (from Equation 4.1) and for the weaker guiding silica device, to illustrate that as the device length increases, the correction needed for the silica structure increases also. Figure 4.3 shows the value of correction needed for this particular case, which is the difference between the traces in Figure 4.2 at particular values of width  $W$ . These two figures are intended to provide a design reference for dry etched silica MMI splitters.

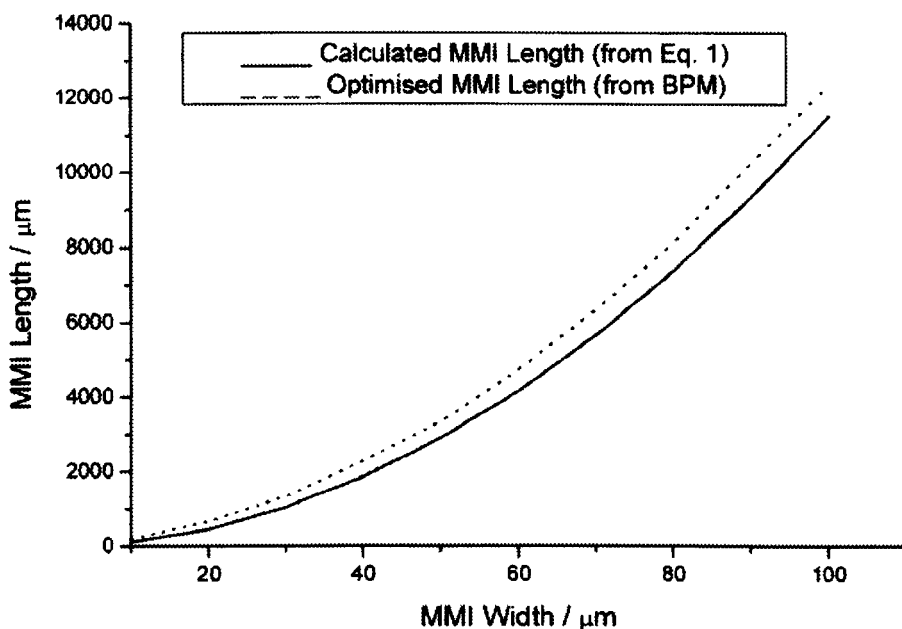


Figure 4.2: Calculated and optimised MMI lengths for a 1 x 2 splitter in dry etched FHD silica. The BPM was used to calculate the optimised length,  $L$ . The length obtained from using Equation 4.1 (solid line) is consistently shorter than the corresponding optimised length.

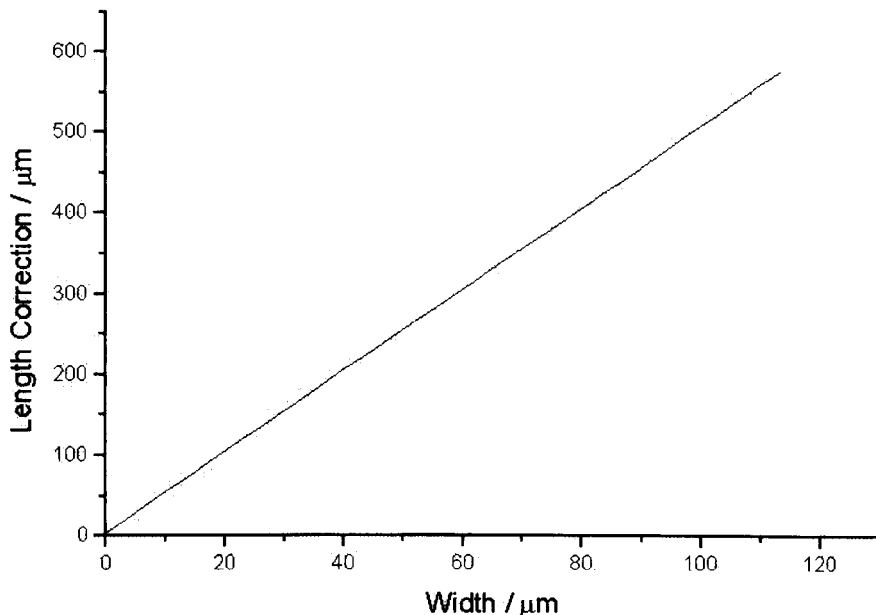


Figure 4.3: Correction ( $\Delta L$ ) needed for the splitter shown in Figure 4.2, to illustrate the difference in device size for a strongly guiding and a more weakly guiding silica MMI splitter. The data from each trace in Figure 4.2 were subtracted from each other to obtain the graph seen here.

MMI splitters have not been applied to fluorescence array sensors to date, to the author's knowledge. However, their compactness and their potential for accurate splitting provide an excellent starting point from which to build such an array-type sensor.

The main problem with using dry etched silica MMI splitters for fluorescence sensing is again the time and resources used in the cladding and microfluidic steps. It was concluded that to build a fluorescence sensor using this method would be, although perfectly possible, a step backwards in the quest for a cheaper, faster and less complex fabrication process. Using an index-matched cladding such as FHD glass to provide a uniform mode profile gives no advantages to a fluorescence sensing system. Therefore, apart from using the BPM to explore their characteristics, no further work on dry etched splitters was carried out.

### 4.2.2 Electron Beam Defined Multimode Interference Structures

An interesting possibility is the use of electron beam direct writing of MMI structures in Ge-doped FHD silica. To date, the only other MMI devices fabricated by a direct writing process were presented by Knappe, using UV writing [Knappe 2003]. The writing resolution and smooth-walled embedded structure of electron beam written waveguides are considered to provide a suitable platform for an MMI fluorescence array sensor, as for the Y-branch sensors described in the previous chapter.

BPM simulations were first used to establish the suitability of the direct writing technique for the MMI splitter configuration, and to find the optimum splitter length. The correction to 'L' needed from the length calculated with Equation 1 as described in the previous section, was found to be smaller than that for similar dry etched silica guides, as the index difference between the slab and the waveguide region induced by the electron beam is larger than the silica core-cladding difference,  $\Delta n$  ( $\sim 0.07$ ). Added to the difference between the slab and thermal oxide undercladding of  $\sim 0.011$ , the overall index difference from the thermal oxide to the electron beam written waveguide is 1.23 % (0.0179). The correction factor ( $\Delta L$ ) for the electron beam written device is therefore smaller than for the dry etch case. The exact correction needed for a 1 x 2 splitter is shown below in Figure 4.4. Data for the equivalent dry etched structure is included for comparison.

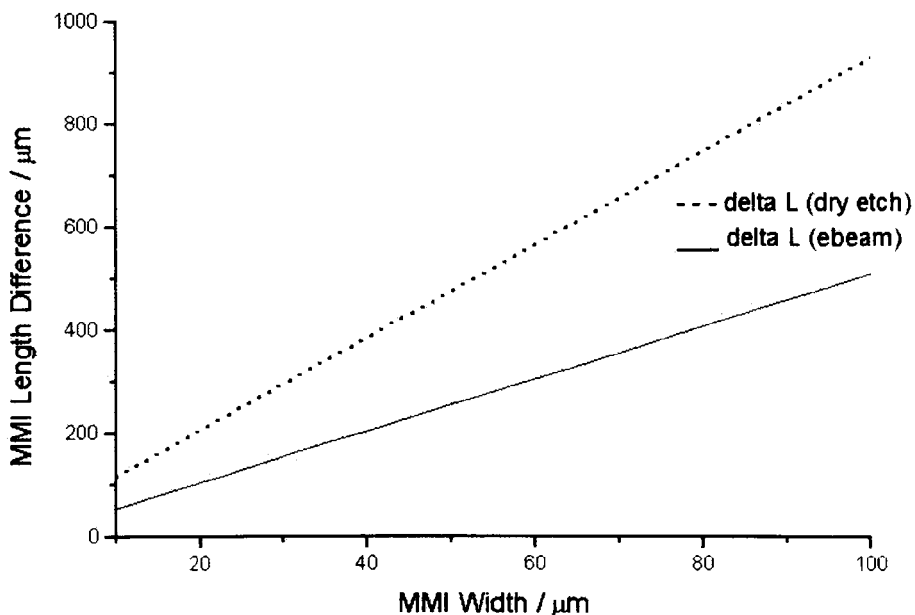


Figure 4.4: Length correction (delta L) needed for an electron beam written 1 x 2 splitter compared to a dry etched silica splitter, when using the BPM to optimise the length calculated from Equation 1. The difference was obtained by subtracting the value calculated with Equation 1 from the value obtained by BPM optimisation.

Clearly, as the MMI width increases, the difference in correction needed becomes larger, increasing to over several hundred microns. Therefore, it can be predicted from the BPM simulation that using electron beam irradiation of silica rather than dry etched silica will result in a more compact device. The potential for producing even stronger guiding waveguides by electron beam densification exists, simply by increasing the total electron dose in the writing process. The predicted length needed for an electron beam written 1 x 2 splitter is shown in Figure 4.5.

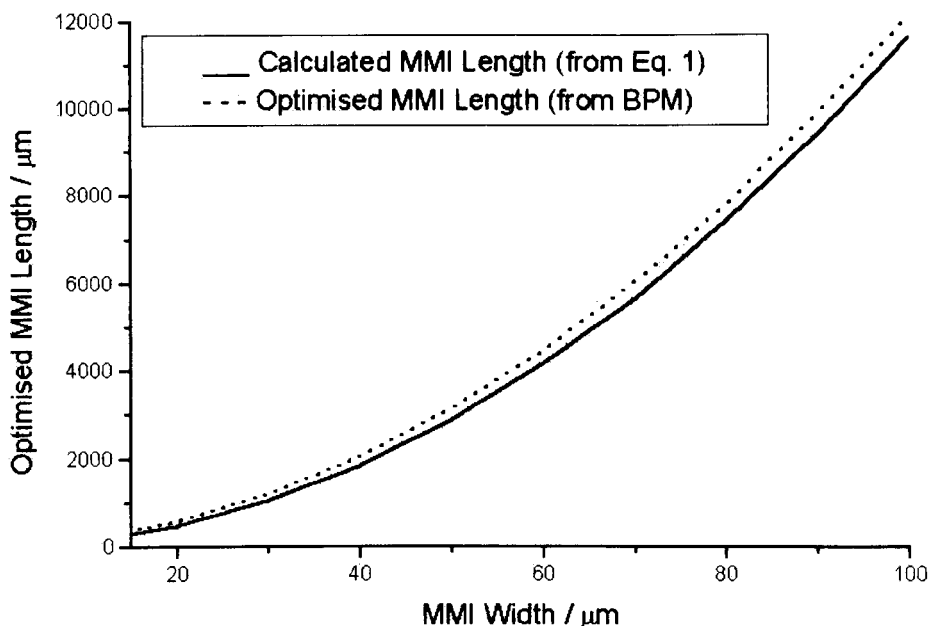


Figure 4.5: Calculated and optimised MMI lengths for a 1 x 2 splitter in electron beam irradiated FHD silica. BPM was used to calculate the optimised length,  $L$ . The length obtained from using Equation 1 (solid line) is consistently shorter than the corresponding optimised length.

Optimisation of a splitter was achieved by maximising the power outputs in a 1 x 2 splitter, or by achieving equal division in a structure with more than two outputs. An example of the 2D BPM simulation result is shown in Figure 4.6 and Figure 4.7, for a 1 x 4 splitter with a pitch of 30  $\mu\text{m}$  written by electron beam. When a 1 x 4 splitter is unbalanced, the outer two waveguides have an equal output, as do the inner two guides.

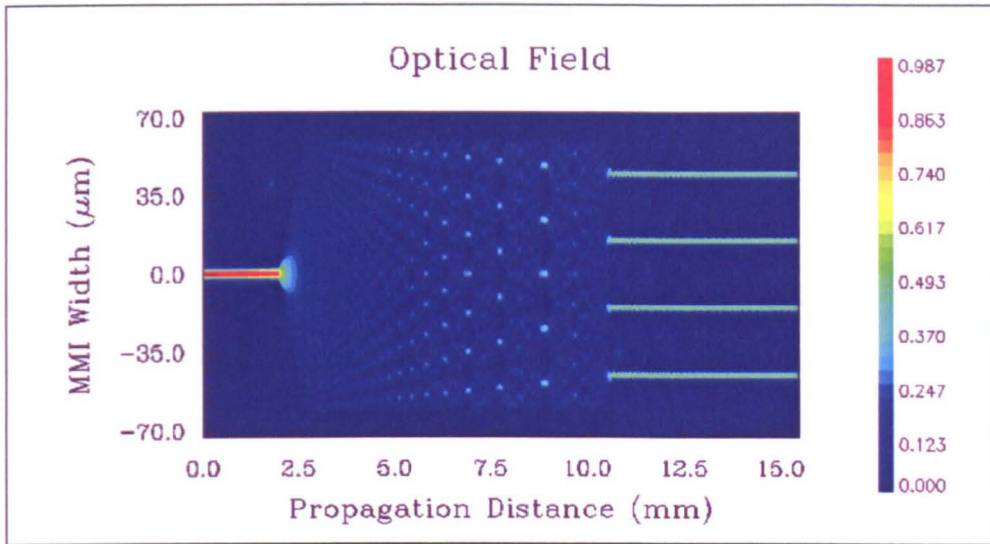


Figure 4.6: Field profile from BPM simulation of a 1 x 4 electron beam written splitter. Some loss can be seen at the end of the multimode section, which is evident even at this optimised length.

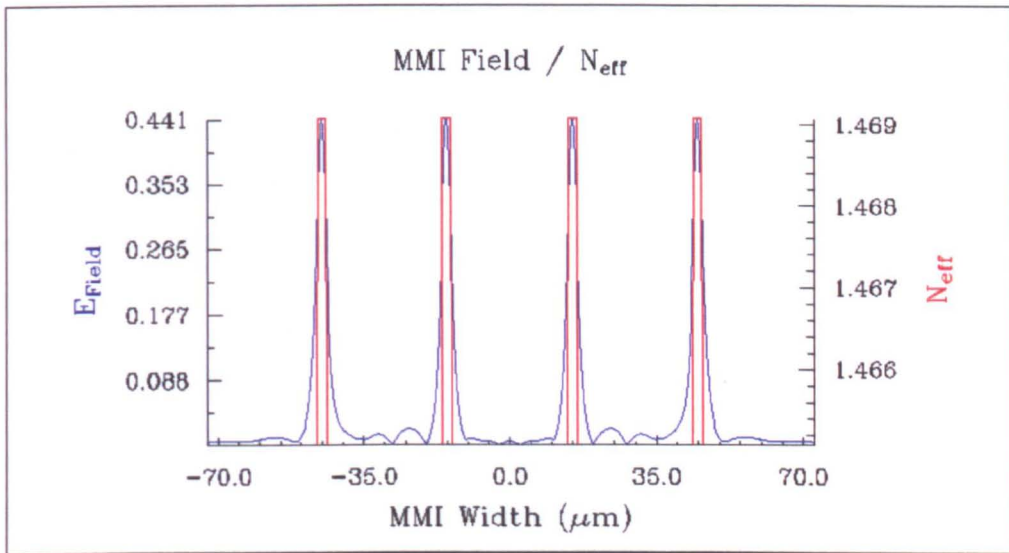


Figure 4.7: Predicted output powers from an optimised 1 x 4 splitter written by electron beam, corresponding to the device shown in Figure 4.6.

Figure 4.7 shows that although equal splitting has been achieved, leakage into the waveguide slab still occurs at the end of the multimode section. As long as the waveguides are embedded into this guiding slab, some leakage will occur.

In practice, several other factors may cause additional leakage into the slab. For example, due to the practical implementation of silica-on-Si technology, irregular FHD film

thicknesses have been observed, and although the MMI splitter area is small, there may be a variation of the order of a few tens of nanometres across the device area. Irregular film thicknesses have also been recognised by others as a fabrication problem in most types of planar silica device [Jensen 2003].

The refractive index profile of the electron beam written waveguides is also not uniform throughout the depth of the guide [García-Blanco 2003]. Therefore, the assumption in the BPM modelling of a step-index profile is not an accurate representation of reality. However, the index profile of the FHD glass itself is also believed to be not completely uniform, so final optimisation of the fabricated MMI splitter would have to be iterative if the true index profile is not accurately defined.

One solution to this problem is to decouple each output waveguide completely by etching a series of channels between the waveguides, as suggested by Mogensen et al [Mogensen 2003]. These channels can be etched simultaneously with the microfluidic channels, and therefore add no time or resource use to the chip fabrication. It is however, technologically challenging to align such channels precisely during the photolithographic step so that they do not have an adverse effect on the splitting ratio of the device. If the channels are not perfectly aligned, the MMI output waveguides will be uneven, thus affecting the final splitting ratio.

### 4.2.3 Fabrication Tolerances

Whilst the high fabrication tolerances of MMI splitters have been reported, an investigation into the tolerances of this particular fabrication method was considered necessary. One possible cause for concern prior to fabrication was the belief that the width of an electron beam written waveguide extends further by approximately  $0.5\ \mu\text{m}$  than the written area under the sample surface [Madden 1990].

To this end, BPM simulations were carried out to determine the possible effect of length and width variations in the multimode section of a splitter. The design used for the  $1 \times 4$  splitter that was finally incorporated into a full sensor device was used as the basis for the simulations. The original, optimised length of the splitter was  $3923\ \mu\text{m}$  and the width  $80\ \mu\text{m}$ .

It was discovered that variations of several microns in the splitter length ‘L’ had a relatively small effect on the splitting ratio, and variations of up to  $\pm 50 \mu\text{m}$  still offered reasonable device performance. The results of the simulations are summarised in Table 4.1.

Length Condition / $\mu\text{m}$	$E_0$ / calculated from BPM (centre arms / outer arms)	Power Imbalance / dB
L - 50	0.455 / 0.439	0.304
L - 10	0.457 / 0.450	0.127
L - 5	0.452 / 0.449	0.043
Optimised (L)	0.450 / 0.449	0.021
L + 5	0.445 / 0.443	0.044
L + 50	0.384 / 0.375	0.181

Table 4.1: Summary of the expected imbalance induced by variations from the optimum MMI splitter length, ordered by increasing length. Values in the second column show  $E_0$ , the optical field for the two centre splitter outputs followed by the two outer waveguides. The optimised length was chosen for both a small imbalance and a high output.

An illustration of the effect is given in Figure 4.8 for the case of L - 50.

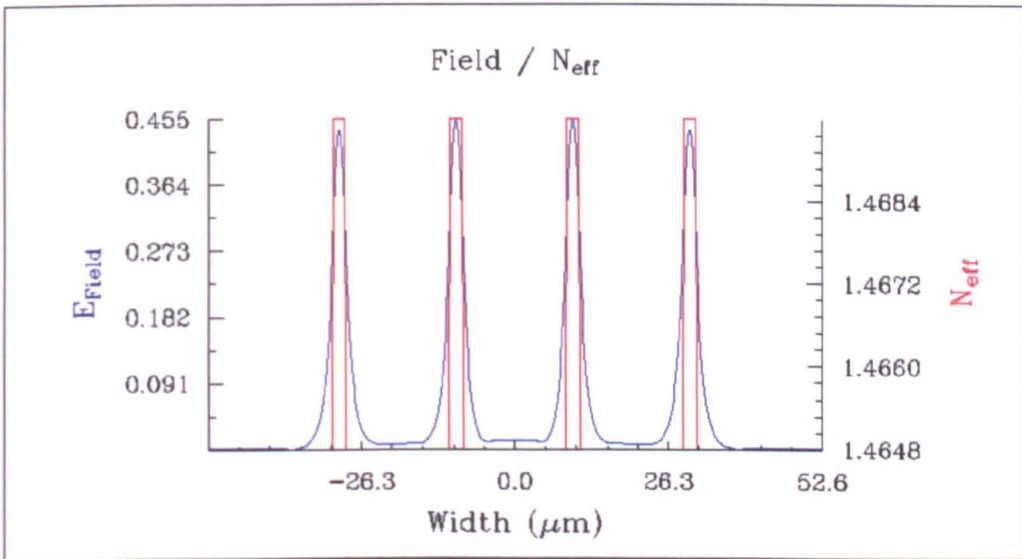


Figure 4.8: BPM field profile showing the effect of reducing the length of a 1 x 4 MMI splitter by 50  $\mu\text{m}$ . The power imbalance in this case was 0.304 dB.

The effect of variations in the width ‘W’ was found to be more significant than the length variations, with even a 1  $\mu\text{m}$  increase in width having an easily observable effect on the final imbalance. Table 4.2 shows the results obtained for width variations of up to  $\pm 2 \mu\text{m}$ . An increase in width of 10  $\mu\text{m}$  was found to have such an adverse effect that the splitter ceased to function.

Width Condition / $\mu\text{m}$	$E_0$ / calculated from BPM (centre arms / outer arms)	Power Imbalance / dB
W - 2	0.254 / 0.262	0.259
W - 1	0.325 / 0.328	0.081
Optimised (W)	0.450 / 0.449	0.021
W + 1	0.364 / 0.357	0.167
W + 2	0.369 / 0.358	0.044

Table 4.2: Summary of the expected imbalance induced by variations from the optimum MMI splitter width, ordered by increasing width. It should be noted that the pitch of the output waveguides was not altered as the width was increased. There appears to be no clear trend in the power imbalance values.

Finally, a combination of length and width errors was modelled with the BPM to determine what may happen during ‘real’ fabrication. An increase in length of 5  $\mu\text{m}$  and an increase in width of 1  $\mu\text{m}$  were chosen, as these values are the predicted worst-case fabrication imperfection. The field profile for this situation is shown in Figure 4.9. The predicted power imbalance for this case was 0.263 dB.

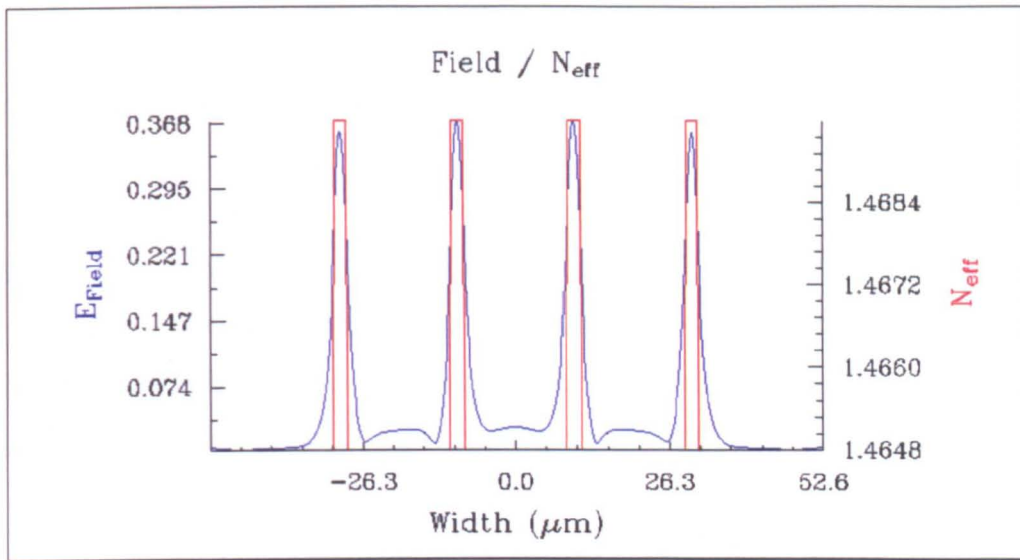


Figure 4.9: Field profile of the expected imbalance in the MMI output for the expected worst-case fabrication errors. The power imbalance was 0.263 dB.

### 4.3 Fabrication and Waveguide Characterisation

#### 4.3.1 Waveguide Fabrication

A 2  $\mu\text{m}$  thick layer of Ge doped FHD glass was deposited on a Si/SiO<sub>2</sub> wafer to give a single-mode slab waveguide at 632.8 nm, with 0.75% relative index difference from the thermal oxide undercladding, measured using the prism coupler. Dopant flow rates of 100 sccm of GeCl<sub>4</sub> and 65 sccm BCl<sub>3</sub> were used. The thickness of the layer was determined by etching through the FHD glass and thermal oxide with concentrated hydrofluoric acid and using a Talystep profilometer to measure the thickness etched. The thermal oxide was 7  $\mu\text{m}$  thick. The wafer was then diced into 1 x 1.5 cm pieces using a fine diamond saw.

Various splitter configurations were written on the FHD silica using an electron dose of 1 C.cm<sup>-2</sup>, a current of 100 nA, an acceleration energy of 50 keV and a resolution of 0.3125  $\mu\text{m}$ . The pitch of the output waveguides was varied between 17.5 and 50  $\mu\text{m}$ . 17.5  $\mu\text{m}$  was chosen as the minimum pitch to minimise coupling between adjacent output waveguides, and to allow space for future integration of microfluidic channels.

### 4.3.2 Microfluidics

Figure 4.10 shows the design of the prototype fluorescence device with a reference waveguide, prior to sealing of the microfluidic channels with a flat layer of polydimethylsiloxane (PDMS). Microfluidic channels and the analytical chambers were etched 6  $\mu\text{m}$  deep into the devices using a  $\text{CHF}_3$  dry etch, at a rate of  $60 \text{ nm}\cdot\text{min}^{-1}$ . A mask of 75 nm NiCr and AZ4562 photoresist was used to produce smooth channel sidewalls. The chamber dimensions of the prototype device were  $600 \times 50 \times 6 \mu\text{m}$ . The reference waveguide enabled verification of light coupling into the excitation waveguide.

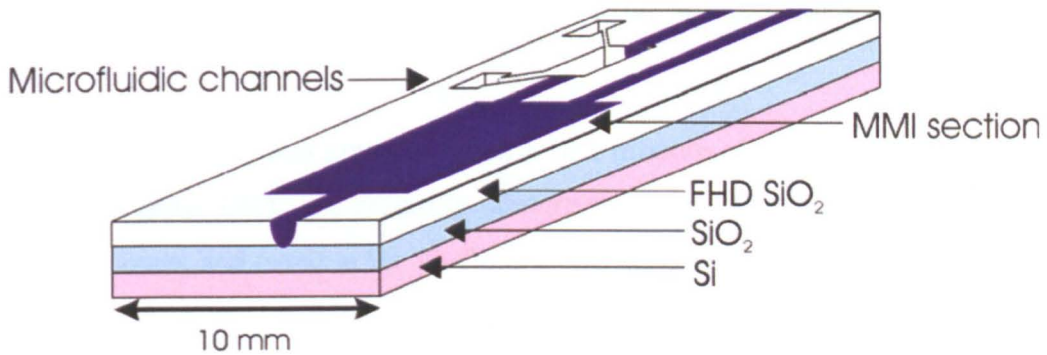


Figure 4.10: Schematic of the sensor chip prototype layout (the waveguides shown are not to scale). The prototype was used to ensure that fluorescence measurements could be made using an MMI splitter structure.

Figure 4.11 shows a complete  $1 \times 4$  array device incorporating a  $500 \mu\text{m}$  wide and  $6 \mu\text{m}$  deep microfluidic channel intersecting all output waveguides to allow simultaneous fluorescence measurements to be made. Future devices would have a discrete microfluidic chamber at each waveguide output, with the inlet and outlet microfluidics sited within the PDMS layer. The purpose of the single channel was to allow verification of the optical performance of the chip, and this type of channel has also been used for the analysis of flowing particles [Mogensen 2003].

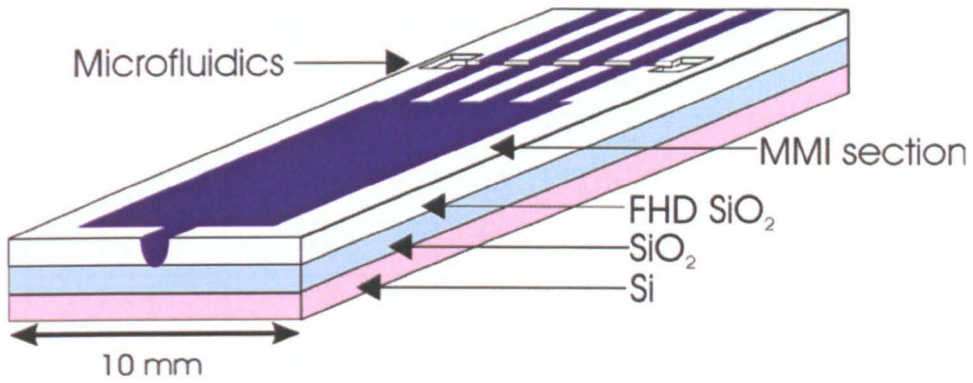


Figure 4.11: Schematic of the array chip layout (the waveguides shown are not to scale), incorporating a 500  $\mu\text{m}$  wide microfluidic channel. The channel was etched through the entire depth of the waveguides and into the thermal oxide undercladding.

The PDMS overcladding was prepared using a 10:1 mixture of precursor and activator (RS Electronics Supplies, UK). The resulting mixture was spun onto clean glass slides at 600 rpm for 30 seconds, and cured at 90 °C. Once cured, the PDMS was peeled from the slides and sealed to the waveguide chip, acting as both overcladding and as a seal for the microfluidic layer. The seal was obtained simply by pressing together the device and the PDMS, and was sufficient to allow non-pressurised flow by capillary forces along the channel without any leakage. If a permanent seal were desired, exposure of both sealing surfaces to an  $\text{O}_2$  plasma could be used. Holes were punched in the PDMS to allow filling of the channels through the reservoirs.

### 4.3.3 Optical Characterisation

The input and output waveguides were single-mode at the wavelength of operation and were approximately 2  $\mu\text{m}$  wide. A HeNe laser at 632.8 nm was used to couple light into the waveguides through a x40 lens with a N.A. of 0.65 at the input and a x20 lens with a N.A. of 0.45 at the output. A Labmaster optical power meter was used to measure the waveguide outputs. Table 4.3 summarises the measured results. It is interesting to note that the measured imbalances are of a similar magnitude as those predicted by the BPM simulations of the fabrication tolerances.

Splitter Type	Pitch 'p' ( $\mu\text{m}$ )	Width ( $\mu\text{m}$ )	Length ( $\mu\text{m}$ )	Maximum Imbalance (dB)
1 x 2	50	100	3150	0.60
1 x 3	35	105	8521	0.35
1 x 4	17.5	70	2890	0.45
1 x 4	20	80	3975	0.18

Table 4.3: Summary of different MMI splitters written in FHD Ge-doped silica. Each of the splitters shown had been optimised by simulating different lengths with the 2D BPM such that the expected imbalance was zero.

Figure 4.12 shows a micrograph of a 1 x 4 MMI splitter written with a dose of  $1 \text{ C.cm}^{-2}$ . Interference filters were used to observe the index contrast.

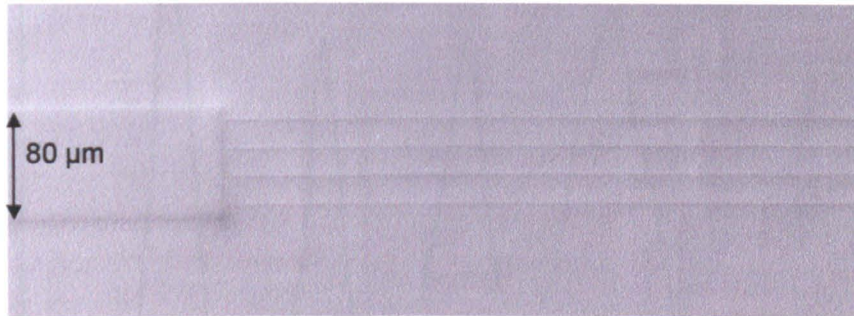


Figure 4.12: MMI splitter written by electron beam. The width of the splitter is  $80 \mu\text{m}$ . Interference contrast (DIC) filters are needed to be able to view the waveguides under the microscope. This particular splitter was used for the final array device.

The output of the splitter is shown in Figure 4.13. A digital camera (Fujifilm, Japan) was used to take this photograph. An intensity map of this output is given in Figure 4.14, where image-processing software (ScionImage from Scion Corp., USA) was used to produce the profile by analysing the intensity along the horizontal plane of the device.

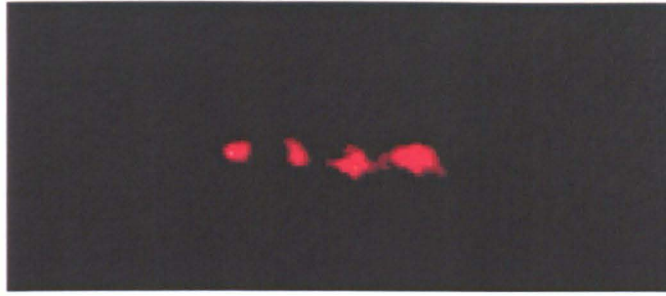


Figure 4.13: Digital photograph of the output of the 1 x 4 splitter shown in Figure 4.12. It should be noted that the quality of the waveguide facets was such that the output image was degraded. Etching of a smooth-walled microfluidic channel into the chip ensured that light incident on the fluorophore was more balanced than seen here. The contrast has been enhanced to show the four outputs more clearly.

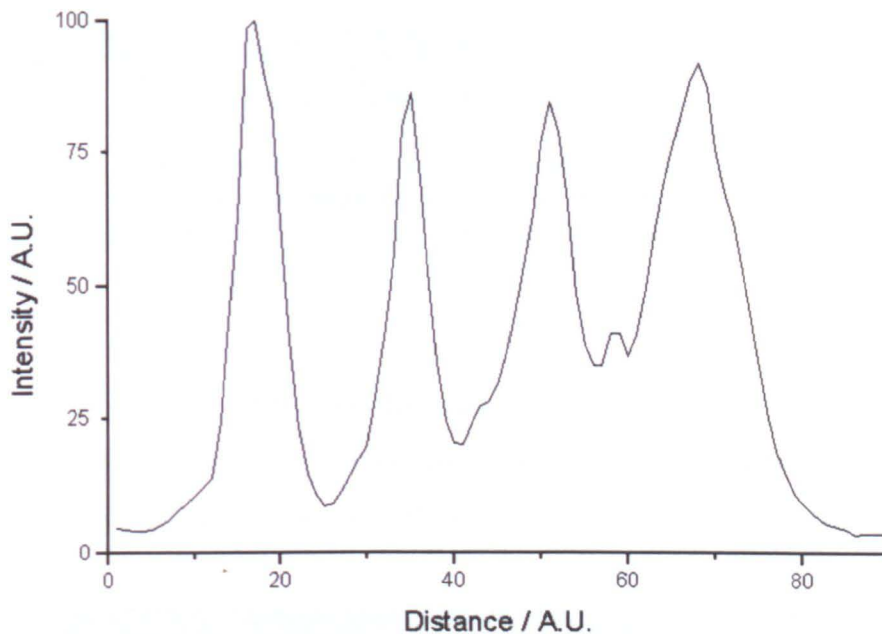


Figure 4.14: Intensity profile of the MMI splitter output in Figure 4.13. The digital image was analysed using image-processing software to produce the data.

#### 4.4 Fluorescence Measurements using MMI Splitters

Fluorescence measurements were made using a Hamamatsu H5700-50 PMT connected through an EG&G lock-in amplifier (model 5205) and optical chopper. Nile Blue dye in methanol, with excitation and emission maxima at 636 and 686 nm respectively was used in solution concentrations ranging from 20 nM to 12.5  $\mu$ M. Omega optical emission filters (670DF40) were used to remove any stray excitation light from the detected signal. Prior to use, devices were cleaned using ultrasonic agitation in acetone and methanol, followed by

immersion in a 7:1 mixture of sulphuric acid and hydrogen peroxide. The Nile Blue fluorophore solution was injected by placing a droplet at one of the inlets to the microfluidic channel, and allowing capillary forces to fill the channel. Figure 4.15 shows the optical setup used.

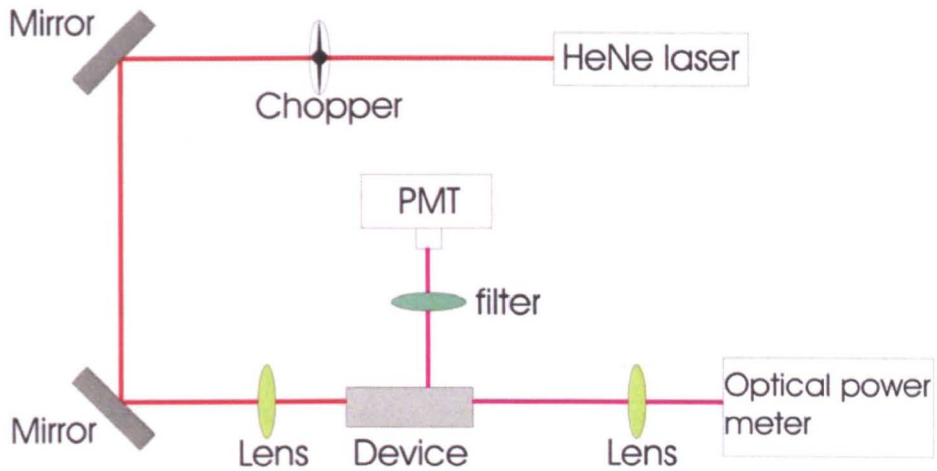


Figure 4.15: Optical setup for fluorescence measurements. The chopper and PMT were connected to a lock-in amplifier so that only light pulses at the frequency of the chopper were detected. The optical power meter was used to characterise the waveguides.

A micrograph of the array chip with the channel intersecting the waveguides is shown in Figure 4.16. Although the channel has been etched through the FHD core layer into the thermal oxide undercladding, some densification of the undercladding can still be seen.

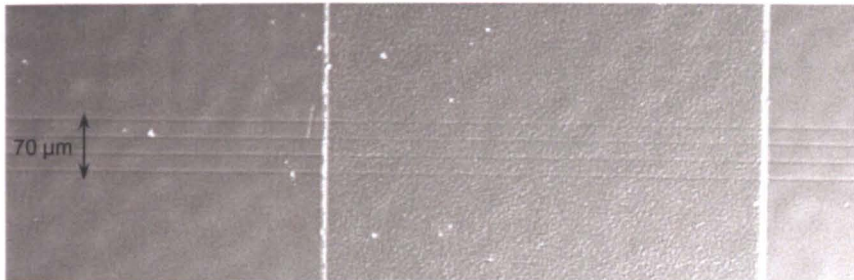


Figure 4.16: Micrograph of a microfluidic channel dry etched through the output waveguides of the 1 x 4 splitter. The channel was etched through the FHD core into the undercladding, where densification of the silica undercladding can also be seen, but to a lesser extent than the densification in the Ge-doped FHD core.

Measurements for the 1 x 2 prototype chip were taken by placing the PMT directly above the microfluidic chamber to allow orthogonal detection. Figure 4.17 shows the fluorescent

intensity measured for each concentration. For the 1 x 4 array device, the channel was filled with a 12.5  $\mu\text{M}$  solution of Nile Blue dye using a pipette tip to introduce droplets through holes punched in the PDMS. The PMT was placed at the waveguide outputs, and the maximum intensity was recorded for each successive signal peak focussed into the objective lens. Inline detection was used in this case, as an inline x20 objective lens was used to separate the output channels. The measurement error, estimated from repetition of the measurements, was  $\pm 5\%$ . Errors in reading the measurement signal may also contribute to the total error. Figure 4.18 shows the normalized peak intensity measured for each channel.

Prior to the addition of fluorescent dye, the signal was measured for the case of an empty microfluidic chamber, and with the chamber filled with methanol. With the empty microfluidic chamber, only the laser light that was not stopped by the filters was measured, whereas methanol has some associated autofluorescence and gave a higher measured signal. The methanol measurement was then subtracted from each measured fluorescent signal to give the data shown in the graph. The output fluorescence intensity measured in Figure 4.18 follows a similar variation to that observed for the waveguide outputs themselves (Figure 4.14).

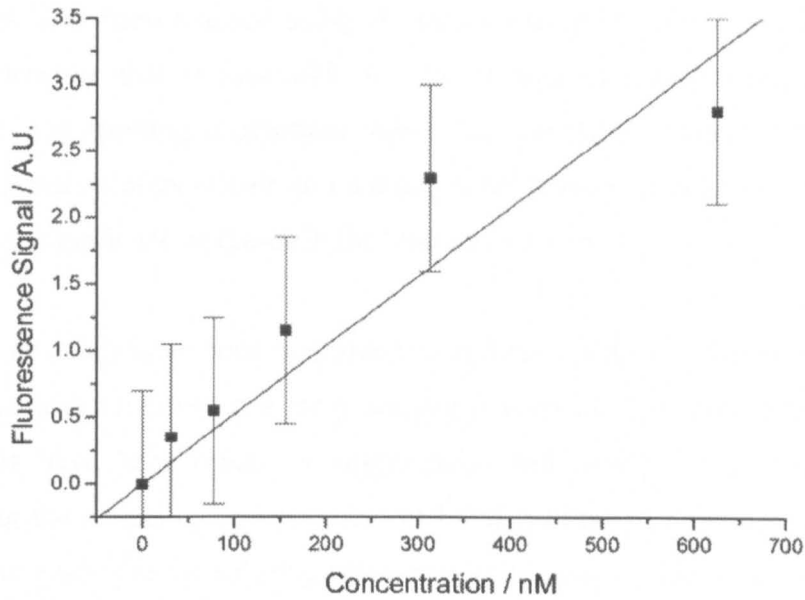


Figure 4.17: Calibration graph for prototype 1 x 2 splitter chip. The PMT was placed directly above the microfluidic chamber. 31 nM was the lowest concentration measured. The linear fit is used here as a guide for the eye. 20 nM was the lowest concentration that could be detected by the system.

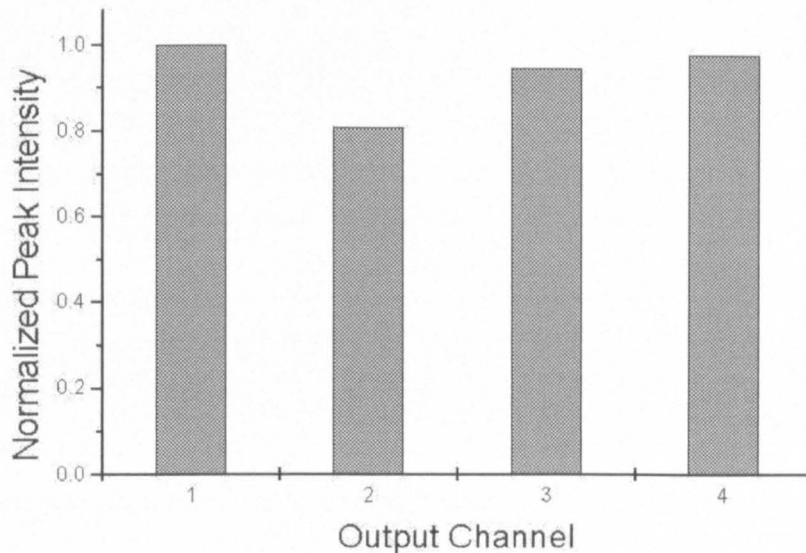


Figure 4.18: Normalized peak fluorescence intensity measured for each output channel, using a 12.5  $\mu\text{M}$  solution of Nile Blue. The PMT was placed at each of the outputs and the peak signal recorded. The data shown has the signal from the methanol-filled channel subtracted, and then each channel was normalized using the corresponding waveguide output peak from Figure 4.14.

## 4.5 Summary

MMI splitters have been realised using electron beam irradiation of FHD silica, giving a waveguide structure that is accessible for the etching of microfluidic circuits and that requires only one splitting component rather than cascaded splitters. Elimination of the need for cascaded splitters allows an increase in the density of analytical sites of an array sensor without significant increases in the total device size.

Microfluidic channels have been integrated with these splitters to form a compact sensing platform suitable for fluorescence array sensing [Cleary 2003, Cleary 2004]. Fluorescence measurements have been made on single point and multipoint excitation chips, thus demonstrating the suitability and potential of MMI splitters in Lab-on-a-Chip technology. Further improvements to the splitting uniformity of the waveguides could be made through further investigation of the intrinsic properties of the densified electron beam waveguides, and then the incorporation of more sophisticated design of the MMI splitter regions.

## **5 Time Correlated Single Photon Detection of Fluorescence from an FHD Planar Silica Sensor Chip**

The aim of the work described in this chapter was to show the suitability of single photon detection for Lab-on-a-Chip functions by integrating a single photon avalanche detector (SPAD) with an FHD glass chip similar to the ones described in Chapter 3.

Experiments were carried out to find the lowest measurable concentration of fluorescent dye, and the fundamental limits on the system were found. In addition, the decay time of the fluorescent dye was measured using the same system.

In previous work on planar optical sensors, fluorescence detection has been with either a PMT or Charge Coupled Device (CCD) camera [Ruano 2000]. Only steady-state measurements of fluorescence intensity have been taken, with no regard to the time evolution of the fluorescent signal. A PMT detector is often limited by its time response and relatively low quantum efficiency [Spinelli 1998], and the CCD camera is more useful for taking optical photographs, which must then be analysed with an intensity profiling program.

Recent advances in the waveguide technology have led to the possibility of more control of the behaviour of the guides, but to make full use of these improvements a more accurate detection system than the ones previously described should be used. One such system is time correlated single photon counting (TCSPC), using the Single Photon Avalanche Diode (SPAD) as a detector. Its use in biological fluorescence experiments is described in this chapter.

### **5.1 Time Correlated Single Photon Counting (TCSPC)**

TCSPC involves the measurement of single photons within precise time windows, defined by a repetitive pulsed source that excites the sample under test [Smith 1996]. Generally, the number of photons detected in each time window is summed, and can then be plotted in a histogram style against the total time elapsed since the excitation pulse.

The applications of TCSPC are wide-ranging. So far they have included quantum well measurements [Massa 1992, Buller 1996, Fancey 1996 (a)], carrier lifetime analysis [Massa 1994], fluorescence lifetime analysis [Birch 1993] and DNA analysis [Neumann 2000]. Most recently, the integration of a SPAD with a capillary electrophoresis system has been described [Rech 2004], opening up the field of single photon counting to Lab-on-a-Chip systems. The use of a combination of extremely sensitive detectors with time resolved counting provides possibilities in detection of smaller and smaller concentrations of analyte, possibly down to the single molecule level in line with the chip fabrication improvements that have taken place in the last few years.

By using time-correlated measurements, more information about the excited state of a particular molecule can be obtained, in comparison with using steady-state measurements of intensity such as the ones described in previous chapters. The lifetime of the excited state of a molecule, i.e. the time taken for the intensity of the excited state to drop to  $1/e$  of its maximum value, can be measured. Typical lifetimes of fluorescent molecules can be anywhere in the femto to nanosecond, and sometimes even in the microsecond range, often depending on the medium in which the fluorescent dye is dissolved [Grofcsik 1995, Hatrick 1997, Li 1997].

Another advantage of using TCSPC for biological measurements is that the measured lifetime of a fluorescent molecule should be independent of the concentration used. Therefore, a molecule can be identified by its lifetime, as long as its concentration in the solution under test is greater than the minimum detectable concentration and lower than the concentration at which particle aggregation and concentration quenching may occur. The intensity of the fluorescence measured, although a useful measure of the amount of a fluorescent dye or labelled molecule present, is therefore not essential in identifying a species, as could be very important in 'real' biological analysis. An example could be in the initial testing of a sample to see if biohazardous agents were present, prior to making any quantitative measurements. With TCSPC, concentration measurements are possible using the same data sets as those used for the lifetime measurements.

The possibility of detection of more than one fluorescently labelled molecule in the same solution becomes clear when using TCSPC. Either molecules that can be excited by the same wavelength but have different decay times, or molecules that are excited at different

wavelengths where the excitation source can be easily switched, could in principle be detected using this type of system.

The property of the fluorescent lifetime being independent of concentration is an important feature when considering reusable optical biochips. As has been mentioned in Chapters 2 and 3, if a chip has to be realigned with the excitation source, for whatever reason, the amount of light reaching the fluorophore to excite it may be different due to the waveguide coupling. Therefore, if a fluorophore can be identified by its lifetime, rather than its intensity, consistent waveguide coupling is no longer a critical issue in detection.

The pulsed source used for excitation will typically have a pulse duration of down to an order of magnitude less than the typical fluorescence lifetime. The rising edge of each pulse marks the beginning of a time window, which stops when a photon is detected. A voltage signal which is proportional to the time window measured is digitised and then used to build up the histogram. Figure 5.1 shows the components of a typical TCSPC setup, and an example of a histogram is shown in Figure 5.2.

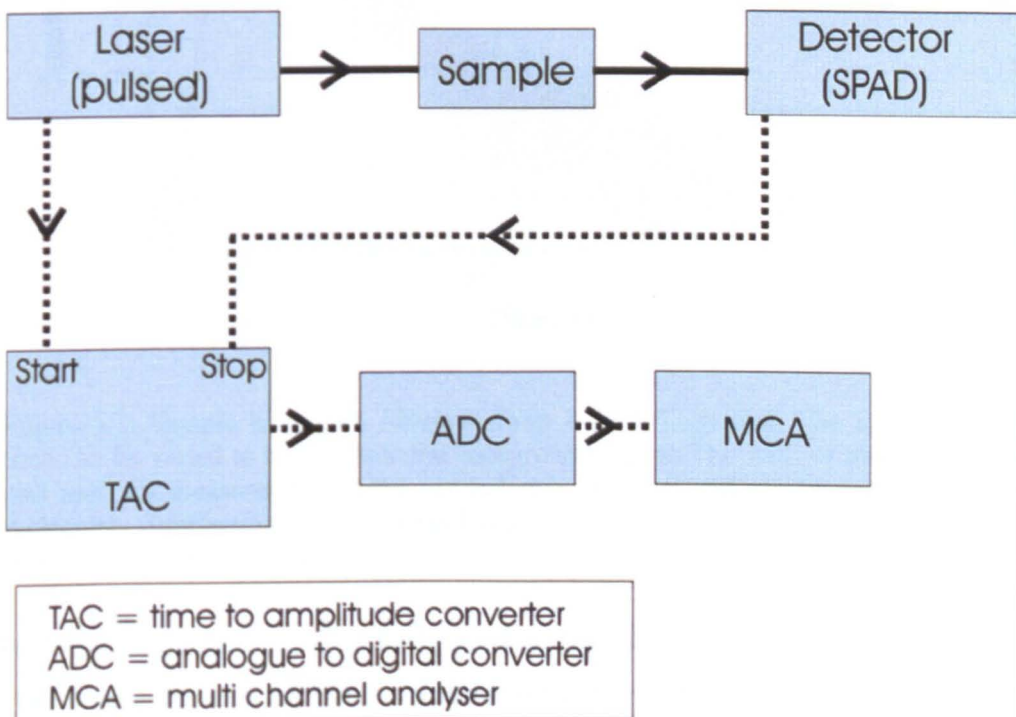


Figure 5.1: Schematic diagram of a typical TCSPC system. The laser is often a diode laser with variable repetition rates and output powers, and the detector may also be a sensitive PMT, but a SPAD is more commonly used.

The TAC starts the timing process when it receives a pulse from the laser and stops when the detector registers a photon, giving an output that is an electrical representation of the time between the laser pulse and the photon detection. After the ADC, the multi channel analyser increments a counter in the channel corresponding to the time measured by the TAC.

The detector can be chosen to match the sensitivity required of the system. PMTs, avalanche photodiodes (APDs) and single photon avalanche photodiodes (SPADs) are all suitable detectors [Cova 1996]. The PMT was originally used in TCSPC systems, but APD's and SPAD's offer the potential to match or supersede the efficiency of PMT based systems, as well as being more compact [Rech 2004].

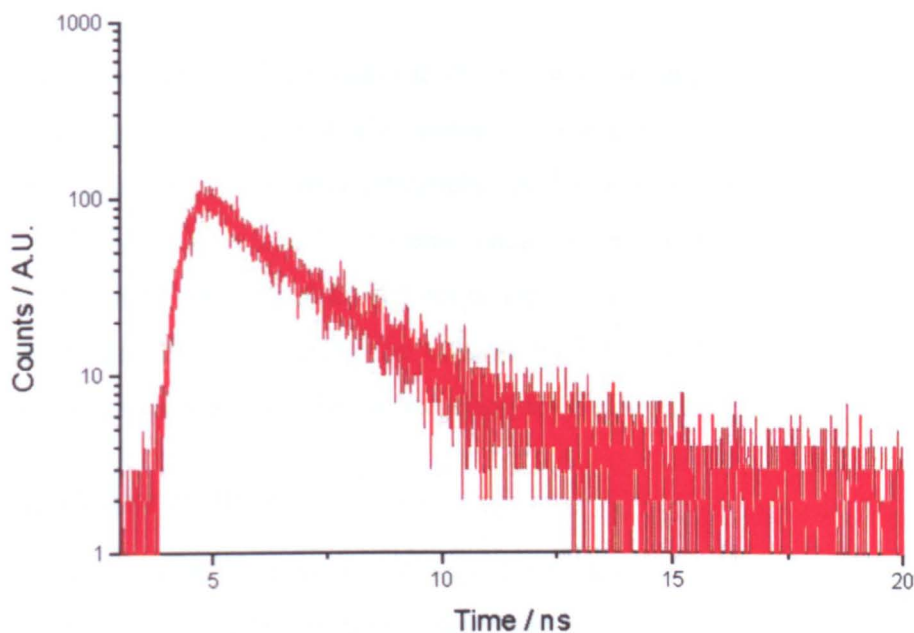


Figure 5.2: Sample histogram obtained from a TCSPC system. The total sampling time can be varied to help reduce the background signal. The ‘tail’ of the graph is the part used for measurement of the excited state lifetime, and can be used to identify molecules. Subtraction of background signals is routinely used to reduce the noise seen in this particular graph.

Reconvolution techniques are normally used to find the decay time,  $\tau$  [Fancey 1996 (b)], where the decay curve is normally in the form of an exponential. Most fluorescent dyes have single or double exponential decay times, but higher exponentials are possible.

## 5.2 The Single Photon Avalanche Diode (SPAD) as a Detector

Pioneered in the 1980s by Cova, the SPAD is a semiconductor device based around a p-n junction diode that can be used to detect single photons [Cova 1996]. Originally developed to improve on detection in situations where a PMT was used, it has successfully been used in both single-molecule detection and fluorescence decay [Weston 2004, Hatrick 1995].

The SPAD is a more sensitive version of the APD, with the main difference being that the SPAD works above the breakdown voltage of the p-n junction [Spinelli 1998]. Silicon is the predominant material for the fabrication of SPAD's, giving a device that has a high efficiency in the visible range, but declining towards the IR range. Germanium SPAD's are less well developed than the Si type, but have shown good potential at higher visible and IR wavelengths [Cova 1996].

By operating at a higher voltage than the breakdown voltage, the p-n junction SPAD has a high electric field. Therefore a single photon (charge carrier) reaching the depletion layer triggers the beginning of a carrier avalanche (multiplication) and a current flow that will continue until the voltage can be lowered back to the breakdown voltage. A quenching circuit based around operational amplifiers is used to sense the beginning of the avalanche, quench the avalanche by lowering the voltage back to the breakdown voltage, and then return the voltage back to the original operating level [Cova 1996].

## 5.3 Chip Fabrication

The chip used was an asymmetric Y branching chip with single-mode electron beam written waveguides, similar to those described in Chapter 3. For completeness, the fabrication of the chip is summarised here, but a more detailed description can be found in Chapters 2 and 3.

Figure 5.3 shows a diagram of the chip layout.

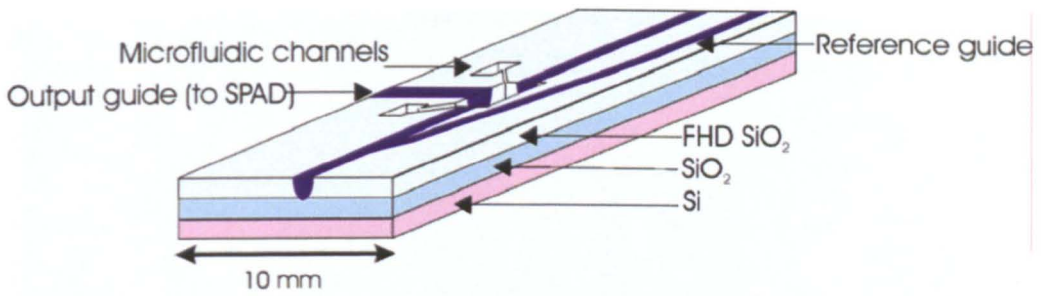


Figure 5.3: Asymmetric Y-branch chip used for TCSPC fluorescence measurements. The reference guide was used to monitor the coupling efficiency of the laser into the device, and the output guide was interfaced to an optical fibre leading to the SPAD.

### 5.3.1 Optical Components

FHD silica wafers were grown with a core/undercladding index difference of 0.7% and a thickness of 2.4  $\mu\text{m}$ . The refractive index was measured with the prism coupler technique, and the film thickness was determined by HF acid etching and Talystep profilometry. The wafers were diced into 1.0 x 1.5 cm pieces using a fine diamond saw. A thin layer (30 nm) of NiCr was evaporated onto the substrate prior to electron beam irradiation to prevent charging. 2  $\mu\text{m}$  wide waveguides were written on the FHD glass, where the refractive index change produced in the irradiated area was  $6 \times 10^{-3}$  for a dose of  $1 \text{ C cm}^{-2}$  and electron energy of 50 keV [García-Blanco 2004].

The BPM program was used to predict the asymmetric Y-branch splitting ratio. The splitting ratio was dependent on the final separation of the excitation and reference waveguides, and a ratio of 80:20 was chosen. Cosine S-bends with a horizontal length of 9000  $\mu\text{m}$  were used, and the output orthogonal waveguide was tapered down to 80  $\mu\text{m}$  at the output for fibre compatibility.

### 5.3.2 Microfluidic Components

Channels 9  $\mu\text{m}$  deep were dry etched through the waveguide core and undercladding using  $\text{CHF}_3$  chemistry. The etch rate of the FHD silica was  $60 \text{ nm min}^{-1}$ . A bilayer mask of NiCr and photoresist was used to produce smooth channel sidewalls. The chamber dimensions were 100 x 50  $\mu\text{m}$ , and the channels were approximately 80  $\mu\text{m}$  wide. Figure 5.4 shows a micrograph of the chip after etching.

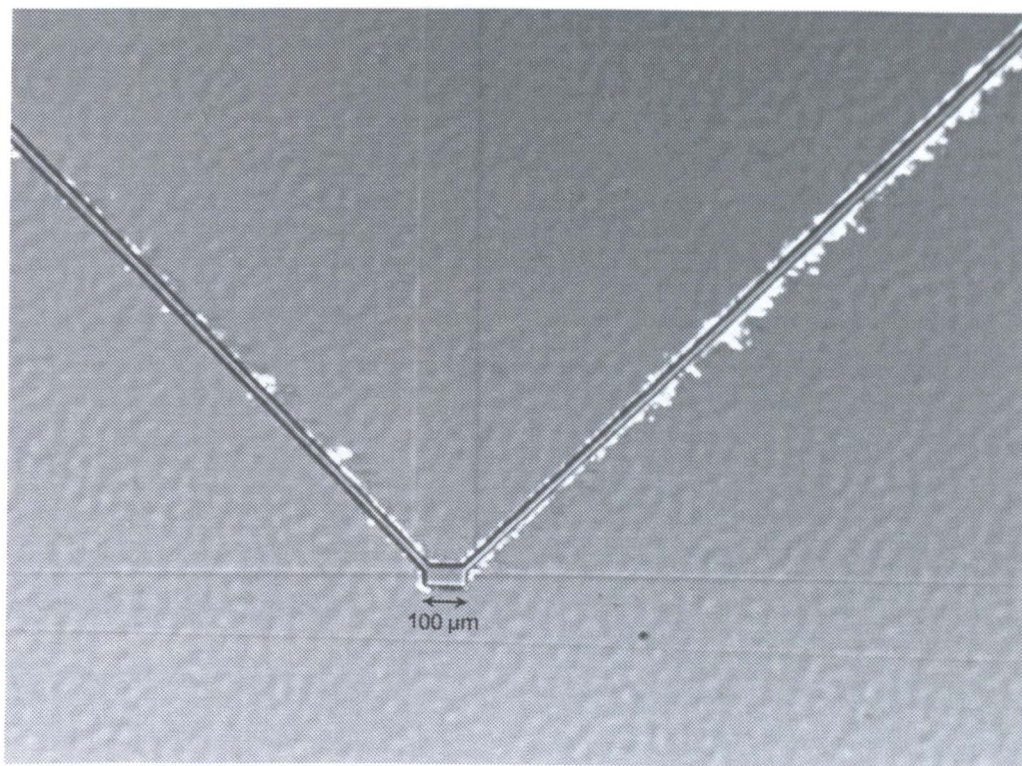


Figure 5.4: Optical micrograph of the chip used for TRPL measurements at 5x magnification. The output guide is tapered to approximately 80  $\mu\text{m}$  at the chip output, although the edge of the chip is not shown in this figure.

From the micrograph above, there is a clearly observable area around the microfluidic channels where some redeposition of photoresist during etching has occurred. This was not a normal occurrence during the course of the project work, and was thought to be due in this case to the use of the thinner S1828 photoresist, rather than AZ4562 as the mask.

A combination of acid cleaning and exposure to an  $\text{O}_2$  plasma for several minutes was used to ensure that no photoresist remained on the chip. Therefore, the marks seen on the chip above are thought to be artefacts in the FHD glass itself. The chip was tested in the TCSPC setup already described, and its performance deemed satisfactory in that time-correlated fluorescence lifetime measurements could be made, so it is believed that the damage was only superficial and may have occurred near the end of the etch. Closer inspection under the microscope showed that the etch quality of the microfluidic chamber walls appeared unaffected, as shown in Figure 5.5.

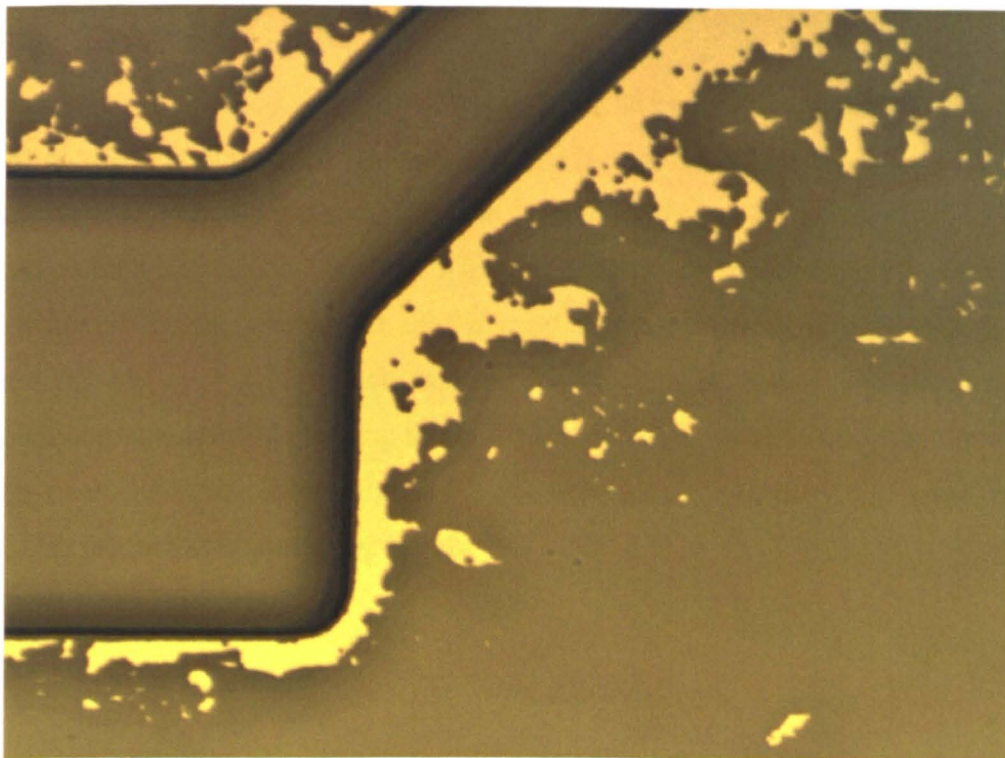


Figure 5.5: Optical micrograph at 100x magnification showing the damage that occurred during etching of the microfluidic channels.

Prior to use, the chip was cleaned in an ultrasonic bath of acetone followed by methanol and rinsed in reverse osmosis (RO) water. This was followed by an acid clean, consisting of a 7:1 mixture of sulphuric acid ( $\text{H}_2\text{SO}_4$ ) and hydrogen peroxide ( $\text{H}_2\text{O}_2$ ).

The PDMS cladding was prepared using a 10:1 mixture of precursor and activator and spun onto clean glass slides at 600 rpm for 30 seconds, then cured at 90 °C. Once cured, the PDMS was peeled from the slides and sealed to the waveguide chip.

Inlet holes were punched in the PDMS, and the fluorescent dye was introduced using a pipette tip. (A complete setup would also have a flow system to introduce the liquid through capillaries, but as this was primarily a feasibility study, it was considered unnecessary to implement the flow system at this time). Nile Blue dye in methanol, with excitation and emission maxima at 636 and 686 nm respectively, was used.

## 5.4 Experimental Setup

Excitation was provided by a pulsed 630 nm diode laser that was capable of producing pulses of picosecond duration. Light was coupled in through a x20 lens with a NA of 0.3, and the reference signal for monitoring the laser coupling collected from the Y-branch waveguide with a x20 lens of NA 0.4. White light imaging was used for alignment of the sample with the beam. The power of the laser was adjusted to give an output at the reference branch of 1  $\mu\text{W}$ , which was monitored by an optical power meter. The orthogonal output waveguide leading to the SPAD was used for collecting the fluorescence from the microfluidic chamber. Figure 5.6 shows the experimental setup used, with the TCSPC instrumentation omitted for simplicity.

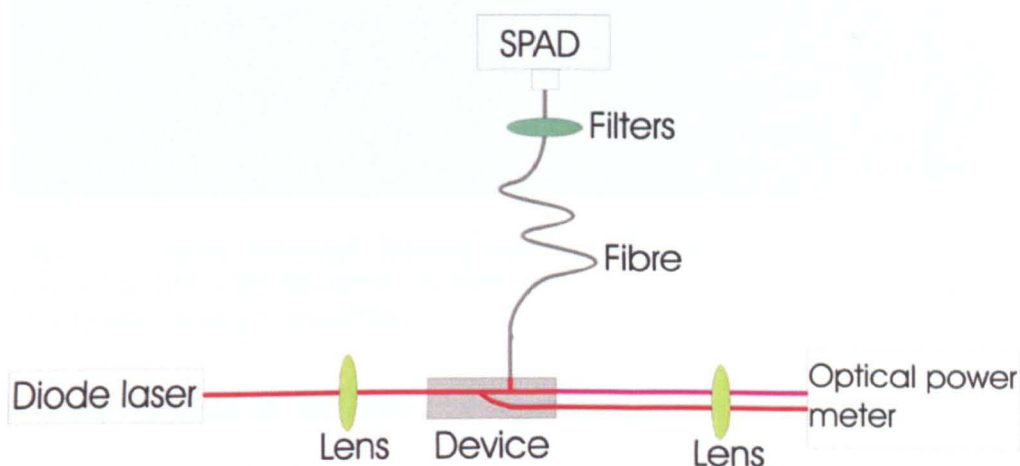


Figure 5.6: Experimental setup used for TRPL measurements. The computer equipment used to collect the data is omitted from this diagram for simplicity, and it is already shown in Figure 5.1. Both ND filters and bandpass filters were used between the chip output (orthogonal waveguide) and the SPAD to prevent saturation of the SPAD at higher dye concentrations.

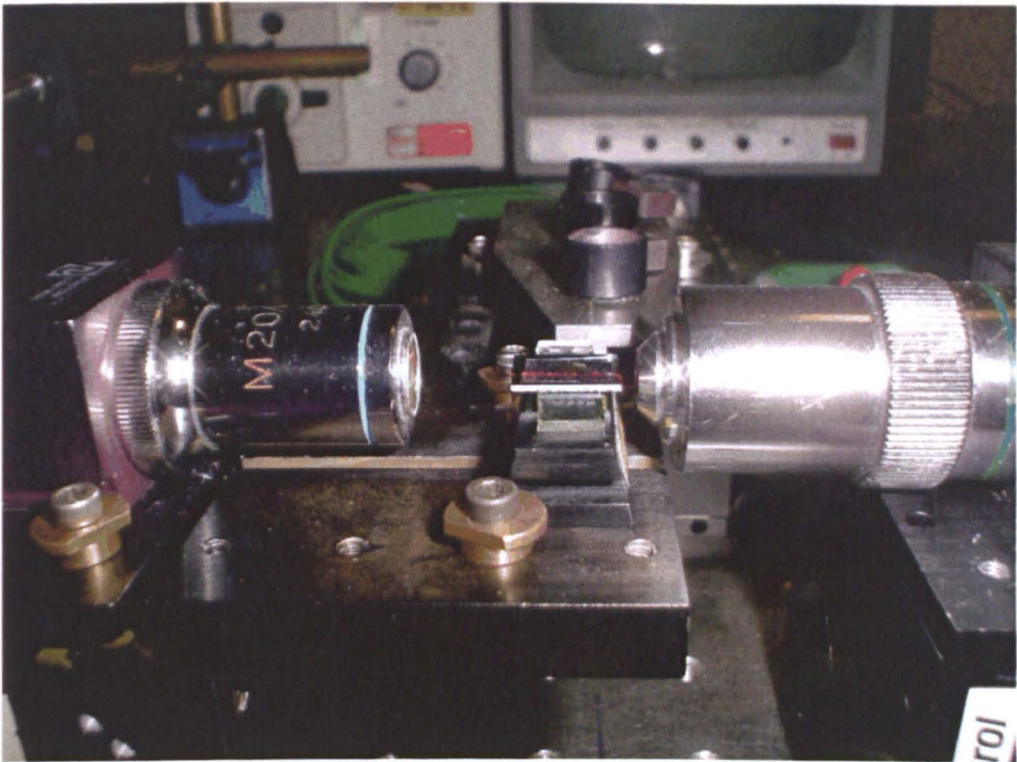


Figure 5.7: Digital photograph showing light being guided through the Y-branch chip used in the TRPL measurements. A fibre was placed orthogonally at the end of the output guide, leading to the SPAD.

## 5.5 Measurement of Different Fluorescent Dye Concentrations

Dye concentrations ranging from 5 mM to 750 pM were prepared by dilution in methanol. As a first test, the ability of the system to identify different concentrations of dye was tested, as shown in Figure 5.8. Clearly, for increasing dye concentration, the peak response of the system increases. Once the neutral density (ND) filters used in each case were accounted for, the response was still seen to increase with concentration.

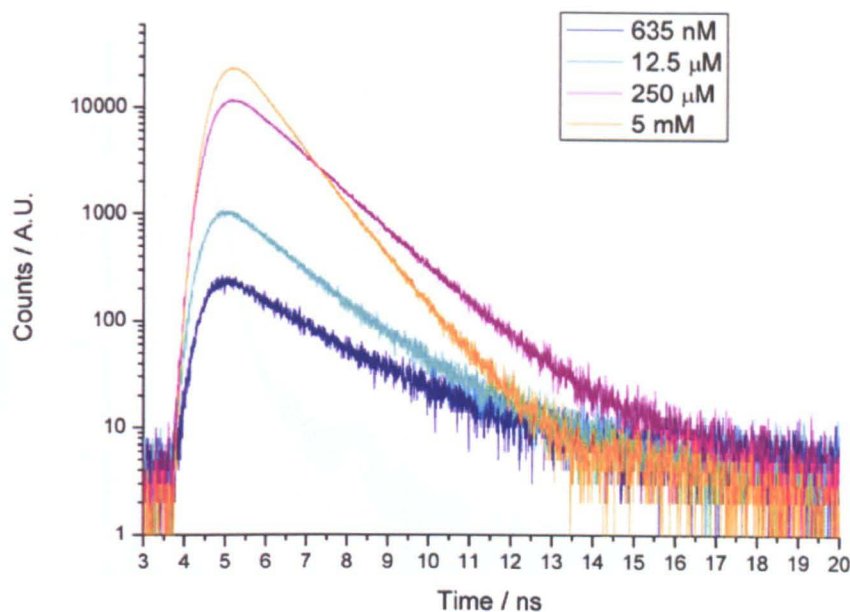


Figure 5.8: Measured response of four different concentrations of Nile Blue dye. The plots shown here are not corrected for the ND filters used.

### 5.5.1 Limitations on the Minimum Detectable Concentration

The most significant limitation of the experimental system used was the source laser, for which the instrumental response is given in Figure 5.9. Although the primary excitation wavelength was 630 nm, harmonics were observed around 690 nm, near to the emission wavelength of the fluorescent dye. Figure 5.10 shows the system response through the chip prior to introduction of any reagents. Bandpass (BP) emission filters (Omega 670DF40) were used when measuring the response, but some residual scattered laser light was still observed due to the sensitivity of the detector. Several narrowband (NB) filters with a 10 nm passband in addition to the standard emission filters failed to eradicate the problem, and as they were found to significantly degrade the overall detected signal they were discarded.

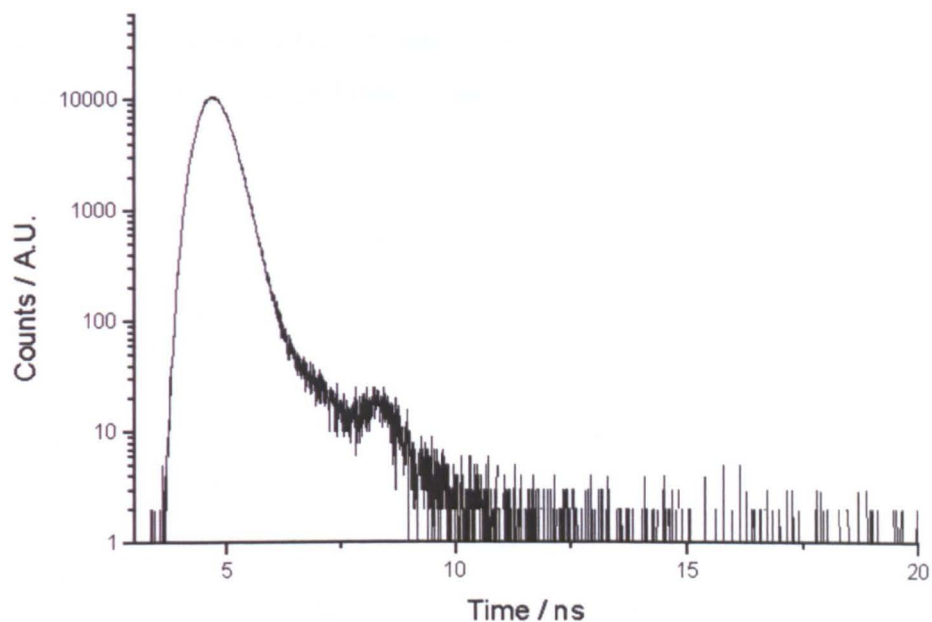


Figure 5.9: Measured response of the system with an empty microfluidic chamber and no filters. This instrumental profile is needed for the calculation of the decay time.

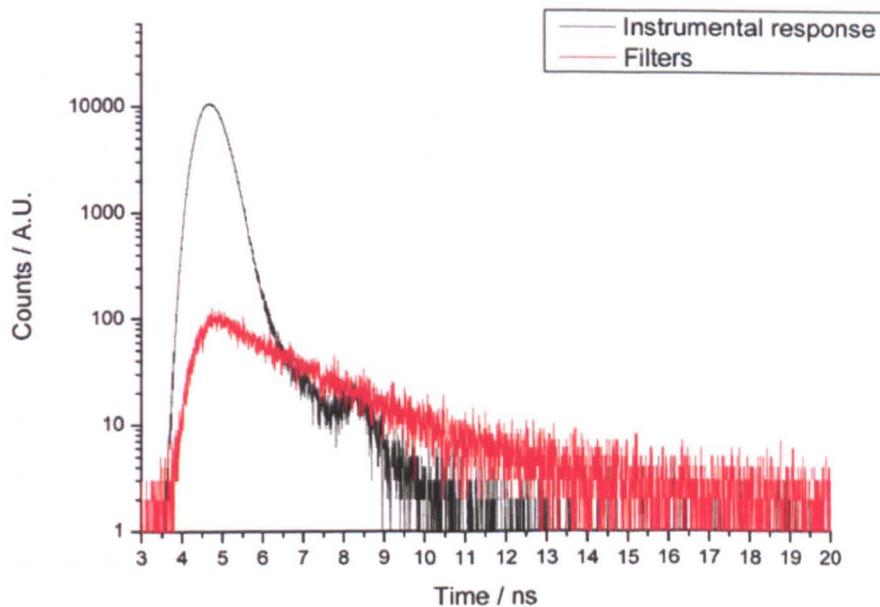


Figure 5.10: Measured response of the system with an empty microfluidic chamber plus bandpass and emission filters.

The second source of unwanted detected signal was the methanol in which the dye was dissolved. Figure 5.11 shows a response taken with the detection chamber filled with methanol only. The standard BP emission filters were used. The conclusion to be drawn from this finding is that methanol itself fluoresces around the detection wavelength of 686 nm.

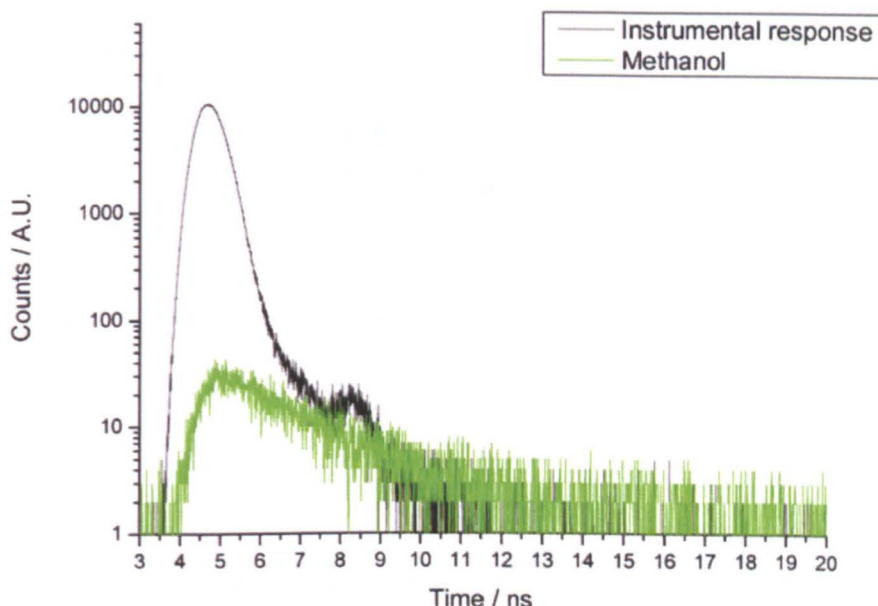


Figure 5.11: System response with the microfluidic chamber filled with methanol. As the response is different from the laser response with filters, methanol itself must have some intrinsic autofluorescence when excited at 630 nm. In previous chapters, this was accounted for by subtracting the measurement taken with the chamber filled with methanol.

Therefore, the minimum concentration detected had to show a response that could be clearly distinguished from the laser and methanol responses. Subtraction of these background signals from the measured signals shows the true measured signal.

## 5.6 Measurement of the Decay Time of Nile Blue Dye

Finding the smallest detectable dye concentration was considered to be the primary goal of this TRPL experiment. However, use of the SPAD detector allowed measurement of the decay times of the dye whilst intensity measurements were also being made. A range of concentrations down to 1.5 nM were measured successfully.

For each measurement taken, the decay time of the dye was recorded. As shown in Figure 5.12, a slight downward trend of measured decay time was observed with increasing concentration. It is thought that the decreasing trend seen was due to quenching at higher concentrations. One possible reason for the observed error could be the polarisation properties of the dye, although this would have to be investigated further.

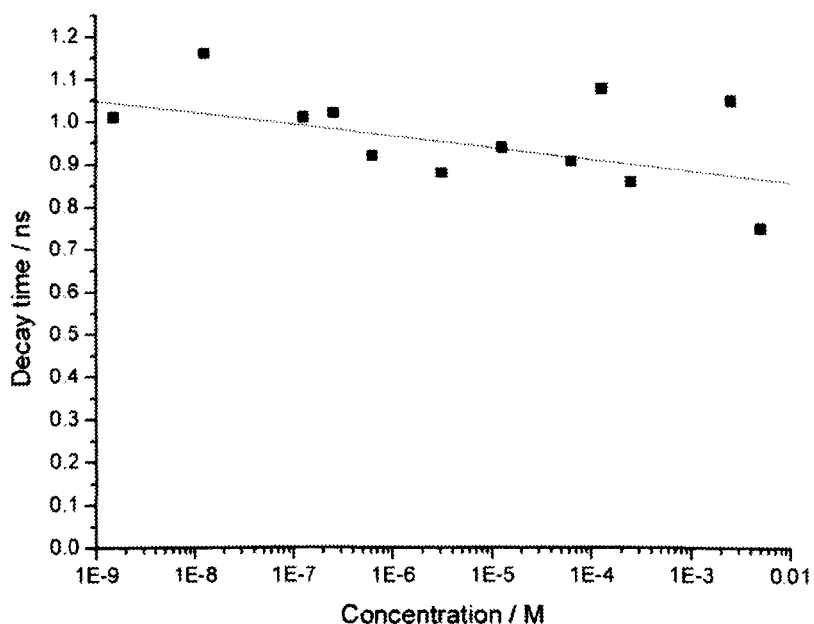


Figure 5.12: Measured decay times for a wide range of dye concentrations. The smallest measurable concentration was 1.5 nM.

## 5.7 Summary

The application of TCSPC to biological analysis with optical sensor chips has been discussed in this chapter. The ability to look at the time evolution of the fluorescent response of Lab-on-a-Chip devices allows investigation of the fluorescence lifetime as well as the fluorescent intensity that is normally measured in non-time resolved situations.

An FHD sensor chip using Y-branches and etched microfluidics has been interfaced to a SPAD to allow time resolved measurements of fluorescence in the microfluidic chamber to be made. Measurements were made of both the intensity and the lifetime of the dye fluorescence excited by a 630 nm diode laser. The fluorescence intensity was shown to increase with increasing dye concentration, but the fluorescent lifetime was mostly independent of the concentration.

As the fluorescent lifetime was shown to be largely independent of concentration, the identification of biological molecules regardless of their concentration is possible using such a system. A cell, protein or DNA strand labelled with a fluorescent molecule of known lifetime could therefore be detected using a TCSPC system such as the one described in this chapter. Concentration information, if needed, could also be extracted through measurement of the peak intensity.

In principle, a TCSPC system could also be used for array measurements, or for scanning along a sample with an optical fibre. Further work on reducing the background, possibly by the investigation of a number of dyes and solvents, would ensure that the system has a better detection efficiency in the case of low fluorescent molecule concentrations.

# 6 UV Laser Irradiation for Optical Waveguide Definition

Work in this chapter covers the development of a new high resolution NiCr masking technique to define waveguide structures in Ge-doped FHD silica using 157 nm UV radiation, and results are shown concerning the production, characterisation and optical measurements obtained from the fabrication of waveguides.

Waveguides written in silica by UV irradiation provide a new opportunity for integration of these optical structures incorporating microchannels for microfluidics and for biological sensing. The possibility of laser micromachining these channels with the same laser also exists, thus allowing both the optical and microfluidic components of a sensor chip to be fabricated consecutively entirely by laser processing [Herman 1999 (a,b)].

## 6.1 UV Photosensitivity of Silica

The photosensitivity of silica to UV and visible light provides a method by which the refractive index of silica can be permanently increased [Hill 1978, Kashyap 1999, Poumellec 2002]. It has been used successfully to write waveguide components, and also high resolution structures, often of the order of a few hundred nanometres such as Bragg gratings [Hill 1993, Albert 1999].

Hill first demonstrated the effect of a continuous wave (CW) argon ion laser at the visible wavelength of 488 nm on silica fibres with a Ge-doped core [Hill 1978]. Further work in this field has concentrated on the exposure of various types of silica to UV irradiation, with the intention of causing permanent refractive index changes of as great a magnitude as possible [Ebendorff-Heidepriem 2004].

As yet, the exact mechanism for the index change is unknown, but the result of the irradiation is currently thought to be similar to that induced by electron beam densification; namely compaction and colour centre formation possibly as a result of bond breaking and vacancies appearing in the irradiated material [Poumellec 1997, 2002]. Compaction of a material is predicted by the Lorenz-Lorentz relationship to provide an increase in refractive index, with silica being receptive to compaction due to its open 3D structure [Ebendorff-

Heidepriem 2004]. Colour centre formation in Ge-doped silica arises from excitation of the Ge-O bonds. Doping of silica cores with Ge results in absorption around 240 nm due to oxygen-vacancy defects brought about by the addition of the Ge [Meltz 1989, Bilodeau 1993]. However, strong photosensitivity in Ge-doped silica has been observed in cases where significantly shorter (up to 157 nm) irradiation wavelengths have been used, exciting other defect states at 195 and 215 nm [Williams 1991, Chen 2001 (b)]. In this case, the increase in refractive index has been explained by some as caused by two-photon absorption, leading to bond-breaking and structural relaxation which cause compaction in the irradiated area [Albert 1999]. However, strong experimental arguments also exist for the case of linear one-photon absorption [Zhang 2001 (a)].

### 6.1.1 Photosensitisation

Poumellec has shown that the refractive index modification of silica can be increased by hydrogen loading or ‘soaking’ of up to one month prior to exposure of the sample to UV irradiation [Poumellec 2002, Chen 2001 (b), Chen 2002 (a)]. Photosensitisation of silica samples by hydrogen loading has been used by a number of authors to enhance the effect of the UV irradiation. Typical increases in photosensitivity have been reported as up to ten times that observed without hydrogen loading [Maxwell 1992, Maxwell 1993, Lemaire 1993, Chen 2002 (b)]. Clearly this method significantly increases the fabrication time, and the irradiation must be performed soon after removal of the sample from the hydrogen, or the sample must be stored in a liquid nitrogen atmosphere.

Bilodeau et al describe the photosensitisation of Ge-doped waveguides without the modification of any surrounding cladding material using a flame-brushing method [Bilodeau 1993]. A predominantly hydrogen flame at 1700 °C was used on both optical fibre and planar FHD waveguide cores. For the Ge-doped FHD glass, an increase in layer refractive index due to the flame was also observed in addition to the increase in photosensitivity. The refractive index change induced by UV irradiation at 249 nm after photosensitisation was  $9.5 \times 10^{-4}$ , a factor of 10 greater than that induced without photosensitisation.

### 6.1.2 Gratings Written in Fibres by UV Irradiation

Excimer lasers with wavelengths as short as 193 nm have been used to write gratings in both doped and undoped silica fibres [Othonos 1997, Kashyap 1999, Albert 1999]. The

periodic fluctuation in refractive index in the fibre allows light to be coupled in and out, and has potential applications in wavelenth division multiplexing (WDM), gain-flattening and noise reduction [Mizrahi 1993].

### 6.1.3 Channel Waveguides Fabricated by UV Irradiation

Current applications of waveguides written in silica by UV are in the telecommunications industry, but the versatility of the technique indicated a potential application in the development of these waveguides for use in biological sensors. Waveguides can be written in a planar Ge-doped layer, yielding a buried structure similar to that formed by electron beam irradiation as described in Chapters 2, 3 and 4.

Svalgaard first reported the use of a 244 nm Ar<sup>+</sup> laser to write waveguides on Ge-doped PECVD planar silica films, where a refractive index change of  $2.5 \times 10^{-3}$  was achieved without hydrogen loading [Svalgaard 1994]. However, the PECVD process may have resulted in the presence of hydrogen in the silica, thus enhancing the index change by photosensitising the silica.

Simultaneous writing of Bragg gratings and planar waveguides in Ge-doped FHD glass was reported by Marques [Marques 2002]. Flame brushing by an oxy-hydrogen torch, such as the one used in the FHD process, was used in this case to photosensitise the glass prior to UV exposure. Photosensitisation using flame brushing results in permanent hydrogenation, as opposed to the hydrogen soaking method described by Poumellec [Bilodeau 1993]. A maximum refractive index change of  $4 \times 10^{-3}$  was obtained using a 248 nm laser.

Svalgaard reported directly-written symmetric Y-branches in silica using a 244 nm focussed laser beam [Svalgaard 1997]. Splitting ratios of almost 50 % were achieved. Knappe has also recently presented MMI splitters written by UV irradiation [Knappe 2003].

If the time-consuming process of photosensitisation by hydrogen loading could be overcome or bypassed, the UV writing technique would be an extremely attractive method of producing optical waveguide components, as the UV lasers used are commercially available.

## 6.2 F<sub>2</sub> UV Lasers for Photonic Fabrication

Researchers at the University of Toronto have pioneered the use of 157 nm radiation for the fabrication of photonic circuits for a number of years [Herman 1999 (a,b)]. To date, this is the shortest wavelength that has been successfully employed to induce refractive index changes in silica [Chen 2003].

### 6.2.1 Background to Waveguide Fabrication

A commercially-available F<sub>2</sub> laser from Lambda Physik (model LPF220i) was used at the University of Toronto. The laser was capable of producing 20 mJ pulses of down to around 3 ns duration with a repetition rate of 100 Hz. Relatively low energy pulses were used to irradiate the silica so as to produce densification of, rather than damage to, the sample surface. The laser can also be used for micromachining of silica, for example for the shaping of ridge waveguides and microchannels [Herman 1999 (b), Herman 2000 (a)].

The laser beam was typically passed through a series of homogenising lenses (9x9 cylindrical lens arrays) to focus the beam and improve the uniformity. The area from the laser output, through the beam-shaping optics to the sample, was housed in a sealed chamber through which nitrogen was pumped so as to avoid absorption of the UV energy by air before it reaches the sample [Herman 2001 (a,b)].

Writing of patterns can normally be achieved in two ways; xyz translation of the sample with respect to a focussed laser beam, or by irradiating the sample through a CaF<sub>2</sub> mask plate. In the case of sample translation, a computer-controlled stage is used to move the sample, and when a mask plate is used, progressive degradation of the plate has been observed due to the irradiation process [Ho 2003]. Therefore, a new masking process was evaluated for the purpose of waveguide writing by flood exposure.

The 157 nm photons generated by the laser are thought to provide absorption near the band edge of Ge-doped silica, as illustrated in Figure 6.1 [Chen 2001 (a,b)].

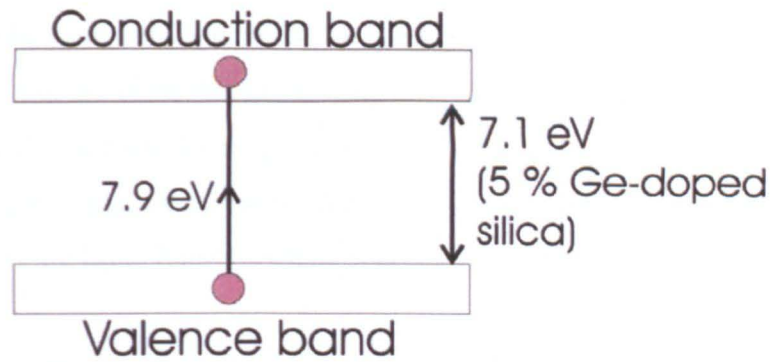


Figure 6.1: The linear single photon transition thought to be responsible for the refractive index change in Ge-doped silica when irradiated by the 157 nm  $F_2$  laser. The 7.9 eV photon energy is close enough to encroach on the bandgap of Ge-doped silica.

## 6.2.2 Refractive-Index Modification of Ge-doped FHD Silica

FHD silica has previously been shown to be suitable for refractive index modification by UV laser [Marques 2002]. The aim of this work was to write waveguides on FHD silica samples that had been fabricated at Glasgow University, and to find a new high resolution masking technique that did not require the production of a separate mask plate.

Each sample to be irradiated was prepared with a surface mask of 100 nm NiCr, allowing the waveguide pattern to be positioned correctly on the sample. There are several advantages to using a mask that is directly attached to the sample to be irradiated. The first is that the initial expense of creating a  $CaF_2$  mask plate is avoided. This is a particularly significant feature in a research or development environment, where a waveguide design may be evolved and improved through time after each irradiation. In this case, a new mask would have to be fabricated for each design improvement.

The second advantage is that by attaching the mask to the sample, pattern alignment can be controlled precisely and only need be done once, after which the position of the mask pattern on the sample is fixed until after the irradiation. The mask can be easily removed in a standard Cr etch solution.

### 6.2.2.1 Sample Preparation

The waveguide patterns in this experiment were defined by electron beam lithography of PMMA, thus allowing extremely high-resolution patterns to be transferred to the sample.

Thin layers can be spun onto wafers in a manner similar to that of photoresist spinning, and as the polymer can be cross-linked by exposure to both electrons and UV light, it has become commonly used for defining nm-scale patterns that can be written with an electron beam. An example is photonic crystal pattern structures, where the PMMA resist can then be used as a masking layer for dry etching precise, repeated structures.

The resolution used for the waveguide masks was  $0.3125\ \mu\text{m}$ , the lowest resolution available on the beamwriter. This resolution was considered sufficient as the waveguide widths were designed to be either  $4$  or  $2\ \mu\text{m}$ .

Fabrication of the mask required the steps shown in Figure 6.2. The process was developed using a similar process for grating fabrication as a basis [García-Blanco 2003].

1. Clean the Si/SiO<sub>2</sub>/FHD substrate using the standard organic clean in acetone, methanol and then RO water.
2. Spin the first layer of PMMA 2010 at 5000 rpm for 60 s, and then bake for 1 hour at 180 °C.
3. Spin a second layer of PMMA 2041 at 5000 rpm for 60 s, and bake for 1½ hours at 180 °C.
4. Coat substrate with 30 nm 60:40 NiCr to prevent substrate charging, as in the case when patterns are to be directly written on the FHD glass. A Plassys electron beam evaporator was used in this work.
5. Expose the reverse of the waveguide pattern using the beamwriter. Therefore all regions of the PMMA where the NiCr mask is to be are exposed to the electron beam.
6. Remove the NiCr in a Cr etch solution before developing the PMMA pattern using a 1:1 mixture of IPA and MIBK for 60 s at 23 °C. The waveguide pattern is at this stage the only area where PMMA is left.
7. Evaporate 100 nm of NiCr on to the sample. A 30 s O<sub>2</sub> plasma ash prior to the evaporation helps to clean the substrate and promote NiCr adhesion.
8. Lift off the remaining PMMA in the waveguide regions by immersing the sample in an acetone bath for approximately 3 hours. Ultrasonic agitation or gentle heating in a warm water bath may be used to shorten the time needed to remove the PMMA.
9. Lift the sample from the acetone bath under a constant jet of acetone or IPA to prevent re-adhesion of the removed NiCr.

Figure 6.2: Process steps for fabrication of a surface NiCr mask on FHD glass. The use of PMMA lift-off allows high resolution masks to be aligned on the sample prior to UV irradiation. The pattern is defined in reverse by electron beam irradiation of the PMMA.

Each 1 x 1.5 cm FHD silica sample contained 3 sets of identical waveguide patterns, with the total vertical area being less than 2 mm. The length of each waveguide mask was 1 cm. The sample was placed vertically, and irradiated through a slit to preserve the other two sets of waveguides. Figure 6.3 shows the set-up inside the sealed irradiation chamber.

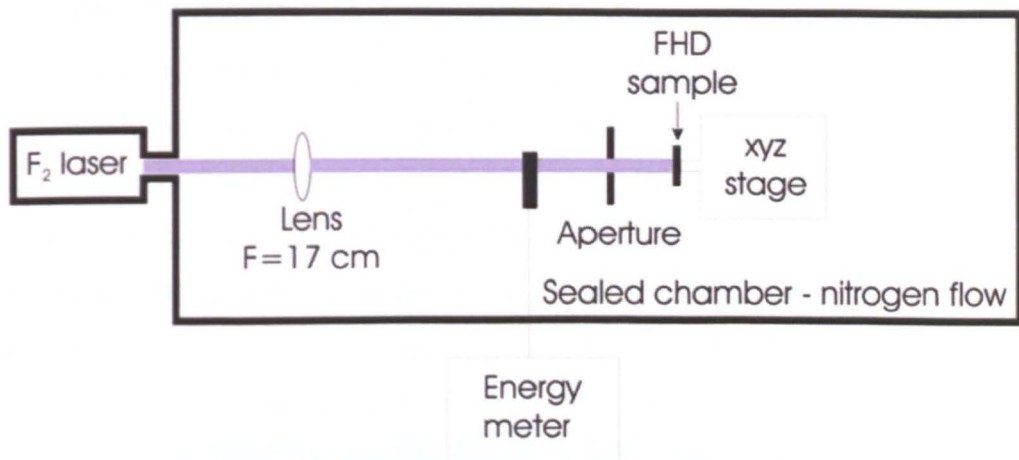


Figure 6.3: Optical arrangement inside the  $F_2$  laser irradiation chamber for writing of straight waveguides and Y-branches. The white-light imaging normally used for aligning the mask with the sample is not needed, as the NiCr mask is already attached to the sample. An aperture was placed directly in front of the sample to prevent irradiation of the rest of the sample. The energy meter was used to monitor the laser energy during the irradiation.

The aperture and sample were placed on a separate base plate, so that the aperture could be aligned to the sample and then the base plate placed inside the chamber. Alignment of the mask with the sample would normally be done with the sample inside the sealed chamber, using gloves attached to the chamber to allow access to the xyz stages. However, as the NiCr mask was already in place on the FHD sample, there was no further need for alignment.

Straight waveguides were investigated before Y-branches, in order to determine the suitability of the FHD glass and the approximate fluences needed to create a waveguide. Three germanium compositions were used: approximately 3, 7 and 10 weight %, corresponding to  $GeCl_4$  flows of 50, 100 and 150 sccm respectively. All other parameters in the FHD process were kept constant, including the boron flow rate of 65 sccm. Refractive indices of the films were measured using a standard prism coupler technique at 632.8 nm. The change in refractive due to the irradiation was determined at a later stage,

and the expected change was only estimated prior to fabrication. All mask fabrication and sample preparation was performed in the clean rooms at the University of Glasgow.

### 6.3 Results from UV Irradiation of FHD Silica

#### 6.3.1 Mask Preparation

An example of a completed mask is shown in Figure 6.4. The apex of the Y-branch is one of the most critical areas in the fabrication of such devices as the accuracy of splitting is dependent on the branch being of the exact dimensions specified in the design. Any deviations in the actual device from the design will result in unbalanced splitting in the case of symmetric branches, as discussed in Chapter 3. Photolithographic processes often do not produce such accurate masks due to the inherent resolution limits, and small features such as Y-branches or thin waveguides are difficult to resolve properly.

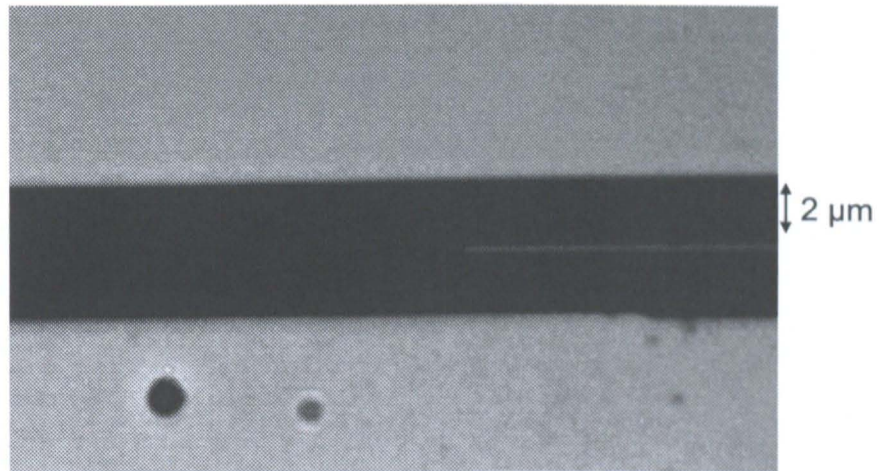


Figure 6.4: Optical micrograph of a completed NiCr mask, showing the apex of an asymmetric Y-branch. The dark area is the FHD silica surface that is to be exposed, and the lighter area is the NiCr.

A more straightforward approach to the mask production would be to evaporate 100 nm NiCr directly on to the FHD glass, then define the pattern using electron beam lithography of PMMA as above, but only exposing the waveguide area, and etching the NiCr directly. However, cracking of the NiCr layer during the 180 °C PMMA baking steps limits the quality of the mask.

The cracking may be related to problems encountered by Marques [Marques 2002], where cracking of thermally evaporated NiCr layers was observed during UV irradiation of masks

patterned by photolithography. However, when using the lift-off process shown in Figure 6.2 above, no damage to the mask was observed after any of the F<sub>2</sub> laser irradiation processes.

### 6.3.2 Fabrication and Characterisation of Straight Waveguides

Sets of 4  $\mu\text{m}$  wide guides on each composition were irradiated to ensure that the process would work before fabricating more complex structures. Table 6.1 summarises the samples and fluences used.

Sample	Germanium Content	Total Fluence (kJ/cm <sup>2</sup> )	Success?
A	3 %	69.0	Yes
B	7 %	33.6	Yes
C	10 %	25.5	No

Table 6.1: Summary of straight waveguides produced by irradiation with the F<sub>2</sub> laser. The 10 % Germanium content is believed to be too high a concentration of Ge.

In the case of sample C, with the highest Ge content, no evidence of any densification or refractive index change could be seen on the sample. This corresponds with the findings of Herman, that as the Ge content increases beyond a threshold, the photosensitivity of the silica is greatly reduced by Ge absorption [Herman 2001 (a)]. In the case of the FHD silica used here, the threshold somewhere between 7 and 10 wt. %. Further experiments varying both the total fluence and the Ge content would be needed to define this point more accurately.

A straight 4  $\mu\text{m}$  wide waveguide written in sample A (3 wt. % Ge) is shown in Figure 6.5. By focussing the microscope below the sample surface, it was possible to see a pronounced stripe below the surface, as in Figure 6.6. It is believed that this is at the interface of the FHD silica and thermal oxide undercladding, where the photosensitive response is expected to decrease approximately tenfold due to the absence of Ge in the thermal oxide [Herman 2000 (b)].

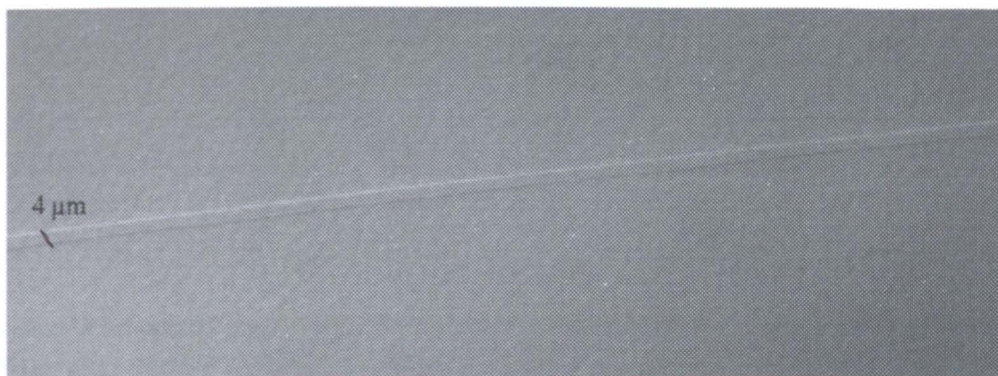


Figure 6.5: Micrograph of a 4  $\mu\text{m}$  wide waveguide written in 3 wt. % (50 sccm  $\text{GeCl}_4$ ) Ge-doped FHD silica. Interference filters were used to allow the waveguide structure to be seen.

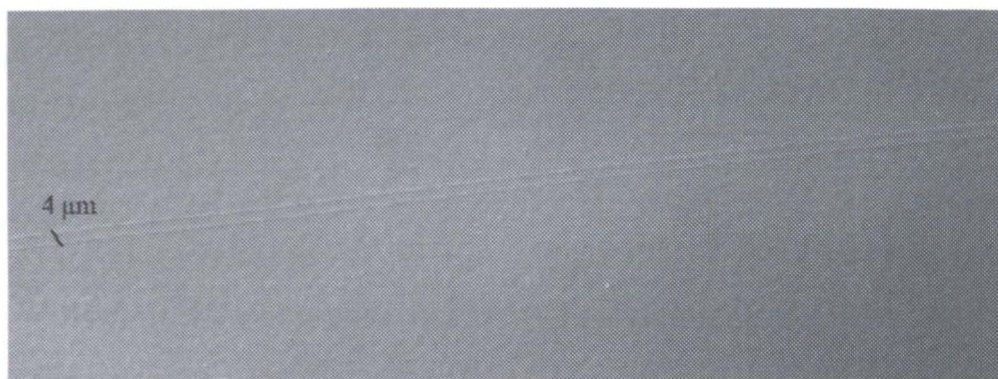


Figure 6.6: Micrograph of the same 4  $\mu\text{m}$  wide waveguide as in the previous figure, focussed on the base of the waveguide which is 2  $\mu\text{m}$  below the surface. This type of image at the interface between core and undercladding is not observable in electron beam written waveguides in the same material.

A HeNe laser at 632.8 nm was used to couple light into the waveguides, as described in previous chapters. A x40 lens with a NA of 0.65 was used at the input, with a x20 lens with a NA of 0.40 at the output. The output of one of the straight waveguides is shown in Figure 6.7. An aperture was used before the camera to remove any light from the FHD slab. Without the aperture, the waveguide output is clearly visible against the slab, as it is much brighter than the slab, and has the appearance of almost a pinpoint.

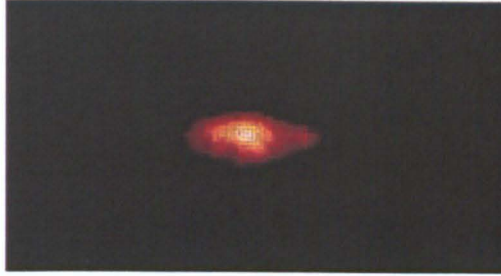


Figure 6.7: Digital photograph of the output of a straight waveguide in ~3 wt. % Ge FHD silica irradiated by the  $F_2$  laser. The guide was approximately  $4\ \mu\text{m}$  wide and  $2\ \mu\text{m}$  high, and was embedded in the FHD waveguide slab layer.

### 6.3.2.1 Losses in the Irradiated Waveguides

While time did not permit the fabrication of straight waveguides that would be single-mode at  $1550\ \text{nm}$  (around  $6\ \mu\text{m}$  square) for the evaluation of losses using the Fabry-Perot technique, the measured output powers were of a similar order of magnitude as those measured for electron beam written waveguides, using the same input power and optical setup. Therefore, total losses can be estimated as approximately on the same scale as those observed for the electron beam written guides.

### 6.3.3 Writing of Symmetric and Asymmetric Y-branch Waveguides

After confirmation that straight waveguides could be successfully produced using the  $F_2$  laser, a series of branching waveguides were fabricated using the same techniques.

#### 6.3.3.1 Y-Branch Design

A generic set of  $2\ \mu\text{m}$  wide single-mode Y-branches was designed using the BPM software as described in Chapter 3 for the case of electron beam written waveguides. The asymmetric design consisted of a straight waveguide, coupled to a cosine S-bend. A straight section at the end was used to ensure that the two branch outputs were parallel. Four final splitting distances 'd' were chosen:  $50$ ,  $60$ ,  $70$  and  $80\ \mu\text{m}$ . Two symmetric branches were included in each set, with separations of  $50$  and  $80\ \mu\text{m}$ . Two  $4\ \mu\text{m}$  wide straight waveguides were also included as a reference. Figure 6.8 shows the layout of each set of guides on the FHD substrate.

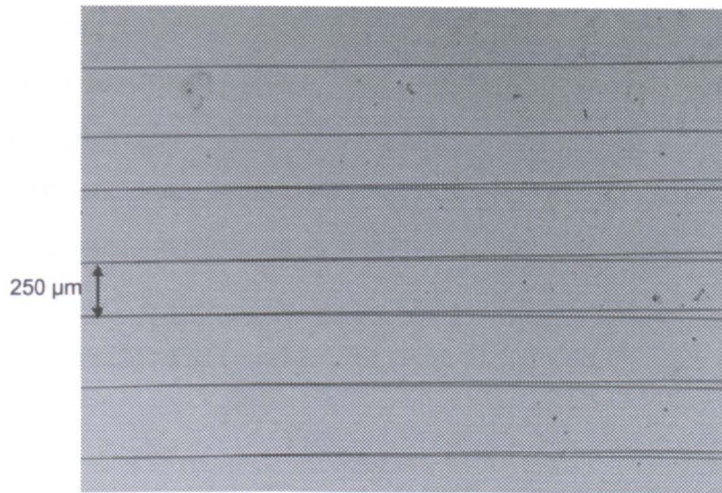


Figure 6.8: Micrograph showing the layout of the Y-branch mask prior to  $F_2$  laser irradiation. Two symmetric branches, and then the asymmetric branches follow the two straight waveguides at the top. The separation between each input waveguide is at least  $200\ \mu\text{m}$ .

The sample was aligned to the aperture in the same way as for the straight waveguides, and irradiated with a total fluence of  $71.6\ \text{kJ}/\text{cm}^2$ . A larger flux than that used in the irradiation of straight waveguides was used, to ensure that waveguides would be formed. No photosensitisation of the samples by hydrogen loading was used. Figure 6.9 shows a micrograph of a symmetric Y-branch after removal of the NiCr mask.

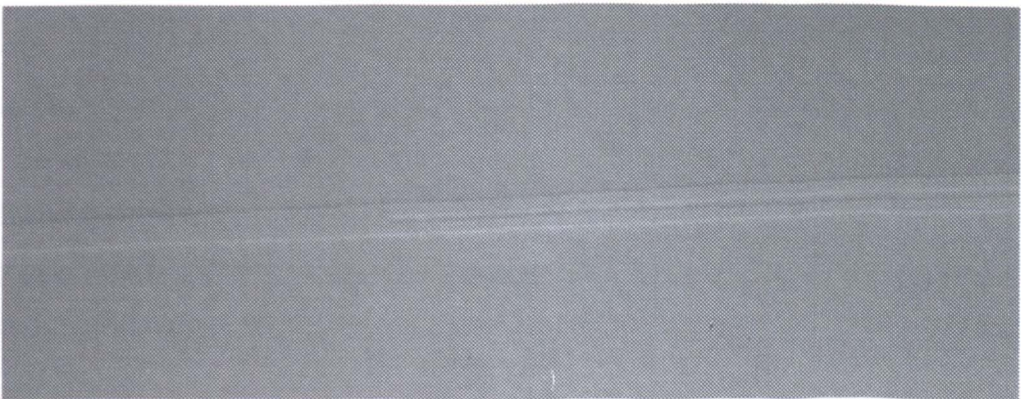


Figure 6.9: Microscope photograph of a symmetric Y-branch waveguide written in 3 wt. % ( $50\ \text{sccm}\ \text{GeCl}_4$ ) Ge-doped silica. The waveguides are  $2\ \mu\text{m}$  wide, and cosine S-bends were used in designing the branch layout. DIC interference filters were used to allow the waveguide structure to be seen.

It was observed using an optical microscope that there was a variation in the amount of densification across the irradiated area, and therefore almost certainly a variation in the refractive index change. The area of lesser densification was situated near the lower edge of the NiCr mask, and was probably caused by beam nonuniformity. In future, closer spacing of the waveguide layout and therefore a smaller area for irradiation should reduce the problem. The output of one of the asymmetric branches is shown in Figure 6.10, where the contrast has been enhanced to show clearly the waveguide outputs.

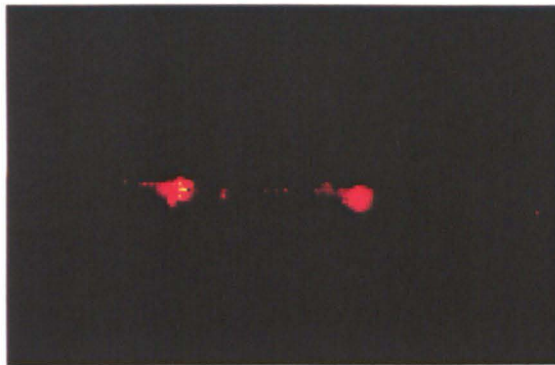


Figure 6.10: Digital photograph of an asymmetric Y-branch waveguide in ~3 wt. % Ge FHD silica irradiated by the  $F_2$  laser. The guide was approximately  $2\ \mu\text{m}$  wide and  $2\ \mu\text{m}$  high, and was embedded in the FHD waveguide slab layer. The left hand spot is the output from the straight guide, and the right hand spot is from the branch.

It was also observed while testing the Y-branch waveguides that the first symmetric branch was not single-moded, as the output powers clearly varied as the input beam was scanned across the waveguide input facet. This particular branch had been subject to the highest total fluence, evidenced by observation of the amount of densification with an optical microscope. While this condition is normally undesirable in a Y-branch, as described in Chapter 3, in this case it provides a guide to the maximum refractive index change induced by the irradiation.

Using the effective index method with the 2D BPM mode solver, the refractive index at which a  $2\ \mu\text{m}$  guide would become two-moded rather than single-mode at  $632.8\ \text{nm}$  was found. Subtraction of the unirradiated index of the FHD layer from this index gave an increase in refractive index caused by the  $F_2$  laser as approximately  $3.7 \times 10^{-3}$ . (This value cannot be applied to all the waveguides in each set as the energy was nonuniformly

distributed). Further examination of *straight waveguides* using microreflectivity could provide a more accurate value of refractive index increase [García-Blanco 2004].

The output of the second (single-mode) symmetric Y-branch was measured using a Labmaster optical power meter, and an imbalance of approximately 0.1 dB (less than 1 %) was found.

#### 6.3.4 Grating Fabrication

For the  $F_2$  laser combined with a NiCr surface mask to be a suitable method of component fabrication, its performance in the fabrication of high-resolution components such as gratings must be examined. Gratings can also be used to couple light into a waveguide, and therefore be used to measure the refractive index of a film or waveguide [Marques 2002].

Several grating masks with a period of 1060 nm were fabricated on 5  $\mu\text{m}$  deep,  $\sim 3$  wt. % Ge FHD samples, with each set of gratings having a 5  $\mu\text{m}$  wide adjacent waveguide, to allow loss measurements of the irradiated waveguides to be made using a tunable laser around 1550 nm. Figure 6.11 shows a micrograph of one such grating after the electron beam lithography of PMMA, immediately prior to the evaporation of the 100 nm NiCr mask layer.

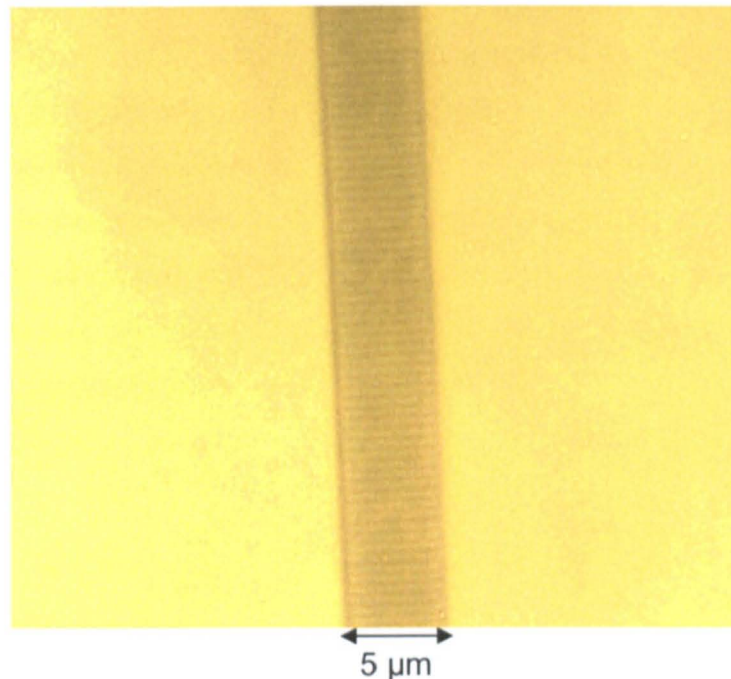


Figure 6.11: Optical microscope photograph of a 1060 nm period grating in PMMA. The width of the grating is 5  $\mu\text{m}$ .

## 6.4 Summary

The photosensitive response of Ge-doped FHD silica was investigated using a 157 nm F<sub>2</sub> commercially available laser. Building upon previous work on photosensitivity at this and other UV wavelengths, a series of straight and single-mode Y-branch waveguides were written in ~3 wt. % Ge-doped FHD silica. Straight waveguides were also successfully written in ~7 wt. % Ge-doped glass, but the threshold where the Ge starts to absorb too much energy is thought to be slightly above this particular composition. Attempts to write waveguides in ~10 wt. % Ge-doped glass were unsuccessful. No photosensitisation of the samples was required prior to the irradiation.

A new masking technology was evaluated during the writing of the waveguides. To eliminate the need for a separate CaF<sub>2</sub> mask plate, a 100 nm layer of NiCr was used as a surface mask, attached to the FHD silica sample. Electron beam lithography of PMMA, combined with lift-off, enabled the formation of extremely high resolution masks. As the waveguide pattern was aligned to the sample during the electron beam lithography stage, no further pattern alignment was necessary prior to UV irradiation. After each irradiation, the mask was found to be completely intact.

Having demonstrated that the NiCr masking technique works, the fabrication of many more complex devices for both conventional integrated optics and optical sensors can now be attempted. In particular, the successful fabrication of gratings, MMI couplers and splitters would provide a significant step forward in this field. Work has been started on the fabrication of high resolution gratings, but more must be done to evaluate completely the effectiveness and stability of the NiCr mask during the UV irradiation. To date, the irradiation and testing of gratings has still to be carried out, but masks have been successfully fabricated at this high resolution.

## 7 Conclusions and Future Work

### 7.1 Conclusions

FHD glass has been used as the basis for a variety of optical fluorescence sensor devices, building upon silica waveguide technology that was originally developed for the telecommunications industry.

Previous work on electron beam written waveguides has been extended through the fabrication of a number of integrated optical devices and the addition of microfluidic circuits. Y-branches, both symmetric and asymmetric, and MMI splitters have been successfully demonstrated for the purpose of direct-excitation fluorescence sensors. Both single-assay and array formats have been demonstrated.

An evanescent sensor chip with asymmetric electron beam Y-branch input waveguides and a dry etched direct collection waveguide has been fabricated and tested. Microfluidic channels were defined completely in the PDMS cladding layer using a thick photoresist to define the channel prior to adding the PDMS. The advantage of this type of chip over those with direct excitation waveguides is that it needs a shorter dry etch time, as only the depth of the output waveguide needs to be etched, rather than the microfluidic channels.

An investigation of the fluorescence lifetime and minimum measurable concentration of the Nile Blue dye (used as the principal dye in this work) has been conducted. Single photons from an asymmetric Y-branch device were detected using a SPAD in a TCSPC setup interfaced by a fibre to the sensor chip. A minimum concentration of 1.5 nM was measured successfully, and the decay time of the dye was measured for a number of different concentrations. While the minimum detectable concentration was limited by the solvent used, different solvents may allow for lower concentrations to be detected.

Finally, asymmetric Y-branch waveguides have been written in Ge-doped FHD silica for the first time using a 157 nm F<sub>2</sub> laser and a NiCr surface mask, thus opening up the possibility of constructing fluorescence sensors using this type of waveguide. Ultrafast pulse micromachining has also been suggested as a quicker method of etching microfluidic channels through these or electron beam waveguides, but has yet to be demonstrated.

## 7.2 Suggestions for Future Work

The work has itself generated a great number of questions that would require further research to be able to answer them fully. A few key points that should be addressed are summarised here.

For the FHD material itself, it would be advantageous to be able to further reduce the wafer bow, film thickness variation and stress birefringence. While these have been studied in industry, complete solutions have not yet been formed. One way to reduce or compensate for birefringence may be to reduce wafer stress by flood exposure to UV light, although more work must be done to verify the effect, and the effect on the refractive index of the FHD film should be examined.

While the devices presented in this thesis have been designed for the red wavelength of 632.8 nm, the nature of both electron beam and UV written waveguides is such that guides of much smaller dimensions can now be fabricated without the need for photolithography. For example, a number of fluorophores can be excited around the green wavelength of a 543 nm HeNe laser, Rhodamine B and Nile Red being two commonly used fluorophores. The advent of diode lasers at many new wavelengths allows the design of devices to match more closely with fluorophores than say, five years ago. FHD silica waveguide devices for green wavelengths would require waveguides of less than 2  $\mu\text{m}$  square for single mode, which is why the high resolution electron beam and UV writing methods are ideally suited to this task.

With regard to the FHD silica material for array sensors, it would be advantageous to reduce the amount of crosstalk between waveguide channels so that each fluorescent element of the array could be identified more clearly and noise would be reduced. One possible method to achieve this would be the development of a technique to etch decoupling channels between the output waveguides, keeping them separate from the microfluidic elements. The main challenge here would be the alignment of the channels to the waveguides, as incorrect alignment could affect the ratio of light reaching each microfluidic sensing element. A second possible method would be to tailor the FHD silica layer so that its refractive index and thickness were such that it would not guide as a slab, just on the boundary of the waveguide cutoff condition. Then by irradiating the waveguide

pattern with a sufficient dose (by electron beam or UV) the index could be increased enough so that the irradiated area would guide light, but the non-irradiated area would still not guide. This second method would be more useful than the decoupling channel etching, as the etching step could then be bypassed without adding any other steps.

The TCSPC route to fluorophore detection should provide a route towards detecting even lower dye concentrations than the ones measured in this thesis. Different combinations of dyes and solvents, by which the background fluorescence from the solvent is minimised should allow for lower concentrations to be detected.

To minimise losses in the waveguide elements of the sensors, more design and fabrication optimisation of both asymmetric Y-branches and MMI splitters could be carried out, in particular to minimise imbalances in symmetric splitting devices. This would of course have to be done in tandem with FHD silica process optimisation to ensure that the films are uniform, and if not, can be compensated for.

Another important step forward would be to apply the devices shown here to real systems, that is, to use a fluorescently-labelled biomolecule or combination of biomolecules in the devices, as well as incorporating a completely integrated and sealed microfluidic flow system.

Finally, the use of other materials such as PMMA for the waveguide elements could be investigated. Although the layers would not be of such high optical quality or as robust as the FHD glass, it may provide a route to lower- cost or disposable devices.

## References

- Albert, J., Hill, K.O., Johnson, D.C., Bilodeau, F., Mihailov, S.J., Borrelli, N.F., Amin, J.,** “Bragg gratings in defect-free germanium-doped optical fibers”, *Optics Letters* 24 (18), 1266-1268, 1999.
- Almeida, R.M.,** “Sol-gel planar waveguides for integrated optics”, *Journal of Non-Crystalline Solids* 259, 176-181, 1999.
- Astle, T.B., Gilbert, A., Ahmad, A., Fox, S.,** “Optical components – the planar revolution?”, *Merrill Lynch In-Depth Report*, 1-17, 2000.
- Auroux, P.-A., Iossifidis, D., Reyes, D.R., Manz, A.,** “Micro total analysis systems. 2. Analytical standard operations and applications”, *Analytical Chemistry* 74, 2637-2652, 2002.
- Bachmann, M., Besse, P.A. Melchior, H.,** “General self-imaging properties in  $N \times N$  multimode interference couplers including phase relations”, *Applied Optics* 33 (18), 3905-3911, 1994.
- Baets, R., Lagasse, P.E.** “Calculation of radiation loss in integrated-optic tapers and Y-junctions”, *Applied Optics* 21 (11), 1972-1978, 1982.
- Barbarossa, G., Laybourn, P.J.R.,** “Wide rejection band multidemultiplexer at 1.3-1.55  $\mu\text{m}$  by cascading high-silica three-waveguide couplers on Si”, *Electronics Letters* 27 (22), 1991.
- Barbarossa, G., Laybourn, P.J.R.,** “Vertically integrated high-silica channel waveguides on Si”, *Electronics Letters* 28 (5), 437-438, 1992 (a).
- Barbarossa, G.,** “Planar silica optical device technology”, PhD Thesis, University of Glasgow, 1992 (b).
- Barbier, D., Green, M., Madden, S.J.,** “Waveguide fabrication for integrated optics by electron beam irradiation of silica”, *Journal of Lightwave Technology* 9 (6), 715-720, 1991.
- Bebbington, J.A., Barbarossa, G., Bonar, J.R., Aitchison, J.S.,** “Rare earth doped silica waveguides on Si fabricated by flame hydrolysis deposition and aerosol doping”, *Applied Physics Letters* 62 (4), 337-339, 1993.
- Bernard, A., Michel, B., Delamarque, E.,** “Micromosaic immunoassays”, *Analytical Chemistry* 73, 8-12, 2001.

- Besse, P.A., Bachmann, M., Melchior, H., Soldano, L.B., Smit, M.K.**, “Optical bandwidth and fabrication tolerances of multimode interference couplers”, *Journal of Lightwave Technology* 12 (6), 1004-1009, 1994.
- Besse, P.A., Gini, E., Bachmann, M., Melchior, H.**, “New 2x2 and 1x3 multimode interference couplers with free selection of power splitting ratios”, *IEEE Journal of Lightwave Technology* 14 (10), 2286-2293, 1996.
- Bilenberg, B.**, “Technology for integrated optics on Lab-on-a-Chip Microsystems”, MSc Thesis, Technical University of Denmark, 2003.
- Bilodeau, F., Malo, B., Albert, J., Johnson, D.C., Hill, K.O., Hibino, Y., Abe, M., Kawachi, M.**, “Photosensitization on optical fiber and silica on silicon/silica waveguides”, *Optics Letters* 18 (12), 953-955, 1993.
- Birch, D.J.S., Sanderson, A., Holmes, A.S., McLoskey, D., Imhof, R.E.**, “Miniaturized single-photon fluorometry”, *Measurement Science and Technology* 4, 797-799, 1993.
- Błahut, M., Karasiński, P., Kasprzak, D., Rogoziński, R.**, “Visualization method of modal interference in multimode interference structures”, *Optics Communications* 214, 47-53, 2002.
- Bonar, J.R., Vermelho, M.V.D., Marques, P.V.S., McLaughlin, J.S., Aitchison, J.S.**, “Fluorescence lifetime measurements of aerosol doped erbium in phosphosilicate planar waveguides”, *Optics Communications* 149, 27-32, 1998.
- Boone, T.D., Ricco, A.J., Fan, Z.H., Tan, H., Hooper, H.H., Williams, S.J.**, “Plastic advances microfluidic devices”, *Analytical Chemistry A-Pages*, 78-86, 2002.
- Bosc, D., Devoldère, N., Bonnel, M., Favennec, J.L., Pavy, D.**, “Hybrid silica-polymer structure for integrated optical waveguides with new potentialities”, *Materials Science and Engineering B57*, 155-160, 1999.
- Buller, G.S., Fancey, S.J., Massa, J.S., Walker, A.C., Cova, S., Lacaita, A.**, “Time-resolved photoluminescence measurements of InGaAs / InP multiple-quantum-well Structures at 1.3  $\mu\text{m}$  wavelengths by use of germanium single-photon avalanche photodiodes”, *Applied Optics* 35 (6), 916-921, 1996.
- Burns, W.K., Milton, A.F., Lee, A.B., West, E.J.**, “Optical modal evolution 3-dB coupler”, *Applied Optics* 15 (4), 1053-1065, 1976.
- Burns, W.K., Milton, A.F.**, “An analytic solution for mode coupling in optical waveguide branches”, *IEEE Journal of Quantum Electronics* QE-16 (4), 446-454, 1980.
- Campillo, A.L., Hsu, J.W.P., Parameswaran, K.R., Fejer, M.M.**, “Direct imaging of multimode interference in a channel waveguide”, *Optics Letters* 28 (6), 399-401, 2003.

- Chen, K.P., Herman, P.R., Tam, R.,** “157-nm F<sub>2</sub> Laser Photosensitivity and Photosensitization in Optical Fibres”, OSA Technical Digest: Bragg Gratings, Photosensitivity, and Poling in Glass Waveguides, 2001 (a).
- Chen, K.P., Herman, P.R., Zhang, J.,** “Large Photosensitivity in Germanosilicate Planar Waveguides Induced by 157-nm F<sub>2</sub>-Laser Radiation”, OSA TOPS 54: Conference on Optical Fiber Communications, WDD81.1-81.3, 2001 (b).
- Chen, K.P., Herman, P.R.,** “Photosensitisation of Silica Planar Lightwave Interleaver for Phase Error Correction”, *Electronics Letters* 38 (1), 24-26, 2002 (a).
- Chen, K.P., Herman, P.R.,** “Trimming Phase and Birefringence Errors in Photosensitivity-Locked Planar Optical Circuits”, *IEEE Photonics Technology Letters* 14 (1), 71-73, 2002 (b).
- Chen, K.P., Herman, P.R., Taylor, R., Hnatovsky, C.,** “Vacuum-ultraviolet laser-induced refractive-index change and birefringence in standard optical fibers”, *Journal of Lightwave Technology* 31 (9), 1969-1977, 2003.
- Chuang, Y.J., Tseng, F.G., Cheng, J.H., Lin, W.K.,** “A novel fabrication method of embedded micro-channels by using SU-8 thick-film photoresists”, *Sensors and Actuators A* 103, 64-69, 2003.
- Cleary, A., García-Blanco, Glidle, A., Aitchison, J.S., Laybourn, P., Cooper, J.M.,** “Towards optical fluorescence sensing using multimode interference splitters”, *Proc. IEEE Sensors II*, 279-282, 2003.
- Cleary, A., García-Blanco, Glidle, A., Aitchison, J.S., Laybourn, P., Cooper, J.M.,** “An integrated fluorescence array as a platform for lab-on-a-chip technology using multimode interference splitters”, in press, *IEEE Sensors*, 2004.
- Coudray, P., Etienne, P., Moreau, Y., Porque, J., Najafi, S.I.,** “Sol-gel channel waveguide on silicon: fast direct imprinting and low cost fabrication”, *Optics Communications* 143, 199-202, 1997.
- Cova, S., Ghioni, M., Lacaita, A., Samori, C., Zappa, F.,** “Avalanche photodiodes and quenching circuits for single-photon detection”, *Applied Optics* 35 (12), 1956-1975, 1996.
- Cullen, T.J.,** “Radiation losses from single-mode optical Y-junctions formed by silver-ion exchange in glass”. *Optics Letters* 10, 134-136, 1984.
- Duffy, D.C., McDonald, J.C., Schueller, O.J.A., Whitesides, G.M.,** “Rapid prototyping of microfluidic systems in poly(dimethylsiloxane)”, *Analytical Chemistry* 70, 4974-4984, 1998.

- Duveneck, G.L., Abel, A.P., Bopp, M.A., Kresbach, G.M., Ehrat, M.,** “Planar waveguides for ultra-high sensitivity of the analysis of nucleic acids” *Analytica Chimica Acta* 469, 49-61, 2002.
- Ebendorff-Heidepriem, H.** “Laser writing of waveguides in photosensitive glasses”, *Optical Materials* 25, 109-115, 2004.
- Erickson, D., Li, D.,** “Integrated microfluidic devices”, *Analytica Chimica Acta* 507, 11-24, 2004.
- Fancey, S.J., Buller, G.S., Massa, J.S., Walker, A.C., McLean, C.J., McKee, A., Bryce, A.C., Marsh, J.H., De La Rue, R.M.,** “Time-resolved photoluminescence microscopy of GaInAs/GaInAsP quantum wells intermixed using a pulsed laser technique”, *Journal of Applied Physics* 79 (12), 9390-9392, 1996 (a).
- Fancey, S.J.,** “Single photon avalanche diodes for time-resolved photoluminescence measurements in the near infra-red”, PhD thesis, Heriot-Watt University, 1996 (b).
- Feit, M.D., Fleck, J.M. Jr.,** “Light propagation in graded index optical fibres”, *Applied Optics* 17 (24), 3990-3998, 1978.
- Feit, M.D., Fleck, J.A.,** “Analysis of rib waveguides and couplers by the propagating beam method”, *Journal of the Optical Society of America A* 7, 73-79, 1990.
- Felton, M.J.,** “Welcome to the microfluidic matrix”, *Analytical Chemistry A-Pages Research Profile*, 419, 2003.
- Fu, L.-M., Yang, R.-J., Lee, G.-B., Liu, H.-H.,** “Electrokinetic injection techniques in microfluidic chips”, *Analytical Chemistry* 74, 5084-5091, 2002.
- García-Blanco, S., Glidle, A., Davies, J.H., Cooper, J.M., Aitchison, J.S.,** “Electron beam induced densification of Ge-doped flame hydrolysis silica for waveguide fabrication”, *Applied Physics Letters* 79 (18) 2889-2891, 2001 (a).
- García-Blanco, S., Kleckner, T.C., Glidle, A., Davies, J.H., Aitchison, J.S., Cooper, J.M.,** “Fabrication of integrated optical circuits by electron-beam modification of flame hydrolysis deposited silica”, *Proc. ECIO, Padeborn*, 121-124, 2001 (b).
- García-Blanco, S., Glidle, A., Davies, J.H., Cooper, J.M., Aitchison, J.S.,** “Waveguide fabrication by electron beam modification of flame hydrolysis deposited silica”, *Proc. OECC/IOCC, Sydney*, 2001 (c).
- García-Blanco, S., Glidle, A., Cooper, J.M., De La Rue, R.M., Jacqueline, A.S., Poumellec, B., Aitchison, J.S.,** “Characterization of the densification induced by electron-beam irradiation of Ge-doped silica for the fabrication of integrated optical circuits”, *Proc. IEEE/LEOS WFOPC, Glasgow*, 17-23, 2002 (a).

- García-Blanco, S., Aitchison, J.S., Cooper, J.M., De La Rue, R.M.,** “Low-loss controlled-birefringence waveguides fabricated by electron-beam irradiation of germanium doped FHD silica”, Proc. IPRC, Vancouver, 2002 (b).
- García-Blanco, S., Aitchison, J.S., Cooper, J.M., De La Rue, R.M.,** “Refractive index characterization of slab waveguides fabricated by electron beam irradiation of flame hydrolysis silica”, Proc. PREP, UK, 2003 (a).
- García-Blanco, S.,** “Electron-beam irradiation of germanium-doped flame-hydrolysis deposited silica for the fabrication of optical waveguides”, PhD Thesis, University of Glasgow, 2003 (b).
- García-Blanco, S., Hnatovsky, C., Taylor, R.S., Aitchison, J.S.,** “Micro-reflectivity characterization of the 2-dimensional refractive index distribution of electron-beam written optical waveguides in germanium doped flame-hydrolysis silica”, Applied Physics Letters, in press, 2004.
- Göpel, W.,** “Bioelectronics and nanotechnologies”, Biosensors and Bioelectronics 13, 723-728, 1998.
- Gowar, J.,** “Optical Communication Systems (Second Ed.)”, Prentice Hall, Hemel Hempstead, 1993.
- Gravesen, P., Branebjerg, J., Jensen, O.S.,** “Microfluidics-a review”, Journal of Micromechanics and Microengineering 3, 168-182, 1993.
- Grofcsik, A., Kubinyi, M., Jones, W.J.,** “Fluorescence decay dynamics of organic dye molecules in solution” Journal of Molecular Structure 348, 197-200, 1995.
- Hadley, G.R.,** “Transparent boundary condition for the beam propagation method”, IEEE Journal of Quantum Electronics 28 (1), 363-370, 1992.
- Hamamatsu, PMT Handbook online, 2004.**
- Harrison, D.J., Manz, A., Fan, Z., Lüdi, H., Widmer, H.M.,** “Capillary electrophoresis and sample injection systems integrated on a planar glass chip”, Analytical Chemistry 64, 1926-1932, 1992.
- Hatrack, D.A.,** “Fluorescence of near infra-red rhodamine dyes”, PhD Thesis, University of Strathclyde, 1997.
- Heaton, J.M., Jenkins, R.M., Wight, D.R., Parker, J.T., Birbeck, J.C.H., Hilton, K.P.,** “Novel 1-to-N way integrated optical beam splitters using symmetric mode mixing in GaAs/AlGaAs multimode waveguides”, Applied Physics Letters 61 (15), 1754-1758, 1992.

- Heideman**, R.G., Lambeck, P.V., “Remote opto-chemical sensing with extreme sensitivity: design, fabrication and performance of a pigtailed integrated optical phase-modulated Mach-Zehnder interferometer system”, *Sensors and Actuators B* 61, 100-127, 1999.
- Herman**, P.R., Oetl, A., Chen, K.P., Marjoribanks, R.S., “Laser Micromachining of ‘Transparent’ Fused Silica with 1-ps Pulses and Pulse Trains, Proc. SPIE 3616: Conference on Commercial and Biomedical Applications of Ultrafast Lasers, 148-155, 1999 (a).
- Herman**, P.R., Goodno, G., Gu, X., Kalbfleisch, J.B., Long, J., Lukacs, M., Marjoribanks, R.S., Dwayne Miller, R.J., Nantel, M., Ness, S., Oetl, A., “Advanced-Laser Processing of Photonic and Microelectronic Components at Photonics Research Ontario”, Proc. SPIE 3618: Laser Applications in Microelectronic and Optoelectronic Manufacturing IV, 240-250, 1999 (b).
- Herman**, P.R., Marjoribanks, R.S., Oetl, A., Chen, K., Konovalov, I., Ness, S., “Laser shaping of photonic materials: deep-ultraviolet and ultrafast lasers”, *Applied Surface Science* 154, 577-586, 2000 (a).
- Herman**, P.R., Chen, K.P., Corkum, P., Naumov, A., Ng, S., Zhang, J., “Advanced Laser Microfabrication of Photonic Components”, Proc. SPIE 4088: Laser Precision Microfabrication, 345-350, 2000 (b).
- Herman**, P.R., Chen, K.P., Corkum, P., Naumov, A., Ng, S., Zhang, J., “Advanced Lasers for Photonic Device Microfabrication”, *Riken Review* 32, 31-35, 2001 (a).
- Herman**, P.R. Li, J., Chen, K.P., Wei, M., Zhang, J., Ihlemann, J., Schäfer, D., Marowsky, G., Oesterlin, P., Burghardt, B., “F<sub>2</sub> Lasers: High Resolution Micromachining System for Shaping Photonics Components”, *OSA TOPS* 56, CLEO Technical Digest 574-577, 2001 (b).
- Hill**, K.O., Fujii, Y., Johnson, D.C., Kawasaki, B., “Photosensitivity in optical fiber waveguides: Application to reflection filter fabrication”, *Applied Physics Letters* 32 (10), 647-649, 1978.
- Hill**, K.O., Bilodeau, F., Malo, B., Albert, J., Johnson, D.C. “Optical Waveguide Photosensitivity”, Proc. LEOS '93, Invited Talk, 1993.
- Ho**, S., Private communication, 2003
- Hosokawa**, K., Fujii, T., Endo, I., “Handling of picoliter liquid samples in a poly(dimethylsiloxane)-based microfluidic device”, *Analytical Chemistry* 71, 4781-4785, 1999.

- Houghton**, A.J., Townsend, P.D., "Optical waveguides formed by low-energy electron irradiation of silica", *Applied Physics Letters* 29 (9), 565-566, 1976.
- Hyde**, J.F., US Patent number 2,272,342, 1942.
- Isutzu**, M., Yoshiharu, N., Tadasi, S., "Operation mechanism of the single-mode optical-waveguide Y junction", *Optics Letters* 7(3), 136-138, 1982.
- Jacobsen**, S.C., McKnight, T.E., Ramsey, J.M., "microfluidic devices for electrokinetically driven parallel and serial mixing", *Analytical Chemistry* 71, 4455-4459, 1999.
- Jensen**, J.B., private communication, 2003.
- Kashyap**, R. "Fiber Bragg Gratings", Academic Press, New York, 1999.
- Kawachi**, M., Yasu, M., Edahiro, T., "Fabrication of SiO<sub>2</sub>-TiO<sub>2</sub> glass planar optical waveguides by flame hydrolysis deposition", *Electronics Letters* 19, 583-584, 1983.
- Kawachi**, M., "Tutorial Review: Silica Waveguides on Silicon and their Application to Integrated-Optic Components", *Optical and Quantum Electronics* 22, 391-416, 1990.
- Kitoh**, T., Takato, N., Jinguji, K., Yasu, M., Kawachi, M., "Novel broad-band optical switch using silica-based planar lightwave circuit", *IEEE Photonics Technology Letters* 4 (7), 735-737, 1992.
- Knappe**, F., Voigt, J., Renner, H., Brinkmeyer, E., "Direct UV writing of Multimode-Interference couplers", *Proc. BGPP, Monterey, California, Paper TuA4*, 184-186, 2003.
- Kunz**, R.E., "Miniature integrated optical modules for chemical and biochemical sensing", *Sensors and Actuators B* 38-39, 13-28, 1997.
- Lagali**, N.S., Paiam, M.R., MacDonald, R.I., "Theory of variable-ratio power splitters using multimode interference couplers", *IEEE Photonics Technology Letters* 11 (6), 665-667, 1999.
- Lai**, Q., Bachmann, M., Melchior, H., "Low-loss 1 x N multimode interference couplers with homogeneous output power distributions realised in silica on Si material", *Electronics Letters* 33 (20), 1699-1700, 1997.
- Lai**, Q., Hunziker, W., Melchior, H., "Low-power compact 2 x 2 thermo-optic silica-on-silicon waveguide switch with fast response", *IEEE Photonics Technology Letters* 10 (5), 1998.
- Lee**, J.N., Park, C., Whitesides, G.M., "Solvent compatibility of poly(dimethylsiloxane)-based microfluidic devices", *Analytical Chemistry* 75, 6544-6554, 2003.

- Leick, L., Povlsen, J.H., Pedersen, R.J.S.,** “Numerical and experimental investigation of 2 x 2 multimode interference couplers in silica-on-silicon”, *Optical and Quantum Electronics* 33, 387-398, 2001.
- Lemaire, P.J., Atkins, R.M., Mizrahi, V., Reed, W.A.,** “High pressure H<sub>2</sub> loading as a technique for achieving ultrahigh UV photosensitivity and thermal sensitivity in GeO<sub>2</sub> doped optical fibres”, *Electronics Letters* 23 (19), 1191-1193, 1993.
- Leuthold, J., Besse, P.A., Hess, R., Melchior, H.,** “Wide optical bandwidths and high design tolerances of multimode-interference converter-combiners”, *Proceedings of ECIO, Stockholm*, 154-157, 1997.
- Leuthold, J., Joyner, C.H.,** “Multimode interference couplers with tunable power splitting ratios”, *IEEE Journal of Lightwave Technology* 19 (5), 700-707, 2001.
- Li, C.C.,** “Integrated Optical Waveguides”, *Corning Report*, 1-26, 2003.
- Li, Y., Baba, M., Matsuoka, M.,** “Femtosecond measurement of fluorescence by two-photon interference”, *Physical Review A* 55 (4), 3177-3183, 1997.
- Livage, J.,** “Sol-gel processes”, *Current Opinion in Solid State and Materials Science* 2, 132-138, 1997.
- Madden, S.J., Green, M., Barbier, D.,** “Optical channel waveguide fabrication based on electron beam irradiation of silica”, *Applied Physics Letters* 57 (27), 2902-2903, 1990.
- Manz, A., Graber, N., Widmer, H.M.,** “Miniaturized total chemical-analysis systems – a novel concept for chemical sensing”, *Sensors and Actuators B* 1, pp. 244-248, 1990.
- Marcuse, D.,** “Mode conversion caused by surface imperfections of a dielectric slab waveguide”, *Bell Systems Journal of Technology* 48, 3187, 1969.
- Marcuse, D.,** “Theory of Dielectric Optical Waveguides”, 2<sup>nd</sup> Ed., Academic Press Inc., 1991.
- Marques, P.V.S., Bonar, J.R., Leite, A.M.P., Aitchison, J.S.,** “Simultaneous UV Direct Writing of Channel Waveguides and Bragg Gratings in Germanium Doped Planar Silica”, *IEEE Journal of Selected Topics in Quantum Electronics* 8 (6), 1316-1322, 2002.
- Mašanović, M.L., Skogen, E.J., Barton, J.S., Sullivan, J.M., Blumenthal, D.J., Coldren, L.A.,** “Multimode Interference-Based Two-Stage 1 x 2 Light Splitter for Compact Photonic Integrated Circuits”, *IEEE Photonics Technology Letters* 15 (5), 706708, 2003.
- Massa, J.S., Buller, G.S., Walker, A.C., Oudar, J.L., Rao, E.V.K., Sfez, B.G., Kuselwicz, R.,** “Quantum-well microresonators fabricated using alloy mixing techniques”, *Applied Physics Letters* 61 (18), 2205-2207, 1992.

- Massa, J.S., Buller, G.S., Walker, A.C., Simpson, J., Prior, K.A., Cavenett, B.C.,** “Photoluminescence decay measurements of n- and p-type doped ZnSe grown by molecular beam epitaxy”, *Applied Physics Letters* 64 (5), 589-591, 1994.
- Maxwell, G.D., Ainslie, B.J., Williams, D.L., Kashyap, R.,** “UV Written 13 dB Reflection Filters in Hydrogenated Low Loss Planar Silica Waveguides”, *Electronics Letters* 29 (5), 425-426, 1993.
- Maxwell, G.D., Kashyap, R., Ainslie, B.J., Williams, D.L., Armitage, J.R.,** “UV written 1.5  $\mu\text{m}$  reflection filters in singlemode planar silica guides”, *Electronics Letters* 28, 2106-2107, 1992.
- McLaughlin, A.J.,** “Hybrid silicon optoelectronic technologies”, PhD Thesis, University of Glasgow, 1998.
- Meltz, G., Morey, W.W., Glenn, W.H.,** “Formation of Bragg gratings in optical fibres by a transverse holographic method”, *Optics Letters* 14 (15), 823-825, 1989.
- Miya, T.,** “Silica-based planar lightwave circuits: passive and thermally active devices”, *IEEE Journal on Selected Topics in Quantum Electronics* 6 (1), 2000.
- Mizrahi, V., Lemaire, P.J., Erdogan, T., Reed, W.A., DiGiovanni, D.J., Atkins, R.M.,** “Ultraviolet laser fabrication of ultrastrong optical fiber gratings and germania doped channel waveguides”, *Applied Physics Letters* 63 (13), 1727-1729, 1993.
- Mogensen, K.B., Petersen, N.J., Hübner, J., Kutter, J.P.,** “Monolithic Integration of Optical Waveguides for Absorption Detection in Microfabricated Electrophoresis Devices” *Electrophoresis* 22, 3930-3938, 2001.
- Mogensen, K.B.,** “Integration of planar waveguides for optical detection in microfabricated analytical devices”, PhD Thesis, Technical University of Denmark, 2002.
- Mogensen, K.B., Kwok, Y.C., Eijkel, J.C.T., Petersen, N.J., Manz, A., Kutter, J.P.,** “A Microfluidic Device with an Integrated Waveguide Beam Splitter for Velocity Measurements of Flowing Particles by Fourier Transformation”, *Analytical Chemistry* 75 (18), 4931-4136, 2003.
- Moore, S.K.,** “Making chips to probe genes”, *IEEE Spectrum*, 54-60, March 2001.
- Natarajan, S.R., Ng, S.L., Yao, J, Tan, P.W., Lam, Y.L.,** “Design of a Multimode Interference Splitter/Combiner for Sensor Applications”, *Proc. Sensors and their Applications XI*, 129-133, 2001.
- Neumann, M., Herten, D.-P., Dietrich, A., Wolfrum, J., Sauer, M.,** “Capillary array scanner for time-resolved detection and identification of fluorescently labelled DNA fragments”, *Journal of Chromatography A* 871, 299-310, 2000.

- Okamoto, K.**, "Tutorial review: recent progress of integrated optics planar lightwave circuits", *Optical and Quantum Electronics* 31, 107-129, 1999.
- Plowman, T.E.**, Durstchi, J.D., Wang, H.K., Christensen, D.A., Herron, J.N., Reichert, W.M., "Multiple-analyte fluoroimmunoassay using an integrated optical waveguide sensor", *Analytical Chemistry* 71, 4344-4352, 1999.
- Polson, N.A.**, Hayes, M.A., "Microfluidics controlling fluids in small places", *Analytical Chemistry A-Pages* 73 (11), 312-319, 2001.
- Poumellec, B.**, Kherbouche, F., Haut, C., "248 nm photosensitivity of reduced SiO<sub>2</sub>-GeO<sub>2</sub> layer on silica substrate: preliminary results on the light-matter interaction", *Applied Surface Science* 109/110, 283-288, 1997.
- Poumellec, B.**, Douay, M., Garapon, J., Niay, P., "Relationship between UV optical absorption and UV excited luminescence in Ge doped silica", *Trends in Applied Spectroscopy* 4, 325-353, 2002.
- Rajarajan, M.**, Rahman, B.M.A., Wongcharoen, T., Grattan, K.T.V., "Accurate analysis of MMI devices with two-dimensional confinement", *IEEE Journal of Lightwave Technology* 14 (9), 2078-2084, 1996.
- Rech, I.**, Restelli, A., Cova, S., Ghioni, M., Chiari, M., Cretich, M., "Microelectronic photosensors for genetic diagnostic Microsystems", *Sensors and Actuators B*, in press, 2004.
- Reyes, D.R.**, Iossifidis, D., Auroux, P.-A., Manz, A., "Micro total analysis systems. 1. Introduction, theory and technology", *Analytical Chemistry* 74, 2623-2636, 2002.
- Robinson, G.**, "The commercial development of planar optical biosensors", *Sensors and Actuators B* 29, 31-36, 1995.
- Rowe-Tait, C.A.**, Hazzard, J.W., Hoffman, K.E., Cras, J.J., Golden, J.P., Ligler, F.S., "Simultaneous detection of six biohazardous agents using a planar waveguide array biosensor", *Biosensors and Bioelectronics* 15, 579-589, 2000.
- Ruano, J.M.**, Ortega, D., Bonar, J.R., McLaughlin, A.J., Jubber, M.J., Cooper, J.M., Aitchison, J.S., "Fabrication of Integrated Microanalytical Chambers and Channels for Biological Assays using Flame Hydrolysis Deposition Glass", *Microelectronic Engineering* 46, 419-422, 1999.
- Ruano, J.M.**, Benoit, V., Aitchison, J.S., Cooper, J.M., "Flame Hydrolysis Deposition of Glass on Silicon for the Integration of Optical and Microfluidic Devices", *Analytical Chemistry* 72, 1093-1097, 2000 (a).
- Ruano, J.M.**, PhD Thesis, University of Glasgow, 2000 (b).

- Ruano, J.M., Glidle, A., Cleary, A., Walmsley, A., Aitchison, J.S., and Cooper, J.M.,** “Design and fabrication of a silica on silicon integrated optical biochip as a fluorescence microarray platform”, *Biosensors and Bioelectronics* 18, 175-184, 2003.
- Sahu, J.K., Wosinski, L., Fernando, H.,** “Reduction of absorption loss in silica-on-silicon channel waveguides fabricated by low temperature PECVD process”, *Proc. Photonics Prague*, 81-85, 1999 (Proc. SPIE 4016).
- Sasaki, H., Anderson, I.** “Theoretical and experimental studies on active Y-junctions in optical waveguides”, *IEEE Journal of Quantum Electronics* 14, 883-892, 1978.
- Seiler, K., Harrison, D.J., Manz, A.,** “Planar glass chips for capillary electrophoresis: repetitive sample injection, quantitation, and separation efficiency”, *Analytical Chemistry* 65, 1481-1488, 1993.
- Shibata, Y., Oku, S., Yamamoto, M., Naganuma, M.,** “Reflection characteristics and cascability of a multi-mode interference 3dB coupler”, *IEE Proceedings – Optoelectronics* 149 (5/6), 217-221, 2002.
- Sigma-Aldrich,** Technical advice online, 2001.
- Soldano, L.B., Pennings, E.C.M.,** “Optical multi-mode interference devices based on self-imaging: principles and applications”, *IEEE Journal of Lightwave Technology* 13 (4), 615-627, 1995.
- Spinelli, A., Ghioni, M.A., Cova, S.D., Davis, L.M.,** “Avalanche detector with ultraclean response for time-resolved photon counting”, *IEEE Journal of Quantum Electronics* 34 (5), 817-821, 1998.
- Svalgaard, M., Poulsen, C.V., Bjarklev, A., Poulse, O.,** “Direct UV writing of buried singlemode channel waveguides in Ge-doped silica films”, *Electronics Letters* 30 (17), 1401-1403, 1994.
- Svalgaard, M.,** “Direct writing of planar waveguide power splitters and directional couplers using a focussed ultraviolet laser beam”, *Electronics Letters* 33 (20), 1694-1695, 1997.
- Syahriar, A., Syms, R.R.A., Tate, T.,** “Thermooptic interferometric switches fabricated by electron beam irradiation of silica-on-silicon”, *Journal of Lightwave Technology* 16 (5), 841-846, 1998.
- Syms, R.R.A., Tate, T.J., Lewandowski, J.J.,** “Near-infrared channel waveguides formed by electron-beam irradiation of silica layers on silicon substrates”, *Journal of Lightwave Technology* 12 (12), 2085-2091, 1994.

- Syms, R.R.A., Tate, T.J., Bellerby, R.,** “Low-loss near-infrared passive optical waveguide components formed by electron beam irradiation of silica-on-silicon”, *Journal of Lightwave Technology* 13 (8), 1745-1749, 1995.
- Takato, N., Jinguji, K., Yasu, M., Toba, H., Kawachi, M.,** “Silica-based single-mode waveguides on silicon and their application to guided-wave optical interferometers”, *Journal of Lightwave Technology* 6,1003-1010, 1988.
- Themistos, C, Rahman, B.M.A.,** “Design issues of a multimode interference-based 3 dB splitter”, *Applied Optics* 41 (33), 7037-7044, 2002.
- Tien, P.K., Ulrich, R.,** “Theory of prism-film coupler and thin-film light guides”, *Journal of the Optical Society of America* 60 (10), 1325-1337, 1970.
- Ulrich, R.,** “Theory of the prism-film coupler by plane wave analysis”, *Journal of the Optical Society of America* 60 (10), 1337-1350, 1970.
- Ulrich, R., Torge, R.,** “Measurement of thin film parameters with a prism coupler”, *Applied Optics* 12 (12), 2901-2908, 1973.
- Van Roey, J., van der Donk, J., Lagasse, P.E.,** “Beam-propagation method: analysis and assessment”, *Journal of the Optical Society of America* 71 (7), 803-810, 1981.
- Verpoorte, E.,** “Chip vision – optics for microchips”, *Lab Chip* 3, 42N-52N, 2003.
- Wang, Q., He, S., Wang, L.,** “A low-loss Y-branch with a multimode waveguide transition section”, *IEEE Photonics Technology Letters* 14 (8), 1124-1126, 2002.
- Ward, G. (editor),** “Integrated optics and optical communications”, MSS Information Corporation, New York, 1974.
- Weston, K.D., Dyck, M., Tinnefeld, P., Müller, C., Herten, D.P., Sauer, M.,** “Measuring the number of independent emitters in single-molecule fluorescence images and trajectories using coincident photons”, *Analytical Chemistry A-Pages*, online edition, 2004.
- Wheeler, A.R., Chah, S., Whelan, R.J., Zare, R.N.,** “Poly(dimethylsiloxane) microfluidic flow cells for surface plasmon resonance spectroscopy”, *Sensors and Actuators B* 98, 208-214, 2004.
- Williams, D.L., Davey, S.T., Kashyap, R., Armitage, J.R., Ainslie, B.J.,** “Ultraviolet absorption studies on photosensitive germanosilicate performs and fibers”, *Applied Physics Letters* 59, 762-764, 1991.
- Wosinski, L.,** “Technology for photonic components in silica/silicon material structure”, PhD Thesis, Royal Institute of Technology (Sweden), 2003.

- Yajima, H.**, “Coupled mode analysis of dielectric planar branching waveguides”, *IEEE Journal of Quantum Electronics* QE-14 (10), 749-755, 1978.
- Yasukawa, T.**, private communication, 2001.
- Yin, R., Yang, J., Jiang, X., Li, J., Wang, M.**, “Improved approach to low-loss and high-uniformity MMI devices”, *Optics Communications* 181, 317-321, 2000.
- Zhang, J., Herman, P.R., Lauer, C., Chen, K.P., Wei, M.**, “157-nm Laser-Induced Modification of Fused-Silica Glasses”, *Proc. SPIE 4274: Laser Applications in Microelectronic and Optoelectronic Manufacturing VI*, 125-132, 2001 (a).
- Zhang, J., Herman, P.R., Sugioka, K.**, “VUV Laser Micromachining and Bulk Modification of Photonic Materials”, *Proc. CLEO 2001* (b).
- Zhao, Y.-G., Lu, W.-K., Ma, Y., Kim, S.-S., Ho, S.T., Marks, T.J.**, “Polymer waveguides useful over a very wide wavelength range from the ultraviolet to infrared”, *Applied Physics Letters* 77 (19), 2961-2963, 2000.
- Zhou, Y., Magill, J.V., De La Rue, R.M., Laybourn, P.J.R.**, “Evanescent fluorescence immunoassays performed with a disposable ion-exchanged patterned waveguide”, *Sensors and Actuators B* 11, 245-250, 1993.